SORPTION OF GASES AND VAPOURS BY ZEOLITE RHO

by

Miguel Angel Rosemblat

A thesis submitted

for the degree of

Doctor of Philosophy

in the

University of London

Department of Chemistry
Imperial College of Science and Technology
South Kensington
London SW7 2AY

December 1979

ABSTRACT

In the third conference of zeolites Robson et al.* reported the synthesis of a new zeolite related to zeolite A which they called zeolite RHO.

The pseudo unit cell of zeolite A contains one α cage, one sodalite cage and three small cubic units. The sodalite and cubic units are not involved in sorption, so it takes place only in the α cages, the passage of molecules into them being controlled by the octagonal windows. In zeolite RHO half unit cell contains one α cage and three octagonal prisms, sorption taking place in both units, the passage of molecules into the structure being controlled by the double set of octagonal windows forming the prism.

This work concerns sorption in the interesting pore system of zeolite RHO. Our first experiments showed that cationic forms of RHO were blocked. Only the hydrogen forms when outgassed at 400°C were good sorbents. They also needed stabilization. The stabilized material was an excellent sorbent.

A sorption study of H-RHO was made. Accurate isotherms were obtained for N_2, O_2, CO_2, Ar, Kr, Xe and for the hydrocarbons CH_4, C_2H_6, C_3H_8, nC_4H_{10}. Heats of adsorption and differential entropies of the sorbed phase were evaluated.

A diffusion study of the hydrocarbons was attempted but the kinetic behaviour of H-RHO was anomalous.

* ("Molecular Sieves", Advances in Chemistry Series 121, Amer. Chem. Soc., (1973) p.106).

ACKNOWLEDGMENTS

I am grateful to Professor R.M. Barrer, F.R.S., for his continual guidance and encouragement during the course of this work.

Thanks to Drs W. Sieber, G. Peeters, A. Sikand and I.S. Kerr for help and advice and to Mr R. Ash for giving me a place in one of his laboratories in the last year of my research.

Finally I want to thank USB/BID and CONICIT for their Scholarships.

Miguel Rosenblat

INDEX

CHAPTER I

RELEVANT LITERATURE

ZEOLITES

The zeolites form a numerous group of structurally diverse, porous, crystalline aluminosilicates. They are found in nature in cracks and cavities of basaltic rocks (1) and as large sedimentary deposits (2). They have also been synthesized in the laboratory, some without any known natural counterpart. The interesting zeolites are found both among the naturally occurring and synthetic phases.

The zeolites are framework aluminosilicates (3). Each SiO_4 tetrahedron is joined to one of four other SiO_4 or AlO_4 tetrahedra by sharing an oxygen atom. Each AlO_4 tetrahedron results in a negative charge which is balanced by a cation, generally alkaline or earth alkaline.

The structural formula of a zeolite is :

$$M_{x/n}[(AlO_2)_x(SiO_2)_y]\ w\ H_2O$$

where M is a cation of charge n. The brackets enclose the framework composition.

The composition of a zeolite is usually expressed in the oxide formula :

$$M_{2/n}O,Al_2O_3\ ,\ a\ SiO_2\ ,\ b\ H_2O$$

a is the silica:alumina ratio. Since according to Lowenstein's rule (4) the AlO_4 tetrahedron is always bounded to a SiO_4 tetrahedron $a \geq 2$. It is generally found that a varies from two to ten.

The framework structures of zeolites are typical and enclose cavities and channels which are occupied by the cations and water molecules. The cations may be exchanged by others to a varying degree and the intracrystalline water in many zeolites is easily and reversibly removed by heating and evacuation (5).

The structure of a given zeolite is its most specific and individual characteristic. Zeolites were early classified according to morphological properties. Smith (6) drew up the first structural classification of

zeolites. His classification which is still valid has been extended by Meier (7).

Meier based his classification in that the zeolite structures could be built up from small assemblages of tetrahedra. He called these assemblages "secondary building units" SBU (Figure 1.1). The primary building units are the SiO_4 and AlO_4 tetrahedra.

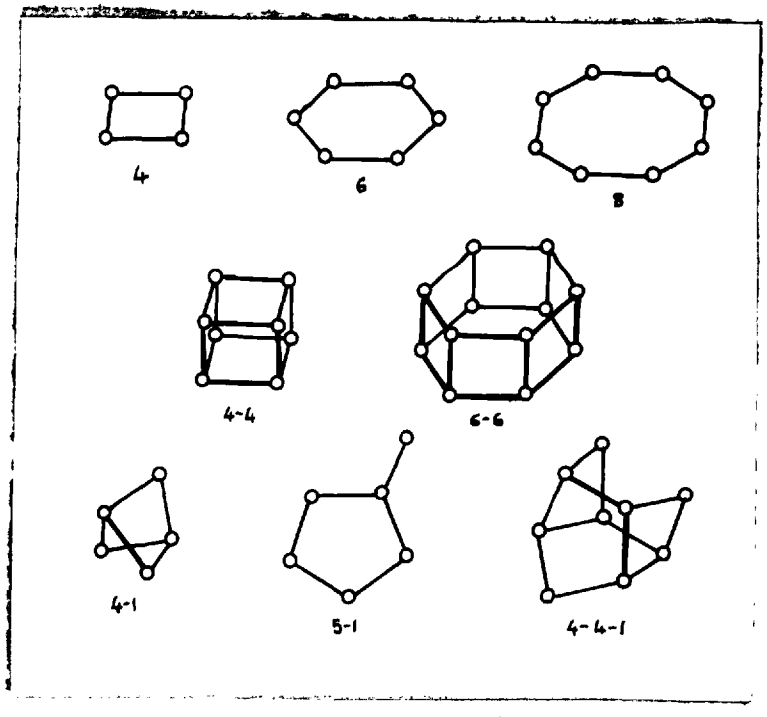

Figure 1.1. The secondary building units found in zeolite frameworks. Oxygen atoms are not shown.

He believed that these SBU could be present in the liquid phase of the reaction mixtures as aluminosilicate anions and were responsible for the growth of zeolite crystals. Zeolites were then classified in seven groups :

1) Analcime group
2) Natrolite group
3) Chabazite group
4) Phillipsite group
5) Heulandite group
6) Mordenite group
7) Faujasite group

The frameworks of the Analcime group can be derived by interconnecting four rings, the frameworks of the Chabazite group from six membered rings, and of the Phillipsite group from four rings lying approximately parallel to each other. The members of the Heulandite, Mordenite and Natrolite groups were not based on SBU and the Faujasite group was based on the presence of 8 cages.

Later Breck (8) classified the zeolites in seven groups all based on SBU, but a given zeolite structure can be built up from several SBU and therefore the classification is arbitrary. For example chabazite can be built up from 4 rings, 6 rings and double six rings, Linde A from 4, 6, 8, 4-4, 6-6 rings, etc. This classification results in bringing together in a group zeolites which have structures and properties which are very different.

The specific ways in which SBU are joined produce definite geometric forms called polyhedra. Some of these are shown in Figure 1.2.

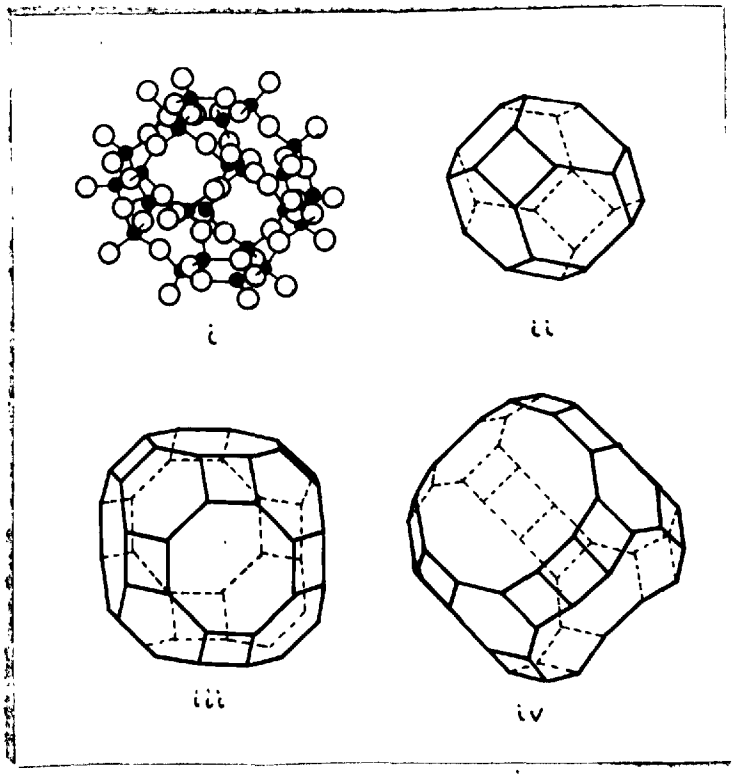

Figure 1.2. i) Sodalite 14 hedron or 8 cage, showing Al, Si (●) and oxygen (O) atoms
ii) β cage
iii) 26 hedron type I or α cage
iv) 26 hedron type II

Many zeolites are well visualized by coordinating these polyhedra. For example, zeolite A results when the sodalite cages are joined to each other through the square faces as indicated in Figure 1.3(a). A cavity at the centre is produced which is the α cage of Figure 1.2 (iii).

In faujasite each 8 cage is tetrahedrally surrounded by four others linked to each other through six membered rings. This creates a 26-hedron of type II of Figure 1.2 (iv) at the centre.

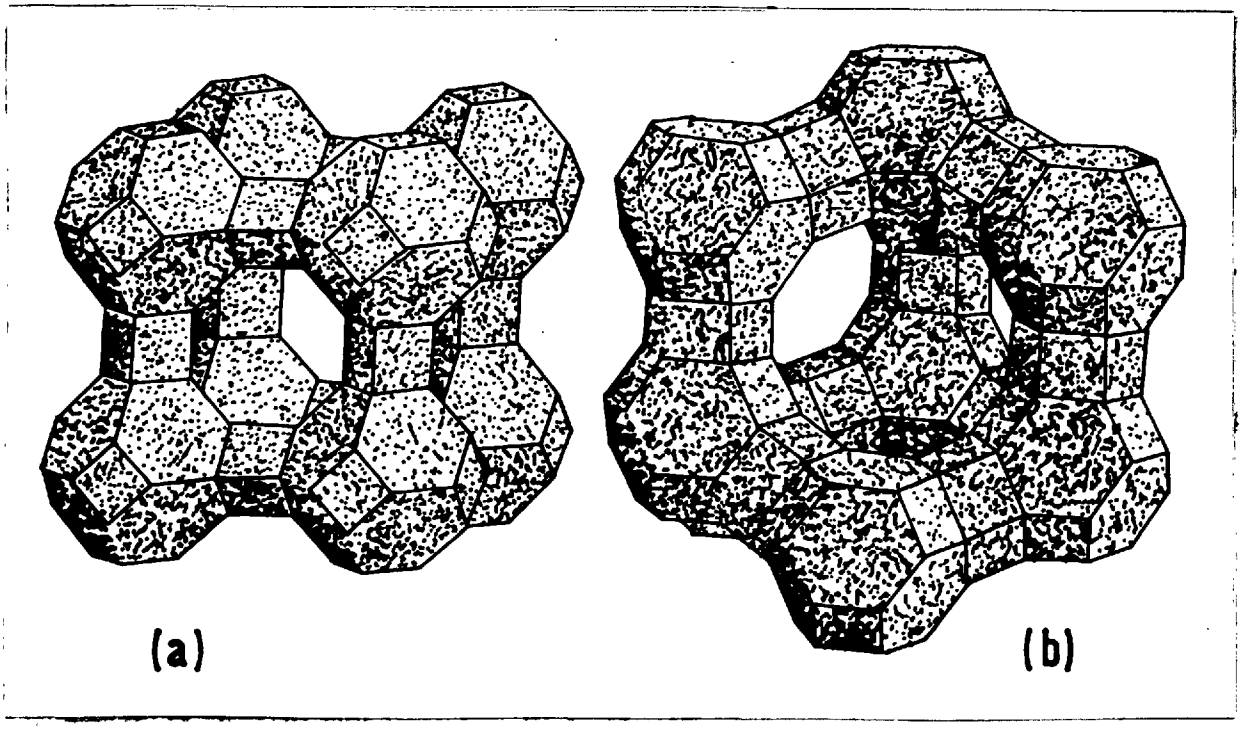

Figure 1.3. Arrangements of the sodalite cages (8 cages) in the framework structures of Linde A (a) and faujasite (b).

The α cage or truncated cubo octahedron is an alternative building block of zeolite A which can be arrived at by connecting the square faces to each other.

When the α cages are joined to each other by oxygen bridges through the octagonal windows the structure of zeolite RHO (Figure 1.4) is produced. Zeolites can also be constructed from layers and chains (9).

Another important aspect when considering the sorption properties of zeolites is the kinds of channels forming the intracrystalline

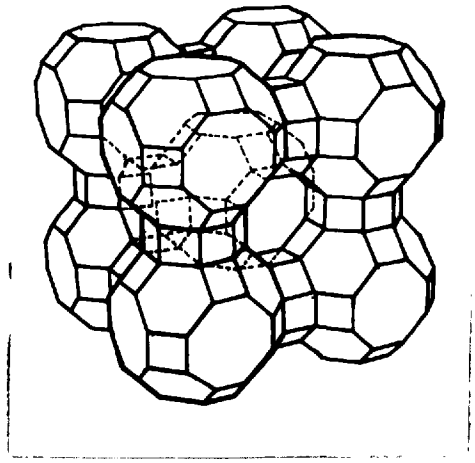

Figure 1.4. Zeolite RHO

volume. If a molecule within the crystal is constrained to move only in one direction the channel system is one dimensional, 1D, if it can move only in a plane 2D and if it can move in three directions, 3D. The channel systems of zeolite A and zeolite RHO are illustrated in Figure 1.5.

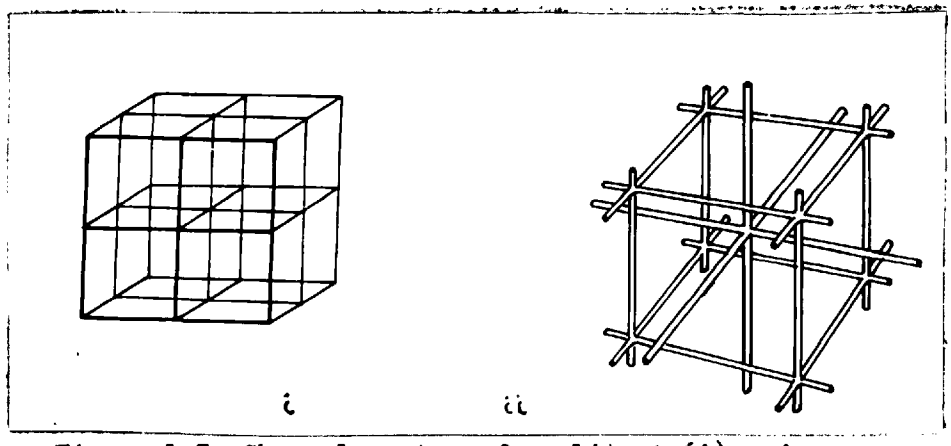

Figure 1.5. Channel system of zeolite A (i) and zeolite RHO (ii).

In zeolite A from the centre of each α cage six directions lead to the centres of one each of six other identical α cages. For zeolite RHO there are two channel systems each of which has the symmetry of that in zeolite A. The two channel systems interpenetrate but are not interconnected.

Zeolites are formed by hydrothermal reactions under alkaline conditions (11). In the laboratory the natural processes are imitated. Many of known synthetic zeolites are not structurally related to minerals, this may be due to the fact that zeolites are not crystallized under equilibrium conditions, that is, are metastable phases.

Important factors in determining the product of a given synthesis are the ratio of Si and Al, the water content, the pH, cations and temperature of the reaction mixture. The pressure is generally the autogeneous vapour pressure of water. The importance of the nature and condition of the starting material (that is whether they are colloidal, oxide or glasses) used in preparing the reaction mixture (12,13) has also been emphasised. These factors influence not only the kinetics of the crystallization process but also the nature of the crystallizing zeolite phases.

The mixing of the starting materials produces a gel which is kept in a closed system, often with ageing at room temperature for some time. Then it is heated at a higher temperature where after some time (induction period) nuclei formed and grow.

The mechanism of crystallization is not yet clear (14). There seems to be a quasi-equilibrium between the solid and liquid phases in the gel :

Amorphous aluminosilicate = aluminosilicate anions
(solid phase) (liquid phase) (1)

When the gel is heated equilibrium (1) moves to the right increasing concentration of the ions in the liquid phase. As a result the probability of condensation reactions between the ions increases giving rise to the formation of primary aluminosilicate blocks and crystal nuclei (15). The formation and growth of crystal nuclei consume the ions in the liquid phase and the solid phase continues dissolving.

Zeolites are the best class of molecular sieves. They have pores uniform in size determined by their crystal structures and molecules larger than the openings giving access to these pores will be excluded. The maximum free dimensions of some windows in planar configurations are given below :

Window	free dimension Å
4	1.15
6	2.8
8	4.5
12	8.0

These dimensions change a little for different zeolites as illustrated by Barrer (10) for octagonal windows.

These windows through which molecules must diffuse are lined in their inner peripheries by oxygen atoms equal in number to the number of tetrahedra forming the ring. The rings are not wholly rigid, and neither oxygen atoms nor penetrating molecules are hard spheres. Therefore molecules somewhat larger in their critical cross-section than the free cross-section of the ring may squeeze through, given a sufficient energy of activation. However the energy barriers will rise as one increases the critical dimensions of the penetrant molecules until the activated diffusion process becomes immeasurably slow.

Apart from the structure, an important factor in determining the molecule sieving property of a zeolite is the cation. Since the charge of the aluminosilicate framework is distributed over all the oxygen atoms we then expect that in the dehydrated state of a zeolite the cations occupy sites with high coordination number of oxygen atoms. These sites can be near or in a window hindering the passage of a molecule through it.

By ion exchange the molecule sieving property of a zeolite can be modified (16). For example in dehydrated zeolite NaA of the twelve cations per unit cell eight are 0.4Å from the six rings into the α cage, one against the four ring and three 1.4Å from the centres of the eight rings. These latter cations regulate the adsorption by partially blocking the eight rings. When exchanged by Ca^{+2} so that there are $4Ca^{+2}$ and $4Na^{+}$ per unit cell the eight positions near the 6 rings are occupied leaving the eight rings completely unblocked.

Ion exchange has been established as a standard way of tailoring molecular sieve zeolites so as to meet the best requirements for a particular separation.

When exposed to a vapour at or below the boiling temperature, the zeolite cavities fill at low relative pressures with the molecular species concerned and when the filling is complete no more intracrystalline sorption occurs. This leads to a rectangular type of adsorption isotherm.

The usual concept of surface area in solids is not applicable with zeolites since the total pore volume is occupied by the sorbate molecules.

According to Gurvitsch rule (17) the quantity of material sorbed at saturation, X_s, at a given temperature is assumed to fill the microporous

of the solid as the normal liquid having a density d_a of the liquid at that particular temperature. The total pore volume V_p is :

$$V_p = \frac{X_s}{d_a}$$

This rule is obeyed to a large extent but some deviations are observed, for example :

Zeolite A contains two types of void spaces: those within the β cages which are accessible only to small molecules and which have a volume of 151 $Å^3$ per unit cell, and the large voids of the α cages of volume 775 $Å^3$ per unit cell.

The application of Gurvitsch rule to the adsorption of gases in zeolite CaA (18) gives :

Adsorbate	T°C	X_s g/g	V_p cc/g	$Å^3$/unit cell
H_2O	25	0.305	0.305	885
O_2	-183	0.276	0.242	700
Ar	-183	0.358	0.261	738
N_2	-196	0.239	0.297	857
n-C_4H_{10}	25	0.131	0.226	655

With the exception of water and nitrogen the observed pore volumes follow the Gurvitsch rule considering that only the α cages are occupied. The amount of adsorbed water and nitrogen cannot be accounted for on the basis that they are normal liquids filling just the large voids. The high value for water is due to its penetration into the β cages, but nitrogen cannot enter into the β cages at -196°C and the only explanation is that the density of nitrogen in the sorbed phase is larger than in the liquid. The smaller value for n-butane is due to the fact that larger molecules pack with more difficulty in a cage and therefore its density is smaller than in the liquid.

Hydrogen forms have been prepared by acid treatment of the silica rich zeolite mordenite (19) and clinoptilolite (20). Together with ion exchange by H_3O^+, aluminium is partially removed from the framework according to :

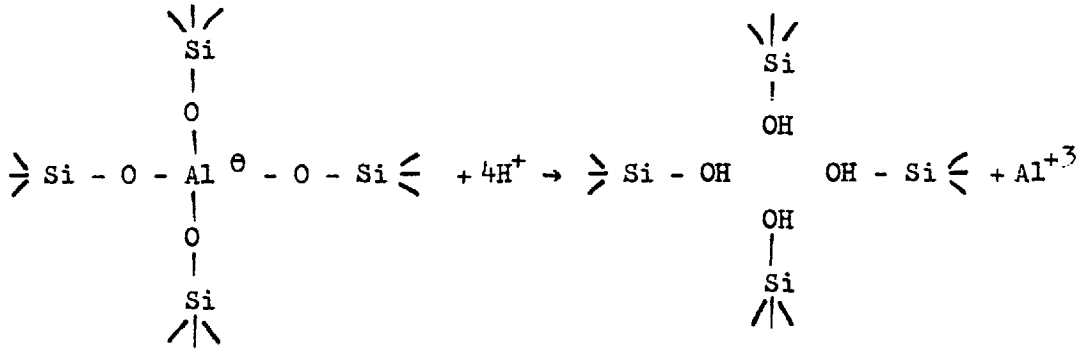

While in silica rich zeolites the replacement of aluminium does not produce the collapse of the structure in other zeolites it does. Nevertheless zeolites which would decompose in acid can be put into the hydrogen form (21) by an indirect method where the cations are exchanged with NH_4^+, which upon subsequent heating will liberate NH_3, leaving the zeolite in the hydrogen form.

When heating the ammonium forms in order to prepare the hydrogen forms two types of procedure can be followed. In the first type de-ammoniation and dehydroxylation are conducted in vacuo which removes the volatilized products, ammonia and water. In the second type the decomposition products are retained, water vapour and ammonia are present in the vapour phase.

The first type results in destabilization, that is the formation of a metastable zeolite which in further contact with water vapour at elevated temperatures will lose crystallinity. The second type results in a stabilized material.

The mechanism of stabilization is not clear (22) but it appears to consist of several steps. The hydrogen form of a zeolite is a first and necessary stage in stabilization. The second step appears to be the extraction of aluminium from the framework. There is evidence that heating the NH_4^+ zeolites in presence of water vapour releases aluminium from the framework (23) The third step appears to be contraction of the structure. Although there are opposing views concerning the nature of the reactions involved in the contraction the most likely possibility is elimination of water with the formation of new Si-O-Si bonds with silica taking positions in the vacated tetrahedral sites.

THEORY OF ADSORPTION

When a highly disperse solid or a porous solid is exposed in a closed system to a gas or vapour at some definite pressure, the solid begins to adsorb the gas. This is made manifest by a gradual reduction in the pressure of the gas and (if the solid is suspended for example on a spring balance) by an increase in the weight of the solid. After a time the pressure becomes constant at a value p, say, and correspondingly the weight ceases to increase any further. The amount of gas thus adsorbed can be calculated from the fall in pressure by application of the gas laws if the volume of the vessel is known, or it can be determined directly as the increase in weight of the solid in the case where the spring balance is used.

The amount, X, adsorbed per gram of solid depends on the equilibrium pressure, p, the temperature T and also the nature of the gas and the solid :

$$X = f(p, T, \text{gas}, \text{solid}) \qquad (1)$$

For a given gas adsorbed on a given solid, maintained at a fixed temperature equation (1) simplifies to :

$$X = f(p)_{T,\text{gas},\text{solid}} \qquad (2)$$

If the gas is below its critical temperature, i.e. if it is a vapour, the alternative form :

$$X = f(p/p_o)_{T,\text{gas},\text{solid}} \qquad (3)$$

is more useful, p_o being the saturation vapour pressure of the adsorbate.

Equations (2) and (3) are expressions of the adsorption isotherm, i.e. the relationship between the amount adsorbed and the pressure, for a given gas adsorbed on a given solid at a fixed temperature.

The first theoretical equation of the adsorption isotherm was advanced by Langmuir.

The Langmuir Theory

In his original treatment of adsorption, Langmuir (24) made the following simplifying assumptions:

1) The surface of a solid is composed of a two dimensional array of energetically homogeneous sites.

2) Only one molecule can be adsorbed per site and saturation of the surface is reached on completion of the monolayer.

3) The adsorbed molecules do not interact with one another.

Using this model, he derived by means of a kinetic argument the isotherm equation :

$$v = \frac{v_m\, b\, p}{1 + bp} \qquad (4)$$

where

v : amount sorbed per gram of sorbent at equilibrium pressure p

v_m : the amount sorbed per gram of sorbent to complete a monolayer

b : is an adsorption coefficient specific to each sorbent-sorbate system :

$$b = K_o\, e^{-q/kT}$$

q : heat of adsorption

K_o : term dependent on the entropy of adsorption

b will be constant if the free energy of adsorption is constant in each site.

In testing whether a given isotherm follows Langmuir equation, equation (1) can be put in the form :

$$\frac{p}{v} = \frac{1}{v_m b} + \frac{p}{v_m} \qquad (5)$$

A plot of p/v against p should give a straight line. This is a necessary condition but not a sufficient condition. The values of v_m and b obtained from the slope and intercept of the straight lines should be reasonable and consistent.

Subsequently Volmer (25) by thermodynamic reasoning and Fowler (26) by statistical mechanics arrived at the same equation, having made the same assumptions as did Langmuir.

About twenty years later Brunauer, Emmett and Teller concluded that adsorption of vapours was not limited to formation of unimolecular layers, but that multimolecular layers were formed. This leads to a generalization of the Langmuir theory, known as the BET theory, and the development of a corresponding equation for the adsorption isotherm.

The BET Theory

Brunauer, Emmett and Teller (27) assumed as did Langmuir that the sorbent surface is an array of energetically uniform sites, that one molecule only is adsorbed per site, and that no mutual interaction occurs between the adsorbed molecules; but further each adsorbed molecule in the monolayer is postulated to be an adsorption site for second layer molecules, and in a like manner further adsorbed layers are built up. The energy of adsorption of second and all higher layer molecules is assumed equal to that of sorbate liquefaction. The total amount sorbed, v, is then the sum of the adsorption in all layers, and taking the value of the nth layer as infinity leads to the isotherm equation :

$$\frac{p/p_o}{v(1 - p/p_o)} = \frac{1}{v_m c} + \frac{(c-1)\, p/p_o}{v_m c} \qquad (6)$$

where

p is the equilibrium pressure

p_o is the saturated vapour liquid pressure

v is the amount sorbed at p

v_m is the monolayer capacity

c is a constant $\cong \exp(E_1 - E_\ell)/RT$

E_1 being the energy of adsorption in the monolayer

E_ℓ the energy of liquefaction.

Brunauer, Emmett and Teller classified the isotherms within the five types of Figure (1.1) and were able to describe them with his equation :

Type I is the Langmuir isotherm which is a particular case of the BET theory.

Type II and Type III are obtained with nonporous sorbents. Type II when E_1 is larger than E_ℓ and Type III when E_1 is comparable or smaller than E_ℓ.

Type IV and Type V are obtained with porous sorbents. The same argument for Types II and III are valid. With microporous sorbents Type I isotherms are obtained.

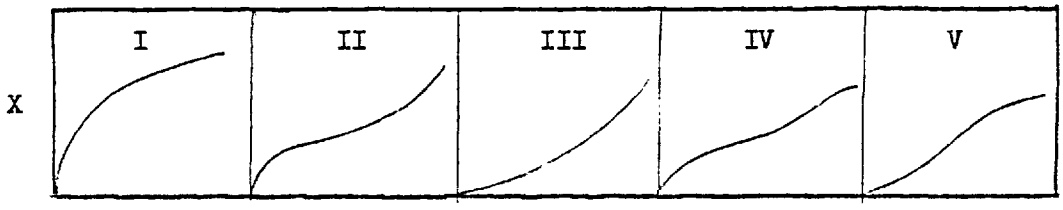

Figure 1.6

Polanyi Theory

Polanyi (28) adopted a completely different approach to the subject of physical adsorption. Whereas the Langmuir and BET theories dealt with specific molecule-site interactions, Polanyi conceived the force of adsorption as an intermolecular potential gradient, the adsorption potential, ϵ_i at a point i at or near the surface of the adsorbent being defined as the isothermal work done by the adsorption forces in bringing a molecule from the bulk gas phase to that point. The resultant picture of the adsorbed phase is shown in Figure 1.7.

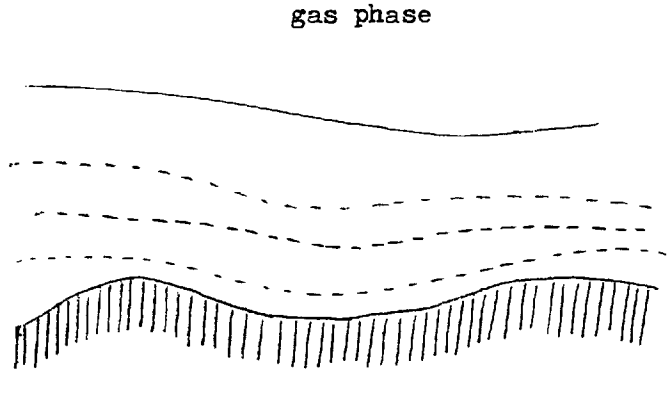

Figure 1.7

The shaded area represents the sorbent surface where the sorption potential is ϵ_o, the dotted lines represent equipotential sorbate forces of potential ϵ_1, ϵ_2, ..., ϵ_i of density δ_1, δ_2, ..., δ_i which together with the adsorbed surface enclose the sorbate volumes w_1, w_2, ..., w_i. The solid line is the gas phase sorbate phase boundary and w_o represents the total volume of adsorption space.

The sorption potential ϵ_1 is some function of w_i:

$$\epsilon_1 = f(w_i) \qquad (7)$$

and the problem is to determine this function between the limits $w = 0$ (ϵ_i max) and $w = w_o$ ($\epsilon_i = 0$). The theory assumes that the adsorption potential is independent of temperature and equation (7), termed the characteristic curve of a particular sorbate-sorbent system, is independent of temperature.

The evaluation of the characteristic curves at different temperatures has been adequately dealt with in the literature (29). As an illustration of the method, the situation for the adsorption of a vapour near its boiling point according to this model is given. Assuming that the gas behaves ideally, the sorption potential, ϵ_i, is simply the work of compressing isothermically the gas from p the equilibrium pressure to p_o the saturation vapour pressure of the liquid and is given by :

$$\epsilon_i = \int_p^{p_o} \frac{RT}{p}\, dp = RT \ln \frac{p_o}{p} \qquad (8)$$

It is further assumed that the sorbed phase is incompressible and that :

$$w_i = \frac{X_i}{\delta_T}$$

where X_i is the quantity sorbed at pressure p and δ_T is the density of sorbate in the liquid state at temperature T. Thus a characteristic curve $\epsilon_i = f(w_i)$ can be constructed. Calculations based on experimental isotherms for a large number of systems have established the existence of such curves and their approximate temperature independence. Despite its ability to represent a large body of experimental data over a considerable temperature range, the application of the Polanyi theory yields little useful information about the solid sorbent.

INTERMOLECULAR FORCES

The forces given rise to adsorption are the same as those involved in any other interatomic or intermolecular interaction phenomena :

Dispersion Forces

Repulsion Forces

Electrostatic Forces

Induction Forces.

Dispersion Forces

When two nonpolar molecules a and b interact there are forces of attraction between them. At any instant the electrons in molecule a are in some configuration which results in an instantaneous dipole moment. This instantaneous dipole moment induces a dipole in molecule b. The induced dipole in b then interacts with the instantaneous dipole in a to produce an energy of attraction between the two molecules.

With the aid of quantum mechanical perturbation theory, London (30) showed that the potential energy, ϕ_D, of two isolated atoms with their centres separated by a distance, r, is given by :

$$\phi_D = -\frac{C}{r^6} \qquad (9)$$

The constant **C** is related to the polarizabilities α_1 and α_2 of the two atoms by :

$$C = \frac{3}{2}\left(\frac{hV_a\ hV_b}{hV_a + hV_b}\right)\alpha_a\ \alpha_b \quad . \qquad (10)$$

in which hV_a and hV_b are characteristic energies of the two molecules approximately equal to their ionization energies. An alternative expression for C involving the diamagnetic susceptibilities χ_1 χ_2 of the atoms has been given by Kirkwood and Muller (31) :

$$C = 6mc^2\ \frac{\alpha_1\ \alpha_2}{\alpha_1/\chi_1 + \alpha_2/\chi_2} \qquad (11)$$

m being the mass of the electron and c the velocity of light.

Repulsive Forces

Repulsive forces arise from the interpenetration of the electronic clouds of the atoms. This may be represented by the empirical expression:

$$\phi_R = \frac{b}{r^m} \qquad (12)$$

where b is an empirical constant and the index m is usually taken as 12. Consequently the repulsion is important only at short separations.

The total dispersion plus repulsion energy of the two atoms is thus given by :

$$\phi_D + \phi_R = \frac{b}{r^{12}} - \frac{C}{r^6} \qquad (13)$$

Electrostatic Forces

Dispersion and repulsive forces are common to all matter and will be present whatever the nature of the solid or gas. If however the gas is polar (has a permanent dipole or quadrupole moment) then electrostatic forces will also make a contribution. The electrostatic contribution due to the interaction of the field F of the solid and the dipole moment u of the molecule is given by :

$$\phi_{Fu} = - Fu \cos \theta \qquad (14)$$

θ is the angle between the axis of the dipole and the direction of the electrostatic field.

The electrostatic contribution due to the presence of a quadrupole moment, Q, of the molecule is :

$$\phi_{FQ} = \tfrac{1}{2} Q^2 \dot{F} \qquad (15)$$

where $\dot{F}$ is the field gradient.

Induction Forces

If the adsorbed molecule has no permanent dipole, it will still acquire an induced moment (of magnitude $F\alpha$ if α is the polarizability of the molecule) when placed in the electrostatic field produced by the solid. The contribution to the interaction energy arising from this cause will at distance, r, from the surface given by :

$$\phi_p = - \frac{\alpha F^2}{2} \qquad (16)$$

where F is the value of the field at distance r.

THE HEAT OF ADSORPTION

The differential change in free energy in transferring isothermically dn moles of gas at the standard pressure p_o, to the sorbed phase where n_s moles of sorbate are sorbed at equilibrium with gas at pressure p, is :

$$\Delta\overline{G}^o_s = \overline{G}_s - \tilde{G}^o_s = \tilde{G}^p_g - \tilde{G}^o_g = RT \ln \frac{p}{p_o}$$

considering p_o = 1 atm

$$\Delta\overline{G}^o_s = RT \ln p \qquad (17)$$

$\Delta\overline{G}^o_s$ is the affinity of sorption.

By definition of G we have :

$$\Delta\bar{G}^{o}_{s} = \Delta\bar{H}^{o}_{s} - T\,\Delta\bar{S}^{o}_{s} \qquad (18)$$

where :

$$\Delta\bar{H}^{o}_{s} = \bar{H}_{s} - \bar{H}^{o}_{g} = \bar{H}_{s} - \tilde{H}^{o}_{g}$$

$$\Delta\bar{S}_{s} = \bar{S}_{s} - \bar{S}^{o}_{g} = \bar{S}_{s} - \tilde{S}^{o}_{g}$$

The heat of adsorption q_{st} is defined as :

$$q_{st} = \tilde{H}^{o}_{g} - \bar{H}_{s} = \tilde{H}_{g} - \bar{H}_{s} \quad \text{since } \left(\frac{dH_g}{dp}\right)_T = o \text{ for a perfect gas}$$

Substituting into (18) :

$$\Delta\bar{G}^{o}_{s} = - q_{st} - T\,(\bar{S}_{s} - \tilde{S}^{o}_{g}) \qquad (19)$$

and equating (17) and (19) :

$$RT \ln p = - q_{st} - T\,(\bar{S}_{s} - \tilde{S}^{o}_{g})$$

$$\ln p = - \frac{q_{st}}{RT} - \frac{1}{R}\,(\bar{S}_{s} - \tilde{S}^{o}_{g})$$

Assuming q_{st} is independent of T, differentiation with respect to the temperature gives :

$$\left(\frac{d \ln p}{dT}\right)_{ns} = \frac{q_{st}}{RT^2}$$

because with the assumption regarding q_{st},

$$\frac{\partial\bar{S}_{s}}{\partial T} = \frac{\partial\tilde{S}^{o}_{g}}{\partial T}$$

This relation integrated between limits T_1 and T_2 gives :

$$\ln \frac{p_2}{p_1} = - \frac{q_{st}}{R}\left(\frac{1}{T_2} - \frac{1}{T_1}\right)$$

where p_2 is the pressure of the gas in equilibrium with n_s moles sorbed at temperature T_2 and p_1 the pressure at temperature T_1.

Then :

$$q_{st} = - \frac{R \ln(p_2/p_1)}{\left(\frac{1}{T_2} - \frac{1}{T_1}\right)} \qquad (20)$$

Further one has :

$$q_{st} = \tilde{H}_g - \bar{H}_s = \tilde{E}_g + P\tilde{V}_g - \bar{E}_s - P\bar{V}_s = \tilde{E}_g - \bar{E}_s + P(\tilde{V}_g - \bar{V}_s)$$

where $-(\tilde{E}_g - \bar{E}_s)$ is the energy of adsorption.

Neglecting $\bar{V}_s$ in comparison with $\tilde{V}_g$:

$$q_{st} = \tilde{E}_g - \bar{E}_s + RT = -(\bar{\phi} - \bar{\phi}_o) + RT - F(T) \qquad (21)$$

This equation relates the heat of adsorption with the potential energy ϕ of the sorbed molecules :

$\bar{\phi}$ is the differential molar value of the potential energy

$\bar{\phi}_o$ is the differential molar zero point energy of the sorbed molecules

F(T) is a function of temperature which occurs because, as the temperature rises, the sorbed molecules acquire vibrational energy in excess of the zero point energy while the gaseous molecules also gain in translational energy. A vibrational mode involves two square terms and a translation only one, so that as an example for adsorbed monatomic gas behaving as a classical oscillator $F(T) = 3/2RT - 3RT = -3/2RT$, and so $q_{st} = -(\bar{\phi} - \bar{\phi}_o) - \frac{1}{2}RT$. The very small temperature coefficient of q_{st} then justifies equation (20) to the experimental accuracy achieved, although a temperature coefficient in $\bar{\phi}$ is also possible (see eqn 22).

From equation (21) at absolute zero one has

$$q^o_{st} = -(\bar{\phi} - \bar{\phi}_o)$$

where $\bar{\phi}$ is now also its value at zero. Contributions to the heat of adsorption arise from dispersion energy, ϕ_D, repulsion energy ϕ_R; polarization energy ϕ_p, field-dipole interaction ϕ_{Fu}, field gradient-quadrupole interaction ϕ_{FQ} and sorbate-sorbate interaction ϕ_{SP}. Thus for the total ϕ :

$$\phi = \phi_D + \phi_R + \phi_P + \phi_{Fu} + \phi_{FQ} + \phi_{SP} \qquad (22)$$

The first three terms are always present and comprise the non-specific part of ϕ. The next two depend upon the presence of permanent dipoles and quadrupoles in the guest molecules. The term ϕ_{SP} includes dispersion and repulsion energies between pairs of sorbate molecules and for polar molecules also dipole-dipole, dipole-induced dipole, quadrupole-quadrupole and similar energy contributions.

Variation of the heat of adsorption with the amount sorbed.

With zeolites is generally found that :

1) For small uptakes q_{st} decreases with amount sorbed, sometimes rapidly sometimes more slowly depending on the sorbate and zeolite. This indicates that there are some local intracrystalline positions where the guest molecules are sorbed more exothermically than in the rest of the intracrystalline volume, and that these positions are proportionally few in number. In other words zeolites are heterogeneous sorbents. Nevertheless the heats do not always show this behaviour, sometimes being constant at small uptakes.

2) At intermediate uptakes the curves tend to be horizontal and thereafter q_{st} may increase due to exothermal sorbate-sorbate interactions.

3) For uptakes approaching saturation of the intracrystalline volume the heats decline and approach $-\Delta H$ of liquefaction as multilayer sorption and capillary condensation between crystals takes over.

The origin of energetic heterogeneity in zeolites

Kington and McLeod (32) showed that heterogeneity arises mainly from variations in ϕ_{Fu}, ϕ_{FQ} and ϕ_P terms with amount sorbed; they considered that if the $\phi_D + \phi_R$ term in equation (22) was constant (ϕ_{SP} is neglected at low amounts) with amount sorbed one could write :

$$q_{st}(1) - q_{st}(2) = \frac{\alpha}{2}(F_1^2 - F_2^2) + u(F_{t_1} - F_{t_2}) + \frac{Q}{4}\left(\frac{\partial F_{t_2}}{\partial t} + \frac{\partial F_{t_1}}{\partial t}\right) \qquad (23)$$

Thus for any sorbate the difference between the heat of adsorption $q_{st}(1)$ and $q_{st}(2)$ at two different amounts sorbed θ_1 and θ_2 depends in the field characteristics of the solid and on the parameters, α, u and Q of the adsorbed molecules.

For different sorbates in a given solid one can write :

$$q_{st}(1) - q_{st}(2) = a\alpha + bu + cQ \qquad (24)$$

a,b,c are constants for any pair of amounts sorbed θ_1 and θ_2, assuming that the same sites are occupied for the different sorbate molecules at those amounts.

Then they considered a series of quadrupolar molecules with no dipole moment so the term bu is zero. The value of a was determined

with argon since it has zero quadrupole moment. So for the quadrupolar molecules we have :

$$[q_{st}(1) - q_{st}(2)] - a\alpha = cQ \qquad (25)$$

and therefore the difference between the heats at two amounts sorbed when corrected for the polarization effect should be a linear function of the sorbate quadrupole moment.

When they plotted the left hand side of equation (25) against Q using values of the heat of adsorption in chabazite they found a linear plot in accord with equation (25) and the hypothesis that heterogeneity originated mainly in the variation of $\phi_{Fu} + \phi_{FQ} + \phi_P$ and not in the variation of $\phi_D + \phi_R$.

In agreement with this, it is generally found that heterogeneity is more in evidence for sorption of molecules with permanent electric moments than for sorption of non-polar molecules.

One should add that although the main source of heterogeneity in zeolites is attributed to the terms ϕ_{Fu}, ϕ_{FQ}, ϕ_P, some contribution from $\phi_D + \phi_R$ could be expected since :

1) In many zeolites there is more than one kind of cavity to which molecules may have access and $\phi_D + \phi_R$ may be different in each kind of cavity (33).

2) In large cavities such as the 26-hedra of zeolite A and RHO, each cavity can provide a variety of environments for a guest molecule (33) where $\phi_D + \phi_R$ is different.

The nature of the sites within the intracrystalline volume of a zeolite responsible for the energetic heterogeneity

a) Energetic heterogeneity is more pronounced in cationic forms than in hydrogen forms of a given zeolite. For example, heats of adsorption vs amount sorbed can be compared in natural (Na,Ca) chabazite (32) with hydrogen chabazite (34).

b) Energetic heterogeneity is more pronounced in a cationic zeolite where the cation has a higher charge density (35). The initial heat and the degree of heterogeneity of NH_3 in a series of ion exchanged zeolites A followed the sequence :

$$Ca,Sr > (Ba,Na) > Li > Na > K > (Rb,Na) > (Cs,Na)$$

The same is found for other gases as Ar and N_2 (36).

c) The heat of adsorption and the degree of heterogeneity is larger in NaX (where the number of cations per unit cell is larger) than in NaY (37).

It is concluded from a, b and c that the more exothermal sites are associated with the cations. Calculations of the field inside zeolite cavities make it clear that these sites are near the cations (38). The values of the terms ϕ_{Fu}, ϕ_{FQ} and ϕ_P decrease rapidly as molecules are displaced away from them.

THE ENTROPY OF ADSORPTION

At constant temperature under equilibrium conditions the differential change in free energy in transferring dn moles of gas at the equilibrium pressure p to the sorbed phase where n_s moles of gas are sorbed is zero.

Therefore we can write :

$$(\bar{H}_s - \tilde{H}_g) - T(\bar{S}_s - \tilde{S}_{gp}) = 0$$

or

$$\bar{S}_s = -\frac{q_{st}}{T} + \tilde{S}_{gp}$$

Knowing q_{st}, to evaluate $\bar{S}_s$, we must know $\tilde{S}_g$ at the equilibrium pressure p and temperature T. $\tilde{S}_g$ is generally available at the standard pressure p_o and the standard temperature T_o, but :

$$\tilde{S}_{g(p,T)} = \tilde{S}_{g_{(p_o,t_o)}} + \Delta\tilde{S}_{g_{p_o \to p}} + \Delta\tilde{S}_{g_{T_o \to T}}$$

Evaluation of $\Delta\tilde{S}_{g_{p_o \to p}}$

$$dS = \frac{dq_{rev}}{T}, \quad dH = dq - pdV + pdV + Vdp = dq + Vdp$$

At constant T, $dH = 0$ and $dq = -Vdp$

Therefore :

$$\Delta S_{g_{p_o \to p}} = -\int_{p_o}^{p} \frac{V}{T}dp = -\int_{p_o}^{p} \frac{R}{p}dp = -R \ln \frac{p}{p_o}$$

assuming perfect gas.

Evaluation of $\Delta\tilde{S}_{g_{T_o \to T}}$

$$dS = \frac{dH}{T} = \frac{CpdT}{T}$$

Then :

$$\Delta\tilde{S}_{g_{T_o \to T}} = \int_{T_o}^{T} \frac{CpdT}{T} = Cp \ln \frac{T}{T_o}$$

considering Cp constant between T_o and T

Therefore :

$$\tilde{S}_{g_{(p,T)}} = \tilde{S}^{o}_{g} + R \ln \frac{p_o}{p} + Cp \ln \frac{T}{T_o}$$

and finally :

$$\bar{S}_s = \tilde{S}^{o}_{g} + R \ln \frac{p_o}{p} + Cp \ln \frac{T}{T_o} - \frac{q_{st}}{T} \qquad (24)$$

MODELS OF THE INTRACRYSTALLINE SORBED PHASE

A sorbate in the interior of a solid (in the same way as a monolayer on the exterior of a solid) may be considered as being either mobile or localized. If the sorbed molecules encounter potential barriers within the solid greater than their thermal energy then they will tend to be caged within a region of the solid and the phase will be localized. If the thermal energy is large enough to permit passage over these energy barriers, then the sorbed molecules will retain some translational motion and the phase will be mobile.

The concept of a sorbed phase either completely localized or completely mobile is over simplified, and the possibility of a localized-mobile transition should be considered. A localized phase can become mobile with increasing temperature (39) and a phase which is mobile at low concentrations can become more localized at high concentrations (40).

Molecules sorbed within the network of a zeolite cannot possess three degrees of translational freedom, since the molecules are confined to move along channels in the structure. Therefore the following models for the intracrystalline sorbed phase will be considered; localized, mobile with two translational degrees of freedom and mobile with one translational degree of freedom. For each model the isotherm equation and the entropy is given.

Localized Model

This is the Langmuir model referred to in page 15. It applies equally well to sorption on a three dimensional array of sites. Equation (4) can be written as :

$$p = K_2 \frac{\theta}{1-\theta} \qquad (27)$$

where $\theta = \frac{v}{v_m}$. v_m here is the amount sorbed at saturation of the intracrystalline volume.

The entropy of a localized phase may be conveniently separated into thermal entropy and configurational entropy :

$$\bar{S}_s = \bar{S}_{therm} + \bar{S}_{conf} \qquad (28)$$

The thermal entropy includes entropy originating from the electronic states of the molecule, vibrations about chemical bonds, rotations and restricted rotations and vibrations about the mean position of a site. The configurational entropy arises from the number of distinguishable arrangements of N molecules in N_A sites which is given by :

$$\bar{S}_{conf} = R \ln \left(\frac{1-\theta}{\theta} \right) \qquad (29)$$

$$\theta = N/N_A$$

In testing the validity of this model one may consider the difference between the experimentally observed $\bar{S}_s$ and the value of $\bar{S}_{conf}$ calculated from (28). If a simple localized theory is valid then this difference which is the differential thermal entropy of the system, must be a constant independent of θ. Furthermore, the magnitude of $\bar{S}_{th}$ must be reasonable. For example the frequency of vibration about the mean position on the site can be obtained from the value of $\bar{S}_{th}$. This frequency has been discussed by Hill (41) and should normally be in the range 10^{11} to 10^{12} s^{-1}.

Mobile Models

The following cases are considered :

1) Perfect two dimensional gas

A two dimensional gas in which the area accessible to the sorbed molecules is independent of their number, and in which no mutual interaction

between sorbed molecules is allowed. It may be shown that the isotherm required by this model is Henry's law :

$$P = K_p \theta \tag{30}$$

The differential entropy of the two translational degrees of freedom is given by :

$$_2\bar{S}_T = R(\ln \frac{2\pi m kTA}{h^2 N} + 1) \tag{31}$$

where m is the mass of a molecule and A is the total area of surface occupied by N molecules. The model is most unreal except at very low concentrations, since, as a consequence of the supposition of point particles, the phase never becomes saturated with sorbate.

2) Two dimensional gas with co-area

The preceding model based on a two dimensional gas is over simplified and the first step to a more realistic model involves the introduction of a finite co-area for each molecule, but again neglects the possibility of mutual interaction between sorbed molecules.

The corresponding isotherm equation is :

$$p = K_{M''}\left(\frac{\theta}{1-\theta}\right) \exp\left(\frac{\theta}{1-\theta}\right) \tag{32}$$

where $K_{M''}$ is a constant for any sorbate and temperature.

The differential entropy is given by :

$$_2\bar{S}_T = R \ln \left[\frac{2\pi m KT}{h^2} b^{2/3} \frac{(1-\theta)}{\theta}\right] + R\left(\frac{\theta}{1-\theta}\right) \tag{33}$$

where m is the molecular weight of the sorbate and b is the co-volume of the molecule and is equal to the intracrystalline volume per gram of sorbent divided by the number of molecules sorbed per gram at saturation.

3) Two dimensional Van der Waals gas

A sorbed phase in which the molecules have a finite area and exhibit mutual interaction.

The isotherm equation is :

$$p = K_{M''I} \frac{\theta}{1-\theta} \exp\left(\frac{\theta}{1-\theta} - \alpha\theta\right) \tag{34}$$

$\alpha = \frac{2a'}{b'KT}$ a' and b' are two dimensional Van der Waals constants.

The entropy of this model is identical to that of the previous model.

4) One dimensional gas

A sorbed phase with one translational degree of freedom. The isotherm for this model has the same form as the model 2 :

$$p = K_{M'} \frac{\theta}{1-\theta} \exp \frac{\theta}{1-\theta} \tag{35}$$

thus any system which obeys an isotherm of this type has translational freedom but is insufficient to determine the number of degrees of freedom involved.

The entropy is given by :

$${}_1\bar{S}_T = R \ln \frac{(2\pi m KT)^{\frac{1}{2}}}{h} b^{1/3} \frac{(1-\theta)}{\theta} + R\left(\frac{1}{2} - \frac{\theta}{1-\theta}\right) \tag{36}$$

DIFFUSION

Diffusion is a process which leads to an equalization of concentrations within a single phase. The equations of diffusion connect the rate of flow of the diffusing substance with the concentration gradient responsible for this flow. Fick's first equation of diffusion may be stated in the form :

$$J = - D \frac{\partial C}{\partial x} \tag{37}$$

where D is the diffusion coefficient for the substance under consideration. Equation (1) allows the diffusion coefficient to be determined provided an arrangement in which both J and $\partial C/\partial x$ are accessible to measurement. This is possible in certain cases in which there is no change in concentration with time and a steady state prevails.

Generally for diffusion in zeolites, it is not possible to investigate diffusion under steady state conditions and it is necessary to determine the change of concentration with time caused by diffusion within a given sorbate-zeolite system. Fick's second equation in one dimension, when D does not depend upon C, is

$$\frac{\partial C}{\partial t} = D\frac{\partial^2 C}{\partial x^2} \tag{38}$$

This equation has to be solved for appropriate boundary conditions to enable the diffusion coefficients to be determined experimentally.

Two methods may be employed to measure diffusion coefficients in zeolite crystals :

a) Sorption or desorption is measured keeping the sorbate pressure constant.

The boundary conditions for any crystallite are:

$c = c_{\infty}$ just within the surface for all $t > 0$

$c = c_o$ throughout the crystal at $t = 0$

The solution of the second Fick's law assuming all crystals have the same shape and size (for example spheres of radius r_o) is (41) :

$$\frac{Q_t - Q_\alpha}{Q_{\infty} - Q_o} = 1 - \frac{6}{\pi^2} \sum_{n=1}^{\infty} \frac{1}{n^2} \exp\left(-\frac{D n^2 \pi^2 t}{r_o^2}\right) \tag{39}$$

For larger times, all but one exponential term become negligible and the equation reduces to:

$$\ln \frac{Q_{\infty} - Q_t}{Q_{\infty} - Q_o} = \ln \frac{6}{\pi^2} - \frac{D \pi^2 t}{r_o^2} \tag{40}$$

so that a plot of the left side against t gives a straight line of slope $(D \pi^2/r_o^2)$. Once D is known, it can be substituted in the full equation, which then can be tested for all t.

For small times an alternative form of solution to equation (39) reduces to

$$\frac{Q_t - Q_\alpha}{Q_{\infty} - Q_o} = 6\left(\frac{Dt}{\pi r_o^2}\right)^{\frac{1}{2}} \tag{41}$$

Linear plots of the left side against $\sqrt{t}$ then give D/r_o^2.

b) Constant volume-variable pressure sorption or desorption

At time t = o for sorption a dose of gaseous sorbate is introduced into the sorption volume and left to distribute itself between gas phase and crystals. Exact analytical solutions are available provided sorption follows Henry's law (42).

For spheres of radius r_o :

$$\frac{Q_t - Q_\alpha}{Q_\infty - Q_o} = 1 - 6K(K+1) \sum_{\alpha_n} \frac{\exp - \alpha_n^2 \tau}{9(K+1) + \alpha_n^2 r_o^2 K^2} \tag{42}$$

where $\tau = \frac{Dt}{r_o^2}$ and α_n is the nth positive root of the relation :

$$\tan \alpha r_o = \frac{3 r_o \alpha}{3 + K r_o^2 \alpha^2} \tag{43}$$

and where :

$$K = \frac{V_g}{k V_s} = \frac{(Q_\infty)_g}{Q_\infty} = \frac{(Q_o)_g - (Q_\infty - Q_o)}{Q_\infty} \tag{44}$$

In this last expression k is the Henry's law constant and K denotes equilibrium ratio of gas in the gas phase and in crystals. V_g and V_s are volumes of gas phase and crystals respectively; $(Q_\infty)_g$ and $(Q_o)_g$ are amounts of gas finally and initially in the gas phase.

Diffusion coefficients can also be measured using the time lag L procedure (43).

The plots of Q_t/Q_∞ against t approach the value one for large enough values of t. In these curves (Figure 1.8) the cross hatched area up to time t is :

$$I_t = \int_o^t \left(1 - \frac{Q_t}{Q_\infty}\right) dt = t - \int_o^t \frac{Q_t}{Q_\infty} dt$$

and we can write

$$\int_o^t \frac{Q_t}{Q_\infty} dt = t - I_t \tag{45}$$

For large t, I_t will be a constant called the time lag L and therefore

$$\int_o^t \frac{Q_t}{Q_\infty} dt = t - L.$$

Accordingly if $\int_o^t \frac{Q_t}{Q_\infty} dt$ is plotted against t, a straight line of unit slope is approached asymptotically, the intercepts on the axis of t and of $\int_o^t Q_t/Q_\infty \, dt$ being equal. This intercept is, L, the total

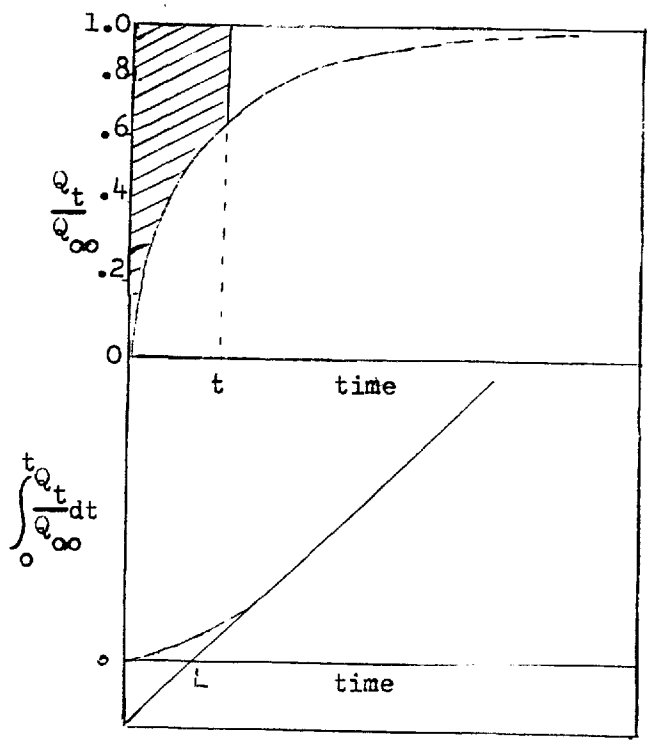

Figure 1.8

cross-hatched area in the upper part of the figure when t = ∞.

Q_t/Q_∞ as a function of time is available for ideal systems ~~(1,2),~~ for spheres equation (42) (31). By integrating $1-Q_t/Q_\infty$ between t = o and t = ∞ L is obtained for these ideal cases (43).

For example for spheres all of radius r_o:

For constant pressure sorption kinetics :

$$L = \frac{r_o^2}{15D} \tag{46}$$

Similarly for constant volume-variable pressure sorption kinetics in the Henry law range of sorption :

$$L = \frac{r_o^2}{15D} \left(\frac{\alpha}{1+\alpha}\right) \tag{47}$$

where α = amount in gas phase/amount in the crystals. Hence measuring L from the experimental sorption kinetics the value of D can be determined. If D depends on concentration of diffusant, L gives an averaged value of the diffusivity.

Energy of activation

Diffusion processes within porous crystals normally obey the Arrhenius equation $D = D_o \exp(-E/RT)$. If D is determined over a range of temperature then E and D_o are readily calculated. However E can be found without prior determination of D. If one considers the plots of Q_t/Q_∞ against time at each of two different temperatures T_1 and T_2 and measures the times t_1 and t_2 taken for Q_t/Q_∞ to reach the same value at each of the two temperatures then one must have :

$$D_1 t_1 = D_2 t_2$$

Accordingly

$$\ln t_1/t_2 = \ln D_2/D_1 = \frac{E}{R}\left(\frac{1}{T_1} - \frac{1}{T_2}\right) \qquad (48)$$

This method is applicable for any distribution of crystal size and shape.

Factors influencing intracrystalline diffusion

The relationship between molecular dimensions of the diffusant and its activation energy is illustrated below for zeolite NaA (44) :

Molecule	Dimensions (Å)	E (kcal/mol)
Ar	3.8	4.7
Kr	3.9	8.1
O_2	2.8 x 3.9	4.5
N_2	3.0 x 4.1	8.3

The larger the dimension of the molecule the larger the activation energy. For O_2 and N_2 the length of the molecule and the cross-sectional diameter are given. It is the cross-sectional diameter which is more important in governing the passage through the narrow points of the diffusion paths.

Activation energies can change considerably with the dimensions of the channels of the zeolite. For example the energies of activation in zeolite KA (45) and K-mordenite (46) are compared below :

	E (kcal/mol)	
Gas	KA	K Mordenite
Ar	12.6	8.4
Kr	16.4	10.0
H_2	9.9	2.5
N_2	16.2	4.8

The cations also play an important part in determining the rate of sorption and activation energy. For example for argon in Mordenite (46) :

Cation	E (kcal/mol)
Li	7.3
Na	9.3
K	8.4
Ba	9.8
Ca	11.5

Sorption of n-paraffins $C_3 \rightarrow C_7$ in chabazite (47), $C_5 \rightarrow C_8$ in erionite (48) and of C_4, C_6, C_9 in Sieve A (49) has been studied. It is found that sorption rates decrease with increasing chain length.

In chabazite, erionite and zeolite A access to intracrystalline channels is through 8-ring windows, somewhat distorted in the first two zeolites and nearly planar in zeolite A. The maximum and minimum free dimensions are 3.7 and 4.1 for chabazite, 3.6 and 5.2 for erionite and 4.3 for sieve A. In Ca rich forms of these three zeolites sufficient 8-ring windows are unblocked by cations to allow the passage through them of n-paraffins. On the basis of the free dimensions of these zeolites the most ready diffusion of n-paraffins might be into erionite and zeolite A. However an additional factor should be considered. In zeolite A the 8-rings lie in sets parallel to each other but in erionite and chabazite the rings are not parallel. When in zeolite A a molecule passes through a window it is in a favourable position to pass through the next one. This is not so in erionite and chabazite (50).

A study of C_1 to C4 paraffins in synthetic mordenite by Satterfield and Frabetti (51) has shown that diffusion coefficients for desorption are many times smaller than those for sorption and the coefficients are reduced substantially by grinding the crystals.

Satterfield and Frabetti's work has been supplemented by Eberly (48) who studied diffusion of nC_5 to nC_9 paraffins in erionite and 5A molecular sieve. In erionite they found desorption rates to be smaller than sorption rates. For n-heptane the diffusion coefficient was seventy times smaller for desorption. Ruthven and Loughlin (52) found that, provided the effect of the crystallite shape and size distribution is taken into account, no significant differences exist between the adsorption

and desorption curves, suggesting that the sorption process is truly reversible and that the diffusivity is the same for both adsorption and desorption.

It has been assumed that the diffusion coefficient does not depend upon intracrystalline concentration. For the dilute range of sorptions - where Henry's law is valid - this is correct. However, for extended ranges of concentration the diffusion coefficient can be strongly dependent in concentration. (53)

CHAPTER II

EXPERIMENTAL

Synthesis

Zeolite RHO was synthesized according to the method of Robson et al. (54), from aluminosilicate hydrogels containing sodium and caesium cations. The procedure was as follows:

Aluminium isopropoxide was dissolved in 50% NaOH solution at 100°C. After cooling to room temperature the required quantity of CsOH was added. The resulting solution was poured into 31% colloidal silica with vigorous mixing. The gel formed was aged for seven days at room temperature and then it was transferred to an oven at 90°C. After several days crystallization took place. Crystals were separated from the mother liquor, washed and stored.

X-ray examination and electron micrographs

X-ray powder photographs were taken using a Guinier camera with CuK_α radiation in order to identify the product of the synthesis, detect possible crystalline impurities, observe change of phase and check stability of samples. Electron micrographs were taken in order to determine crystal shape, calculate average crystal size and observe homogeneity of samples.

Analysis

Zeolite RHO was analysed for water, silica, alumina, sodium and caesium as follows:

(a) Water

Water was determined by loss on ignition (55). About one gram of zeolite was accurately weighed in a platinum crucible and heated over a burner for 20 - 30 min., then cooled and weighed. The procedure was repeated until constant weight.

(b) Silicon and Aluminium

The percentage of silicon was determined by the standard wet semimicro method (56). After a sodium carbonate fusion of the zeolite is made (57), the melt which contained the silicate in acid decomposable form was treated with hydrochloric acid. The acid solution of the

decomposed silicate was then evaporated to dryness on a water bath to separate the gelatinous silicic acid as insoluble silica; this residue was heated to 393 K to partially dehydrate the silica and render it as insoluble as possible. The residue was extracted with hot dilute hydrochloric acid to remove salts of aluminium and other metals which are present. The greater portion of the silica remained undissolved, and was filtered off. The filtrate was evaporated to dryness and the residue heated to 393 K as before in order to render the small amount of silicic acid that escaped dehydration insoluble. The residue was treated with dilute hydrochloric acid as before, and the second portion of silica was filtered off on a fresh filter. The two washed precipitates were combined and ignited in a platinum crucible at about 1320 K to give silicon dioxide, which was then weighed.

The result obtained may be high due to impurities of alumina being weighed with the ignited residue. To establish the amount of impurity the weighed residue in a platinum crucible was treated with an excess of hydrofluoric acid and a little concentrated sulphuric acid; the silica was expelled as volatile silicon tetrafluoride and the loss in weight represented the amount of pure silicon dioxide present.

Aluminium was determined by precipitation as aluminium 8-hydroxyquinolate (58) after the removal of silicon.

Sodium and Caesium

For sodium and caesium analysis an accurately weighed amount of sample was treated in a platinum crucible with a mixture of sulphuric acid and hydrofluoric acid (59). The mixture was evaporated to dryness over a steam bath and the procedure repeated. The solid residue from the second evaporation was dissolved by adding hydrochloric acid and heating on a steam bath for half an hour. The clear solution was transferred to a volumetric flask and made up to volume with distilled water.

Sodium was analyzed by flame photometry using a Unicam SP 90 dual absorption/emission instrument. It was examined at 589.0 nm on emission.

Caesium was determined as caesium tetraphenylborate (60).

Ion Exchange Experiments

Ion exchange experiments were carried out in the as synthesized product of zeolite RHO (containing Cs^+ and Na^+) with Na^+, Ca^+ and NH_4^+. The extent of Cs^+ exchanged was determined by analysing it in the solution as the tetraphenylborate.

Also ion exchange was carried out in the NH_4-RHO with Na^+ and Ca^{+2}. The extent of ion exchange was determined by analysing NH_4^+ in the solution by the Kjeldhal method (61).

The conditions of ion exchange were: 0.5N solutions, the equivalents in the solution being ten times the equivalents in the zeolite and the temperature being that of the room. In other experiments more concentrated solutions (1N, 2N) were used as well as higher temperatures (90°C).

The Sorbates

The n-paraffins were obtained from the National Physical Laboratory and were at least 99.9% pure. The gases were obtained from the British Oxygen Company and were spectroscopically pure.

Apparatus

Two separate apparatuses were used: a volumetric and a gravimetric sorption unit. The pumping system of each was identical.

The Pumping System The pumping system is shown schematically in Figure 2.1. It consisted of a mercury diffusion pump A, backed by a rotary oil pump. A 5 litre buffer volume C was inserted between the pumps so that the diffusion pump could be run for long periods without the oil pump. The mercury pump could be isolated by closing taps T_2 and T_3 and opening T_1. A 2 litre oil trap D was inserted between the pumps in case of a power failure.

The low vacuum line G was evacuated by a rotary oil pump H with its two litre oil trap bulb K and operated independently of the high vacuum system. The vacuum system was capable of providing a high vacuum of 10^{-6} Torr. The vacuum was measured by a McLeod gauge J.

The Volumetric Sorption System The volumetric sorption unit consisted of a four bulb gas burette A, a manometer B, a sorption cell C and a gas line D. A diagram showing the complete volumetric unit is shown in Figure 2.2.

Figure 2-1

The Pumping System

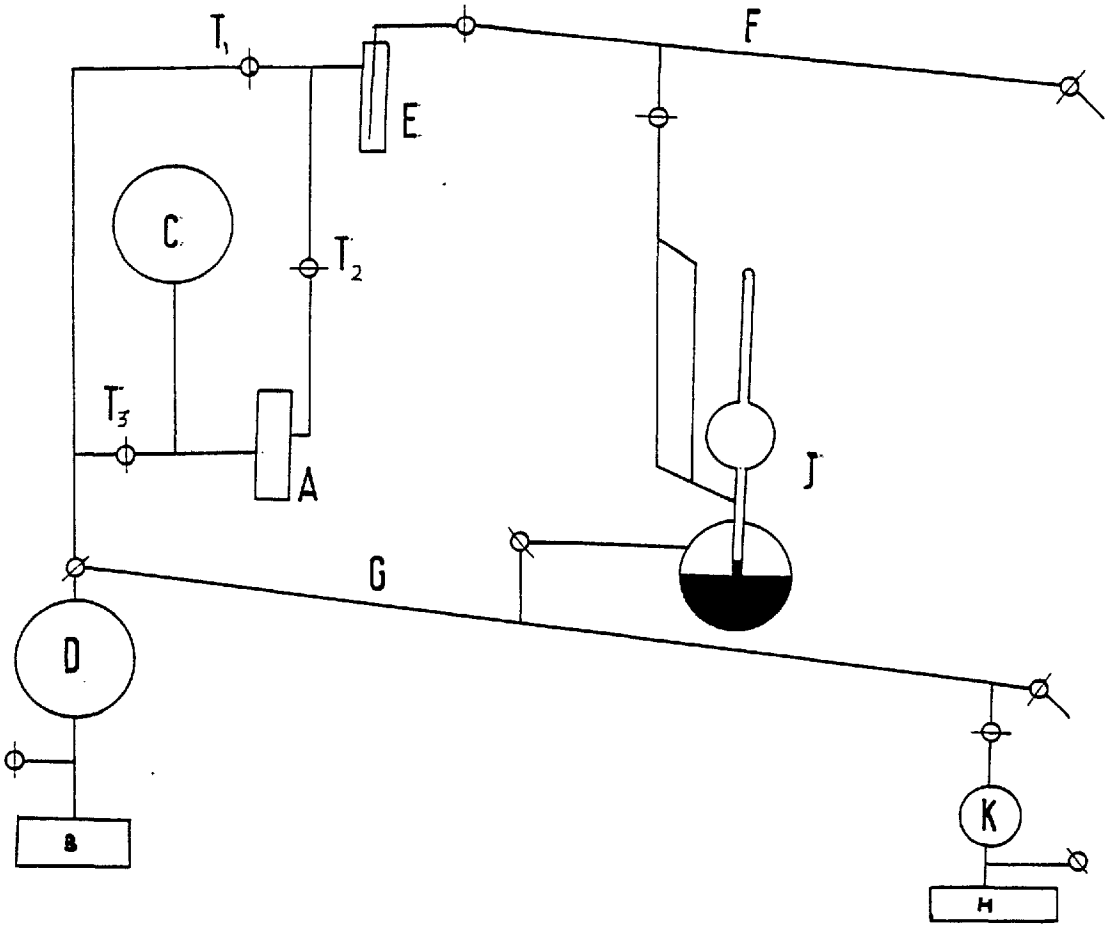

Figure 2-2

The Volumetric System

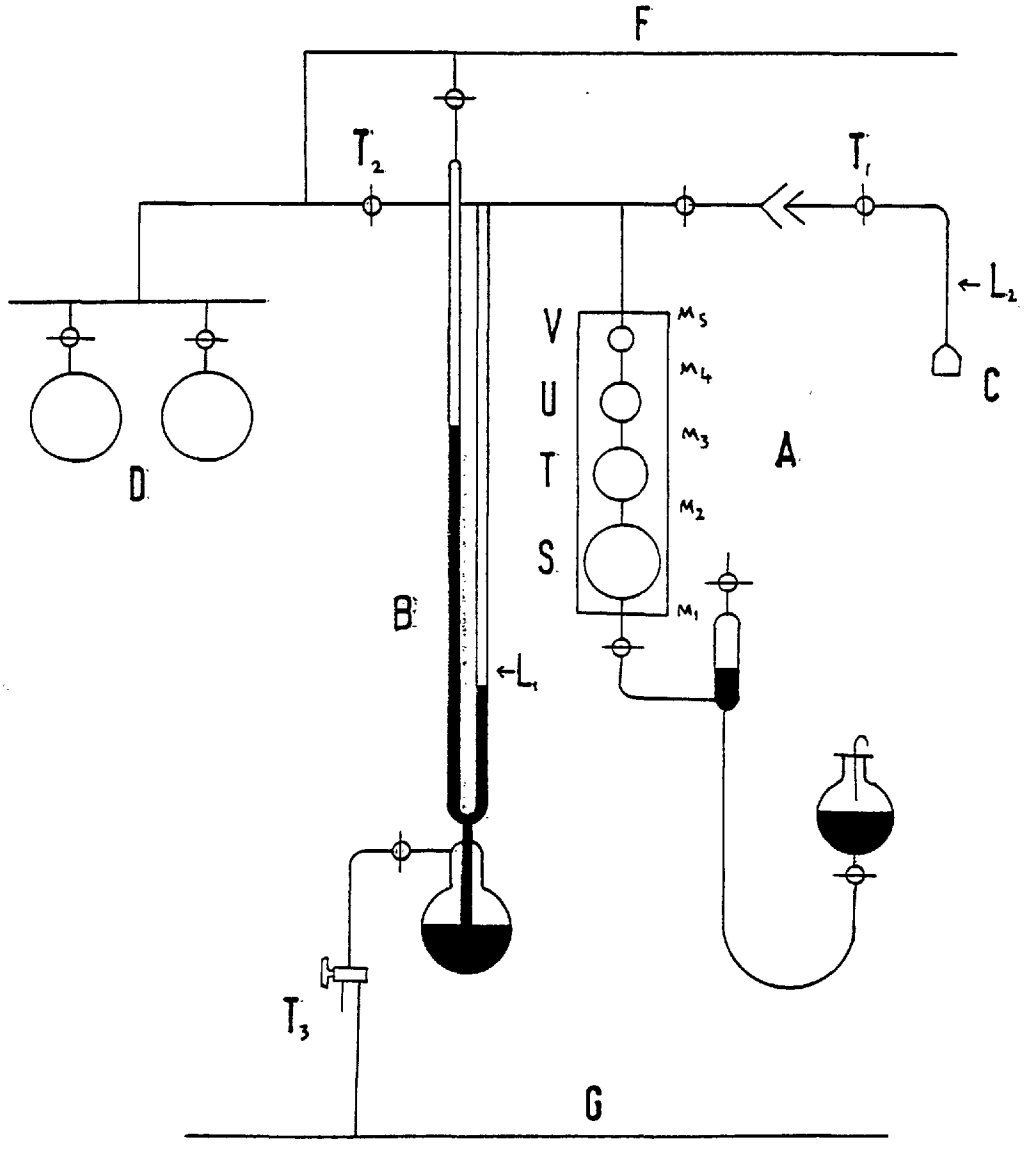

The gas burette consisted of four bulbs, V, U, T, S, interconnected by short lengths of small capillary tubing on which marks M_1, M_2, M_3, M_4, M_5 were made. The volume of each bulb is determined by mercury weighing. An air jacket containing a thermometer surrounded the gas burette.

The sample under examination was put into the sorption cell C, a small plug of glass wool placed in the neck and the cell was then glass blown onto a stopcock and B7 cone/socket assembly for attachment to the volumetric line.

Through tap T_2 the volumetric system is connected to the high vacuum line. With tap T_3 the level of mercury in the manometer was controlled. L_1 and L_2 are reference marks made on the manometer and sorption cell respectively.

The Gravimetric Sorption Unit The gravimetric sorption apparatus consisted of four McBain-Bakr silica spring balances, a manometer B, a spiral gauge C and storage bulbs D_1 and D_2. These are shown in Figures 2.3, 2.4 and 2.5.

The apparatus was used at temperatures up to 413 K so that the balance cases and system contained no ground glass taps or cone/socket joints. Each balance case was made of 35 mm pyrex tubing and was tapered at the base to minimize the amount of space required in the thermostat bath. The balance case was connected to the gravimetric line through a greaseless tap E.

All tubing and taps connecting the balance cases, the spiral gauge and storage bulb were wrapped in Electrothermal 'heat by the yard' asbestos which was carried below the level of the thermostat bath by glass inseals D. The resistance wire was kept at 413 K and prevented condensation of vapours when vapour pressures greater than the saturated vapour pressure at room temperature were desired.

The sample under examination was suspended in the balance case as follows: F was a dolly filled with lead shot, with lengths of welding rod sealed into the handle. This allowed the dolly to be moved from outside the case by means of a magnet, thus allowing the bucket to be placed in the centre of the balance case.

Figure 2-3 The Gravimetric System

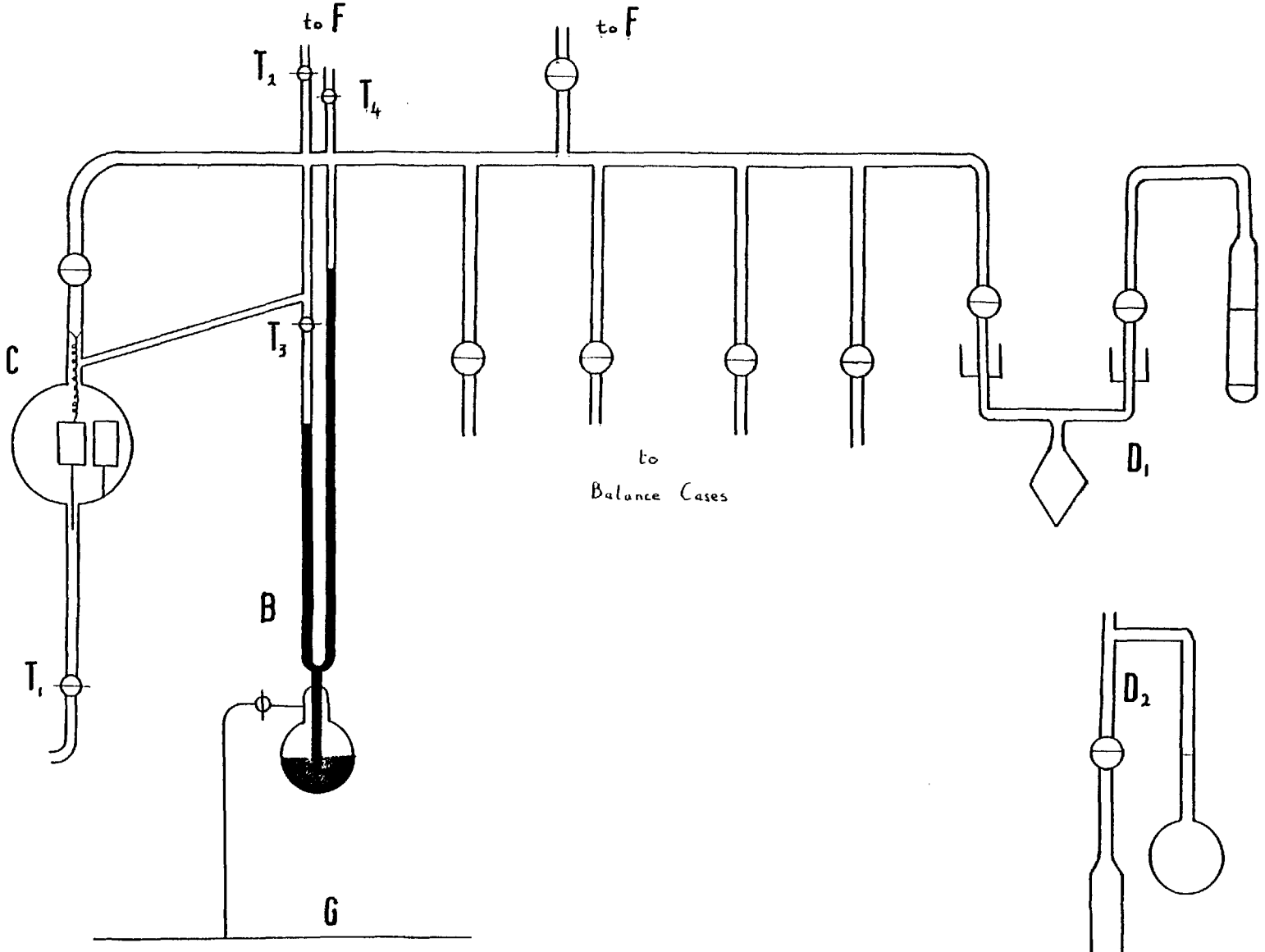

Figure 2-5

The Spiral Gauge

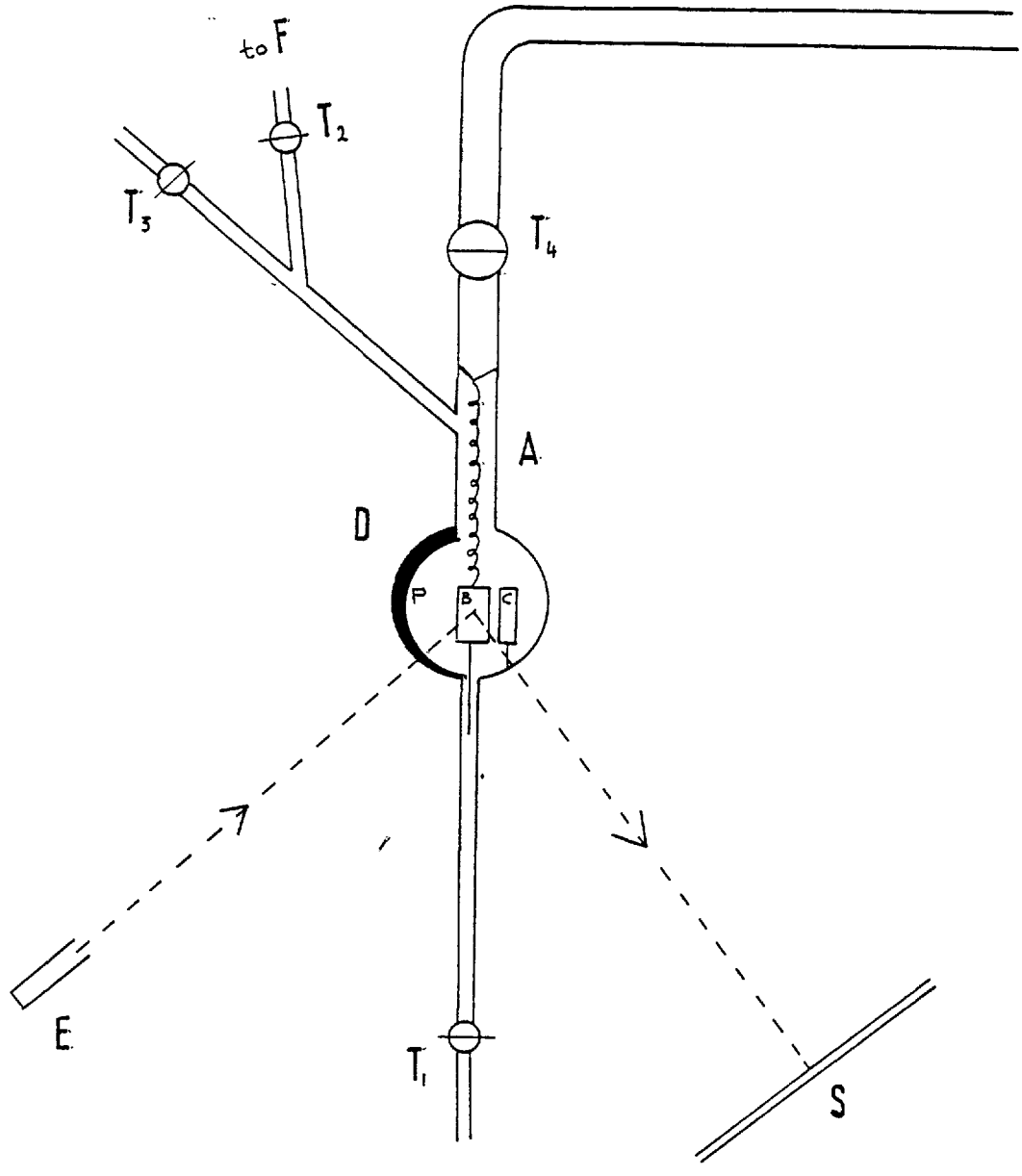

Figure 2-4 Gravimetric Balance Case

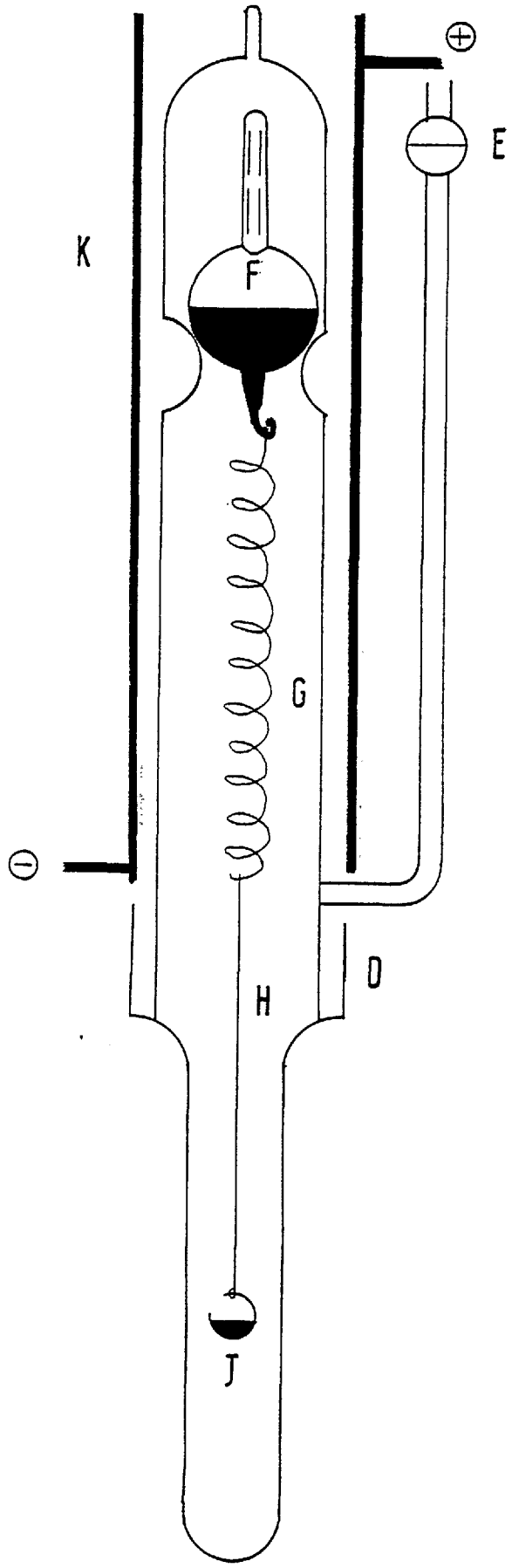

To the dolly was attached a sensitive silica spring G. H, a fine thread of silica glass, was attached to the bottom of the spring to extend the sample bucket J to a convenient depth in the well of the balance case.

The balance case was sealed by glass blowing a cap onto the top of the case. A furnace was arranged around the case and maintained at 413 K at all times.

One arm of the manometer was attached to the high vacuum line and the other to the spiral gauge. The spiral gauge consisted of a sensitive hollow glass spiral sealed into the gravimetric line (Figure 2.5). The spiral held a platinum coated mirror, B. Mirror C was also platinum coated but was fixed to the outer case as a reference mark. The spiral assembly is sealed into an outer case D containing a stopcock T_1. A projection lamp E was positioned so as to be incident upon the two mirrors. The reflected image is focussed onto a graduated scale S via an optical flat F sealed into the outer case.

Bulbs containing the lower n-paraffins were glass blown onto the storage vessel and the complete system is shown in Figure 2.3, D_2. The sorbate was released from the bulb by breaking the seal by dropping a piece of iron covered in glass onto it using a magnet.

The storage bulb, D_1, for n-hexane is shown in Figure 2.3. It consisted of a pear-shaped container between greaseless taps. In-seals were incorporated in the design so that the bulb could be immersed in the thermostat.

Thermostats, Cryostat, Temperature Control and Measurement

Thermostat The thermostat was used in the range 298 K to 413 K. A diagram of it is shown in Figure 2.6. It consists of a 3 litre tall beaker, A, wrapped in asbestos paper. Electrothermal heating tape is wound evenly round the beaker and covered with two more layers of asbestos paper, B. The beaker is placed inside a 5 litre beaker C, and the free space packed with asbestos wool, D.

MS 550 silicone oil, E, was used as bath liquid and the oil was stirred by a stirrer S. The main heating of the bath was supplied by a Variac connected to the electrothermal tape of the bath and temperature

Figure 2-6

The Thermostat

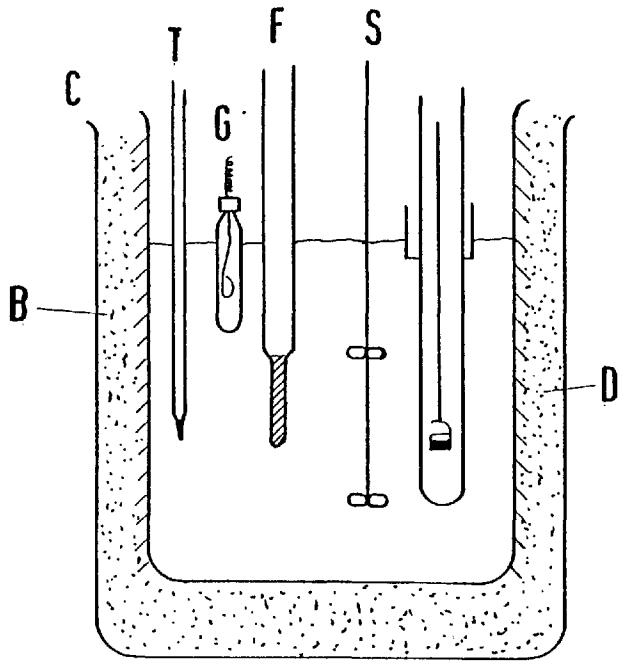

Figure 2-7

The Cryostat

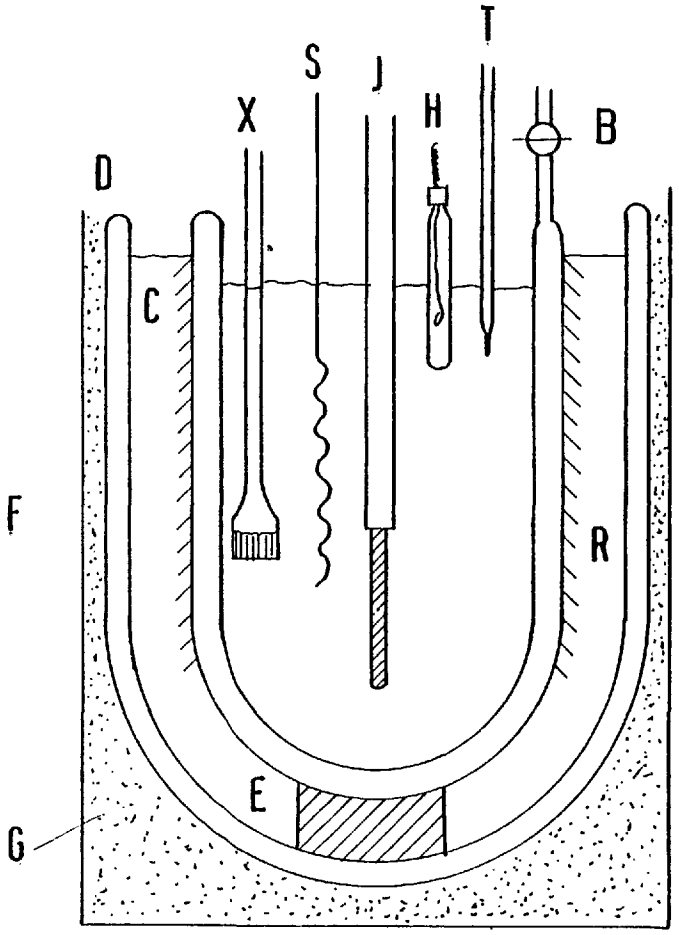

control was obtained by operating a TS7 bimetallic spiral F, and a 25 W heating bulb, G, in conjunction with a sunvic relay. All temperatures were measured with certificated thermometers, T, and temperature control and measurement was better than 0.1°.

Cryostat The cryostat was used from room temperature to 173 K. A diagram of it is shown in Figure 2.7. It consisted of a dewar vessel A tightly wound with copper foil which could be evacuated through B. This dewar was placed inside a larger dewar D contained in a box, G, which is filled with asbestos wool. The small dewar is supported in the larger one by a cork ring, E. In the small dewar A, the thermometer T, a glass stirrer S, heating lamp H and bimetallic spiral J were placed.

Petroleum ether (boiling range 373 - 393 K) was used as bath liquid. In R ice was used as refrigerant in the range 298 - 273 K, cardice in the range 273 - 213 K and liquid nitrogen in the range 173 - 213 K. Removal of heat from the bath was compensated by a 25 W lamp, H, operating in conjunction with a TS7 bimetallic spiral and a relay. The cryostat gave temperature control better than ± 0.1°.

Temperatures were measured with an alcohol thermometer which was calibrated against vapour pressure thermometers. The types of thermometers used and the range of temperature over which each was effective are listed below:

Thermometer	Temperature range (°C)
SO_2	- 10 to - 40
NH_3	- 40 to - 75
CO_2	- 75 to -100

Carbon dioxide was obtained spectroscopically pure in a glass cylinder from B.O.C. Ammonia was obtained in a metal cylinder from B.O.C., 99.98% pure. It was distilled two times. Sulphur dioxide was obtained from a B.D.H. canister 99.98%. It was dried over phosphorous pentoxide and twice distilled.

A vapour pressure thermometer is shown in Figure 2.8. Bulb C contains the purified vapour, bulb V is made to enlarge the volume of the thermometer. The manometer M is filled with mercury. Arm M_1 is evacuated and sealed. Then the rest of the thermometer is evacuated through tap T. Tap T is shut again and the vapour allowed inside the thermometer. B is cooled so the pressure inside the thermometer falls

Figure 2-8

Vapour Pressure Thermometer

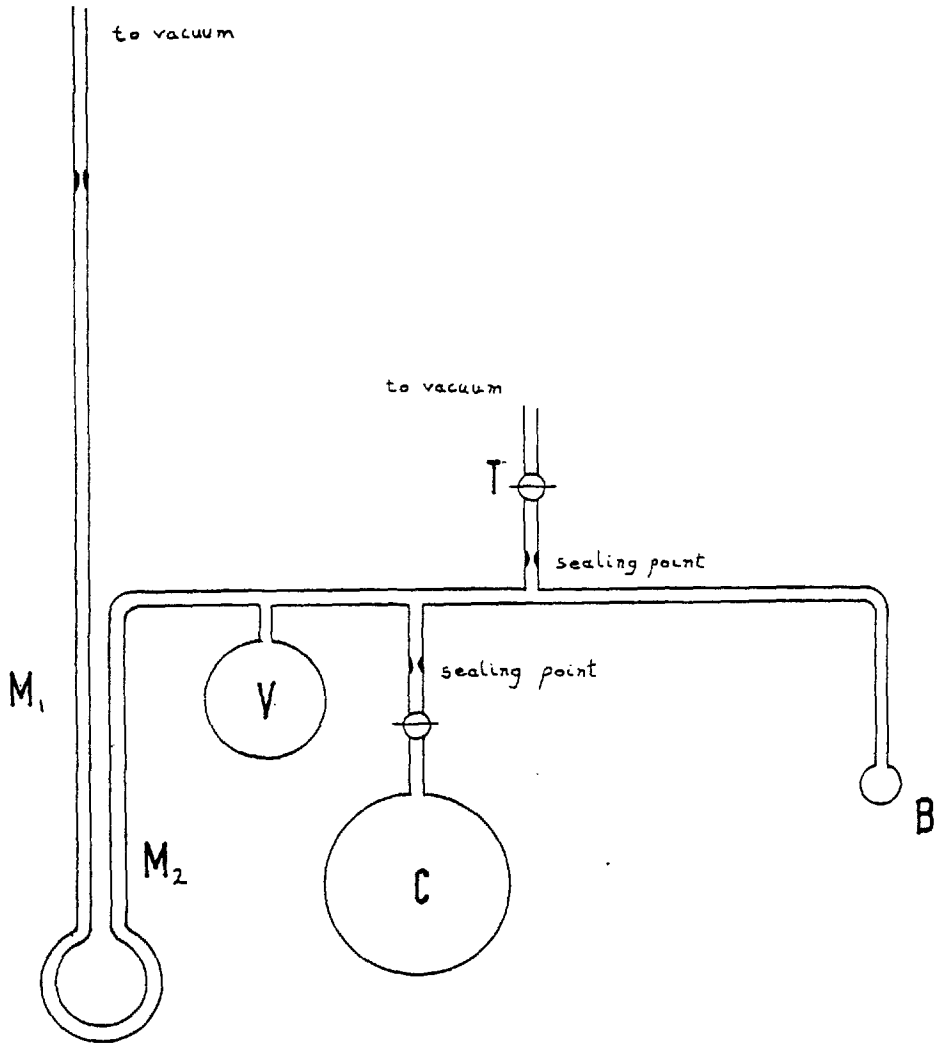

falls below atmospheric and then the thermometer is sealed at the sealing points. The thermometer is then ready for use.

Procedure

Volumetric System

(1) Calibration of doser volume. The doser volume V_d comprises the volume enclosed between mark L_1, tap T_2 and the gas burette with mercury at mark M_5 (Figure 2.2). The value of this volume is determined by letting a quantity of helium from the gas line D into the doser volume. With the mercury at mark L_1 the pressure is read. Then the gas is subsequently expanded lowering the level of mercury in the gas burette to M_2, M_3, M_4 and M_5 and the pressure subsequently read as before. Application of the ideal gas law gives four values of the doser volume. An average is taken.

(2) Calibration of cell volumes. The volume of the cell up to mark L_2, V_c, and from mark L_2 to tap T_1, V_x, are determined by mercury weighing.

(3) Preparation of sample and outgassing. About 0.5 g of zeolite was placed in a weighed sorption cell and its weight accurately determined. A small plug of glass wool was placed in the neck of the cell to prevent sample loss when outgassing. The sorbent was opened carefully to the high vacuum and after one hour was surrounded with a furnace and heated over a period of 6 - 8 hours up to 673 K and left for about 16 hours at this temperature.

(4) Measurement of isotherms. Sorption isotherms of O_2, N_2, CO_2, Ar, Kr, Xe, CH_4 and C_2H_6 were measured in the volumetric unit. After outgassing, the cryostat (or thermostat) was brought up to the temperature T_c at which the isotherm was to be determined, with the level of the bath at L_2 in the sorption cell. It was allowed to run for an hour before admitting the sorbate in the sorption cell. Then a dose of sorbate from the gas line D is admitted to the dead volume and the pressure read (of course with the level of mercury at mark L_1). Application of ideal gas law gives the number of moles in the dead volume n_o. Then the sorbate is allowed into the sorption cell opening tap T_1 carefully. The zeolite begins to adsorb the gas and pressure falls. After some time equilibrium is achieved and pressure is constant at p, which is read in the manometer.

The number of moles in the gas phase is :

$$n = \frac{p(V_d + V_x)}{RT} + \frac{pV_c}{RT_c}$$

where T is the temperature of the room.

The number of molecules sorbed is then $(n_o - n)$ and one point of the isotherm is obtained. Then more doses of sorbate are admitted and the procedure repeated.

The Gravimetric System

Sorption isotherms of propane and n-butane and sorption kinetics of n-butane and n-hexane were measured in this apparatus. The extension of the springs versus known weights was measured at 298 K and 413 K, and the sensitivities determined. The initial lengths were recorded.

About 300 mgs of zeolite was placed in the bucket and the balance case sealed by blowing a cap on the top. The balance case was opened to the vacuum carefully to avoid loss of sorbent. The sorbent was then surrounded by a furnace and outgassed at 673 K as already indicated. After outgassing the balance case was isolated from the gravimetric line and cooled. The spring length was measured and the outgassed weight of sorbent determined.

After cooling, the thermostat is set up at the sorption temperature and is allowed to run for one hour before any dose is admitted to the balance case.

Measurement of Isotherms

The inner spiral and outer case of the spiral gauge and manometer should be evacuated. Then the gravimetric line is isolated from the pumping system, tap T_2 shut and T_3 opened. The position of the light image on the scale is marked indicating equal pressures in the inner spiral and outer case of the spiral gauge. Then a dose of sorbate vapour is admitted into the gravimetric line. The light image is displaced because the pressure in the inner spiral is larger than in the outer case.

Carefully the vapour is allowed into the balance case, the spring begins to extend and the light image is displaced. When equilibrium is attained the length of the spring and the position of the image remain constant. Opening tap T_1 carefully air is allowed into the outer case

of the spiral gauge and the manometer until the light image returns to its original position mark. The pressure in the gravimetric line is then the same as the one read in the manometer.

The quantity of gas sorbed is determined by the change of length of the spring. In this way one point of the isotherm is determined. Further doses are then added and the procedure repeated.

Sorption Kinetics

Kinetic runs were made as far as possible at constant pressure by keeping the bulb of the storage system at constant temperature with a cryostat. Before admitting the gas to the gravimetric line a quantity of air was admitted into the outer case of the spiral and manometer and the position of the light image on the scale marked. The pressure on the manometer was read.

Then the sorbate vapour is admitted to the gravimetric line and the image is displaced. The position of the image is returned by letting more air into the outer case and manometer and the pressure read again. The difference in pressure is the pressure of the vapour in the gravimetric line.

The vapour is then allowed carefully into the balance case, a chronometer started and the length of the spring measured with time. When the gas is allowed in the balance case the light image is displaced due to the change of pressure when the gas expands, but then the pressure is re-established and the light image returns to its original position. Constancy of pressure can be checked at any time by observing the position of the image.

CHAPTER III

RESULTS AND DISCUSSION A

Synthesis

Three syntheses were performed :

Synthesis 1 In this preparation the composition of the gel was :

3.00 Na_2O, 0.40 Cs_2O Al_2O_3, 10.01 SiO_2, 103 H_2O, with

$$\frac{Cs}{Na + Cs} = 0.12$$

Crystals were separated after three days at 90°C.

Synthesis 2 In this preparation the composition of the gel was the same as for synthesis 1, but the quantities used were four times larger. Crystals were separated after five days at 90°C.

Synthesis 3 This time the molar fraction of caesium in the gel was 0.16. The quantity of gel was the same as in synthesis 1. Crystals took more time to appear and they were separated after seven days at 90°C.

X-ray

X-ray photographs for the three synthesis preparations were taken. The values of d indexed in a cubic body centered system (up to N = 54) are:

	Zeolite RHO (Na,Cs) form lattice constant 15.0 Å	
$N = h^2 + k^2 + \ell^2$	d	Intensity
2	10.60	vs
4	7.50	vvw
6	6.10	w
8	5.35	w
10	4.75	vs
12	4.35	w
14	4.05	w
16	3.75	w
18	3.55	vs
20	3.35	s
22	3.08	w
26	2.95	s
30	2.75	s

N	d	Intensity
32	2.65	vvw
34	2.55	s
36	-	-
38	2.45	vw
40	-	-
42	2.26	vw
46	2.22	vw
48	2.16	vw
50	2.12	w
52	2.08	vvw
54	2.05	vw

vs : very strong
s : strong
w : weak
vw : very weak
vvw : very very weak

The following impurity lines are present :

14.1 (w), 12.3 (vvw), 8.5 (vvw), 6.9 (vw), 5.6 (vvw), 3.68 (vw) 3.28 (vw), 3.18 (vvw), 3.00 (vvw).

The impurities have been identified as zeolite A and zeolite X (62). These lines are stronger in the synthesis 2 material and weaker in the synthesis 3. When zeolite RHO (in its Na,Cs form) is dehydrated another phase with 14.6 Å lattice constant is produced. The change of one phase into the other is reversible when sorption or desorption of water takes place. Hydrogen forms only presented the 15.0 Å phase.

Electron Micrographs

Electron micrographs have been taken for the three synthesis preparations. The shape of the crystals seems to be cubic. The average value for the sides of these cubes is :

Synthesis 1	3.13×10^{-5} cm
Synthesis 2	4.02×10^{-5} cm
Synthesis 3	5.60×10^{-5} cm

The crystals of the synthesis 3 preparation are the largest ones which agrees with the longest time crystals took to appear.

Chemical Analysis

The crystals of the synthesis 1 preparation were analyzed. The results of the analysis give the formula :

$$0.63\ Na,\ 0.41\ Cs,\ 1.00\ AlO_2,\ 2.86\ SiO_2 .$$

The water content is 0.226 g per outgassed gram of the zeolite.

Unit Cell

The structure proposed by Robson et al. (54) was shown in Figure 1.4. Vertices correspond to Si, Al atoms. Oxygen atoms were not shown but are near the midpoints of the line segments. The unit cell contains two truncated cubo-octahedrons and six octagonal prisms. There are 96 oxygen atoms per unit cell and therefore 48 silicon plus aluminium atoms. Since Si/Al = 2.86 (see analysis) there are 35.6 silicons and 12.5 aluminiums per unit cell.

Ion Exchange Experiments

(a) In trying to remove the Cs^+ from the zeolite, exchange with Na^+ and Ca^{+2} was tried; the results of the first batch were :

Ion	days	% Cs exchanged $= \left(\frac{Cs^+ \text{ exchanged} \times 100}{Cs^+ \text{ initially in zeolite}} \right)$
Na^+	2	8
Ca^{+2}	2	10

The conditions employed were : 0.5 N solutions, room temperature and the number of equivalents in the solution ten times the number of equivalents in the zeolite. The results of the second batch were :

Ion	days	% Cs exchanged
Na^+	10	14
Ca^{+2}	11	15

As a result of these experiments we see that after 12 days of exchange with Na^+ the cationic composition of the zeolite has changed from ($0.63\ Na^+\ 0.41\ Cs^+$) to ($0.69\ Na^+\ 0.35\ Cs^+$) which is a small change. With Ca^{+2} the results are qualitatively the same.

(b) Success in exchanging the Cs^+ was achieved with NH_4^+ :

Batch	days	% Cs^+ exchanged
1	3	76
2	7	100

The conditions were the same as those used in (a).

(c) Then exchange of NH_4^+ by Na^+ was tried :

Batch	days	% NH_4^+ exchanged
1	2	49
2	4	64
3	3	68

The conditions were those used in (a).

In the first two batches we exchanged a good quantity of NH_4^+ arriving at the composition (0.64 Na^+ 0.36 NH_4^+), but in the third batch exchange becomes difficult and we only get to (0.68 Na^+ 0.32 NH_4^+). It can be noticed that after the second batch the composition of the zeolite is comparable to the one of the starting material but with NH_4^+ instead of Cs^+.

(d) Success in exchanging all the NH_4^+ was achieved with Ca^{+2} using higher temperatures :

Batch	days	% NH_4^+ exchanged
1	3	56
2	6	84
3	2	95
4	3	100

The same conditions were used as in (a) except for a temperature of 90°C.

(e) Subsequently it was found that pure calcium forms could be prepared as well from the (Na,Cs) form at 90°C using more concentrated solutions and about seven batches for seven days. In the same way pure Na^+ and K^+ forms could be prepared.

Sorption experiments in samples outgassed at 360°C

All the samples used were prepared from the synthesis 1 material. Zeolite A contains the α cages present in zeolite RHO but joined to each other through single octagonal windows. It contains as well small sodalite cages which normally are not involved in sorption. Zeolite CaA sorbs n-paraffins and we expected that if these molecules could pass through single octagonal windows and enter the α cages of zeolite A, they would also pass through double octagonal windows and enter in the α cages of zeolite Ca RHO.

(1) With this idea in mind sorption of n-butane was examined in a calcium form of zeolite RHO. The following equilibrium points were obtained in a gravimetric system :

$T = 25^{o}C$ $p = 61$ torr w: 0.030 g per outgassed gram
$T = 97^{o}C$ $p = 65$ torr w: 0.017 g " " "

The quantities sorbed are very small. If we consider that the pore volume of the calcium form is 0.33 cc gr^{-1} (as determined from the water content), we have :

$$\frac{V_{n\text{-but.}}}{V_{H_2O}} = \frac{0.030}{0.33 \times 0.528} = 0.16$$

where 0.568 is the density of n-butane liquid at $25^{o}C$. Therefore the sorption of n-butane is only about 16% of the value expected, since according to the structure proposed all the sorption volume should be accessible to n-butane.

(2) The next experiment was sorption of smaller molecules like O_2 and N_2 in a volumetric system :

O_2 77 K $p/p_o = 0.5$ 50 cc STP g^{-1} $VO_2/V_p = 0.19$
N_2 77 K $p/p_o = 0.5$ 38 cc STP g^{-1} $VN_2/V_p = 0.18$

We see that for smaller molecules the sorption is still only a small fraction of the value expected. It was thought that this small sorption could be taking place only at the external surfaces of the crystals but this adsorption was estimated from the electron micrographs and it was found too small to account for the sorption we have observed. According to the structure proposed there was no reason to have only a small fraction of the volume accessible for sorption and it was believed that the sorption found was taking place mainly in impurity crystals, the structure of RHO being blocked.

(3) Sorption of polar molecules was then examined.

CO_2 195 K $p/p_o = 0.5$ 32 cc STP g^{-1}
H_2O $34^{o}C$ $p/p_o = 0.5$ 320 cc STP g^{-1}
NH_3 $101^{o}C$ $p = 200$ torr 158 cc STP g^{-1}

We can see that the dipolar molecules are sorbed in zeolite RHO, but not the CO_2 which has a large quadrupole moment.

Since a cation in an aluminosilicate framework would prefer a site which allows it to be as close to as many oxygen atoms as possible, one would think that the octagonal prisms are a favourable location for them. In this way the blockage of the structure would be produced. Dipolar molecules are sorbed presumably because they can move the cations from the octagonal prisms and enter into the zeolite.

(4) According to this O_2 should be sorbed in a hydrogen form of the zeolite :

The uptake was, at 77 K and $p/p_o = 0.5$, 51 cc STP g^{-1}. However this is the same as the result obtained with the calcium form.

(5) Finally sorption of O_2 was compared in calcium forms of the three synthesis preparations, with the following results :

77 K	$p/p_o = 0.5$	synthesis 1	50 cc STP g^{-1}
		synthesis 2	66 cc STP g^{-1}
		synthesis 3	28 cc STP g^{-1}

According to these results synthesis 2 contains more impurity and synthesis 3 is the purest. This agrees with what is seen in the X-ray photographs. Synthesis 3 has also larger crystals and therefore a smaller contribution of the sorption at external surfaces of the crystals would be expected.

After this group of experiments were completed, it was believed that :

(1) Zeolite RHO was blocked by cations, except for the dipolar molecules NH_3 and H_2O which presumably can move them from the octagonal prisms and penetrate into the crystals.

(2) For the other sorbates the small sorption found takes place in impurity crystals and at the external surfaces of the crystals.

(3) Why H-RHO was still blocked was not understood.

It was then reported by Flank (63) that :

(i) Cationic forms of zeolite RHO sorbed small quantities of O_2. The same happened with hydrogen forms outgassed at 360°C.

(ii) Hydrogen forms when outgassed at 400°C were good sorbents. At 90 K 224 cc STP g^{-1} of O_2 were sorbed.

According to him only after outgassing at 400°C enough NH_4^+ has been removed from the zeolite to make it a good sorbent. That is not surprising because if the octagonal prisms are very good places to allocate cations higher temperatures than the usually necessary could be required to remove the NH_4^+ from them.

Experiments were then made with a view to repeating Flank's results in H-RHO outgassed at 400°C.

Oxygen Sorption Experiments in Hydrogen Forms

Unless otherwise stated all the sorptions given below are values at 77 K and $p/p_o = 0.5$.

(1) The first sample used was an NH_4 RHO prepared from the synthesis 1 material. The ion exchange conditions were :

0.5 N exchange solutions
2 batches in ten days
eqs solution ~ 10 eqs zeolite
room temperature.

Outgassing at 400°C yielded a sorbent which took up 46 cc STP g^{-1} of O_2. If we remember that this sample outgassed at 360°C sorbed 51 cc STP g^{-1}, we see that no increase in sorption has been obtained. It was possible that the ion exchange treatment had not been enough and there were still enough Na^+ and Cs^+ cations to block the structure.

(2) Using the synthesis 2 material two NH_4 RHO samples were prepared :

(a) For preparing this sample the conditions were :

5 N solutions
8 days, 7 batches, 90°C
eqs solution ~ 10 eqs zeolite.

After outgassing at 400°C the sorption of O_2 was 81 cc STP g^{-1}. Here the increase in sorption is probably due to the presence of more impurity in this preparation, and the structure of RHO is still blocked. It is now more difficult to believe that there are still enough Na^+ and Cs^+ left to block the structure.

(b) With this sample the conditions were :

5 N solutions
30 days, 10 batches, 90°C
eqs solution ~ 20 eqs zeolite.

Sorption of O_2 was found to be, after outgassing at 360°C, 70 cc STP g^{-1}; and after outgassing at 400°C 193 cc STP g^{-1}. This sample is a much better sorbent than the one used in (a). It looks as if much longer treatments than are necessary for complete ion exchange with NH_4^+ are required. This is not well understood. Flank (63) had reported that some dealumination occurs during this ion exchange treatment. When all the Cs^+ and Na^+ has been exchanged, there could be oxy-aluminium cations present in the zeolite and further treatment would be necessary to exchange them and leave the pore volume of the zeolite free for sorption.

(3) Using synthesis 3 two ammonium forms were prepared :

(a) This one was prepared using 0.2 N NH_4Cl solutions at 90°C and the long treatments used in 2(b). After outgassing at 400°C sorption of O_2 was 231 cc STP g^{-1}.

(b) This NH_4 RHO was prepared in the same way as the one in (a) but using more concentrated NH_4Cl solutions. Several H-RHO samples were used for sorption.

Sample A : activated at 400°C. Sorption of O_2 was 275 cc STP g^{-1}.

Sample B :

Flank reported that zeolite RHO was unstable to water vapour. This was found in our samples as well. To stabilize his NH_4 RHO he placed it in a furnace at 250°C purged with an 80% steam in air mixture, and raised the temperature to 650°C for one hour.

We attempted to stabilize it by outgassing in a deep bed. After outgassing sorption of N_2 at 77 K and with p = 240 torr, was 255 cc STP g^{-1}. After desorbing the N_2 air was allowed in the bed and it was heated at 500°C for one day. The sample was then outgassed and sorption of N_2 repeated. At 77 K p = 224 torr the uptake was 254 cc STP g^{-1} which shows that the stabilizing procedure has been successful. Sorption of O_2 in this sample is 285 cc STP g^{-1} at p/p_o = 0·5 and T = 77 K.

Sample C :

Another sample of the NH_4 RHO was stabilized by placing it in a deep bed and following the procedure used by Flank, but using air instead of the controlled atmosphere he used. Sorption of O_2 in this sample gives

304 cc STP g^{-1} at 77 K and $p/p_o = 0.5$. This is the highest sorption found so far with any of our H-RHO sorbents. It seems that only after the heating treatment at 650°C has all the NH_4^+ been removed from the zeolite.

Another sample of the NH_4 RHO was stabilized following the same procedure used for sample C. Sorption of O_2 in this sample D is 295 cc STP g^{-1}.

The results of this section are summarized in the table below.

Synthesis	NH_4 RHO	H-RHO	Sorption O_2 (cc STP g^{-1}) 77 K, $p/p_o = 0.5$
1	NH_4 RHO	H-RHO	46
2	NH_4 RHO (a)	H-RHO (a)	81
	NH_4 RHO (b)	H-RHO (b)	193
3	NH_4 RHO (a)	H-RHO (a)	231
	NH_4 RHO (b)	Sample A	275
		Sample B	285
		Sample C	304
		Sample D	295

CHAPTER IV

RESULTS AND DISCUSSION B

Sorption Capacity

The saturation capacities were determined from the isotherms shown in Figures 4.1, 4.2, 4.3 and are indicated in the table below.

Sorbate	Sample	T (^{o}K)	cc STP g^{-1}	Molec volume (cc/mol)	V_p (cc g^{-1})
N_2	A	77	242	34.57	0.37
O_2	A	90	254	28.00	0.32
CO_2	A	195	180	36.67	0.30
Ar	B	90	272	28.73	0.35
Kr	B	90	252	27.9	0.31
Xe	B	195	140	46.8	0.29
CH_4	C	90	218	35.6	0.35
C_2H_6	C	195	133	56.02	0.33
C_3H_8	C	195	90	70.63	0.28
nC_4H_{10}	B	303	52	101.2	0.24

These values should be evaluated at $p/p_o \rightarrow 1$, but in most cases isotherms were not completed up to $p/p_o = 1$, and in those cases where p/p_o was approached capillary condensation between crystals occurred making it necessary to avoid evaluation at $p/p_o \rightarrow 1$. Nevertheless due to the rectangularity of the isotherms the saturation values given can be considered a good approximation.

In principle the values of V_p should be the same for the different sorbates studied since in zeolite RHO there are no subsidiary cages as in zeolite A and X, and the entire sorption volume is accessible to all sorbates.

The differences observed are due to several reasons :

(1) The three samples used have different sorption capacities :

Figure 4-1

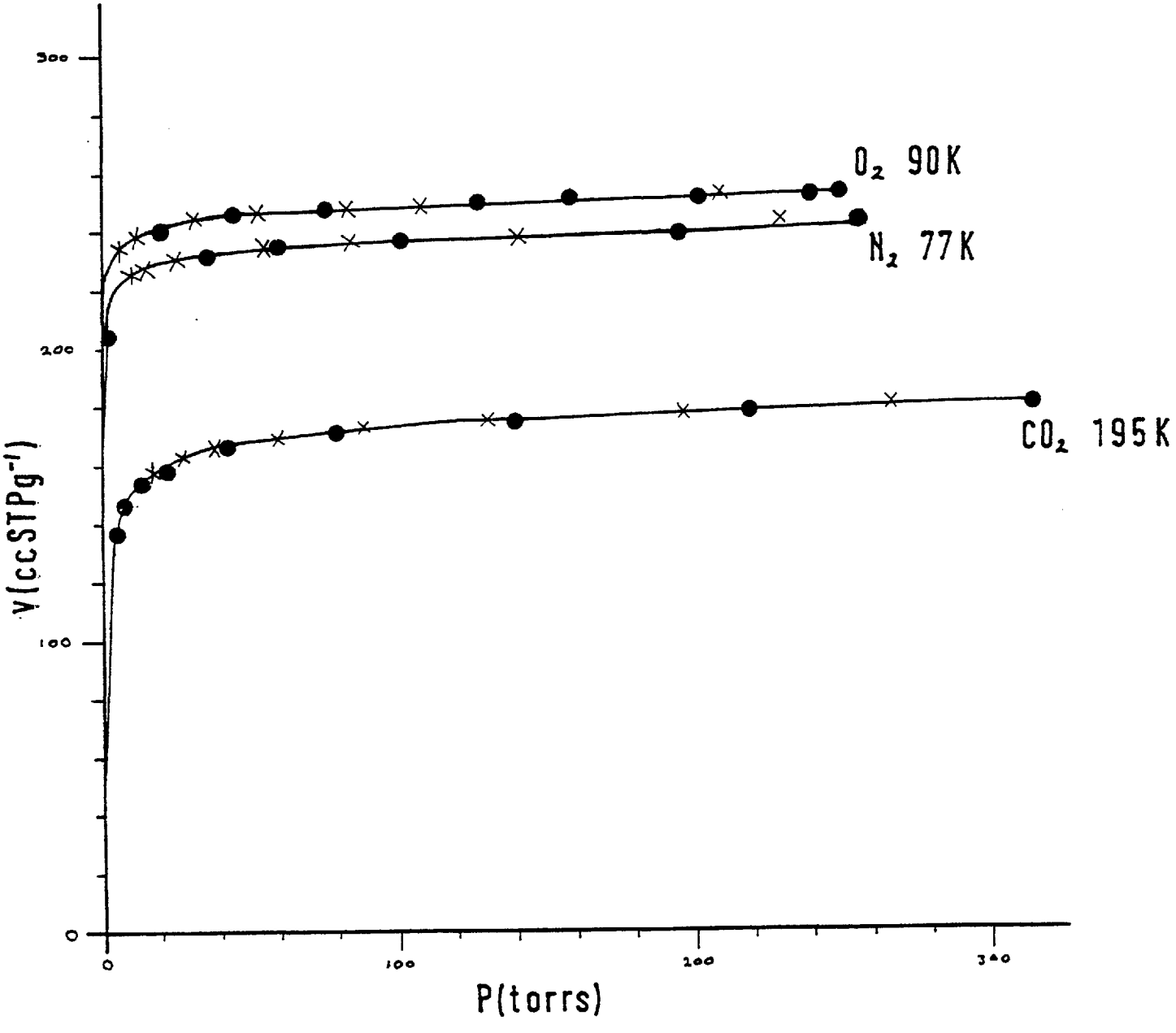
300
200
100
0
0
100
200
340
V(ccSTPg⁻¹)
P(torrs)
O₂ 90K
N₂ 77K
CO₂ 195K

Figure 4-2

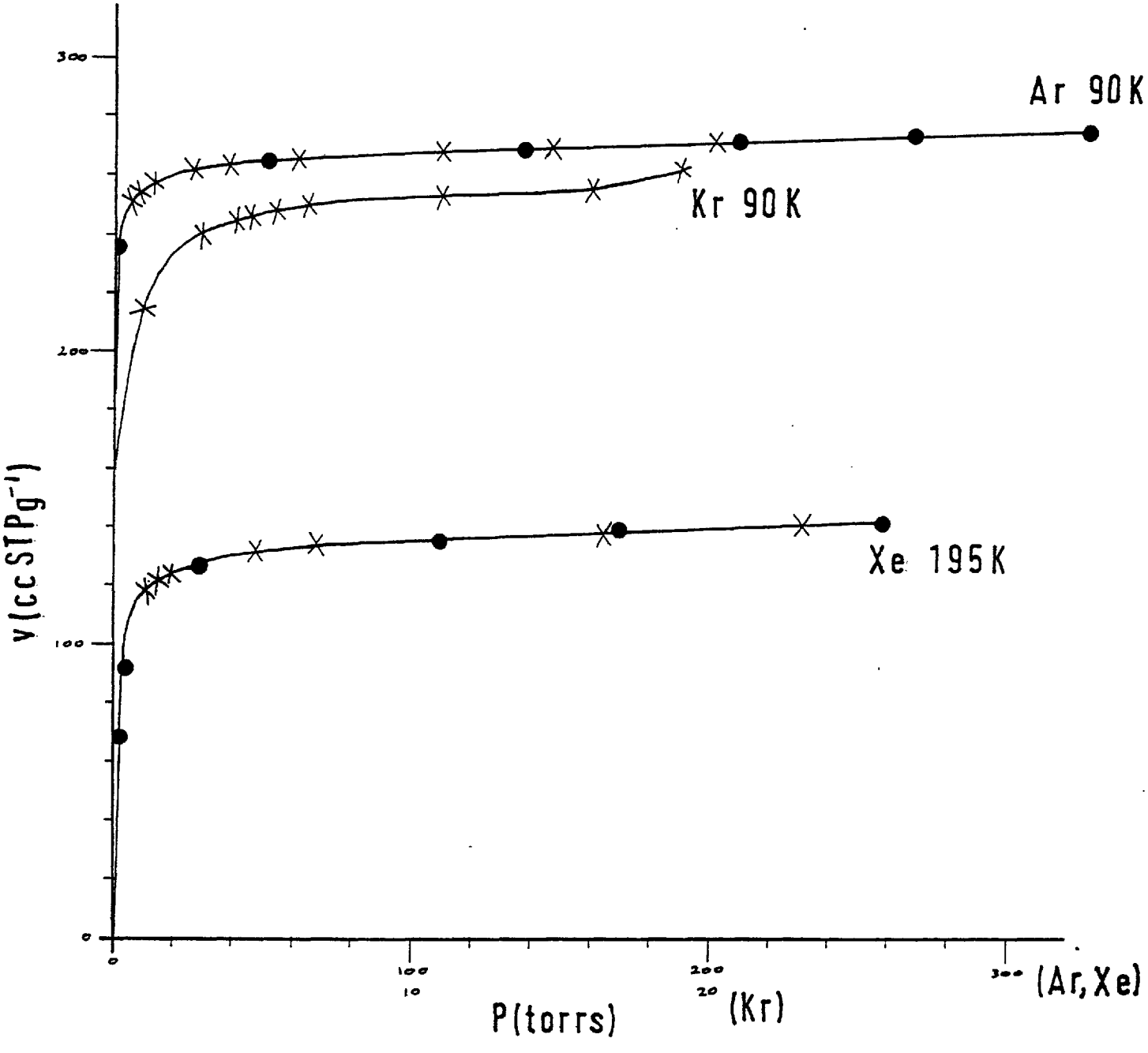
Ar 90K
Kr 90K
Xe 195K
V(cc STP g⁻¹)
300
200
100
0
0
100
10
200
20
300
P(torrs)
(Kr)
(Ar, Xe)

Figure 4-3

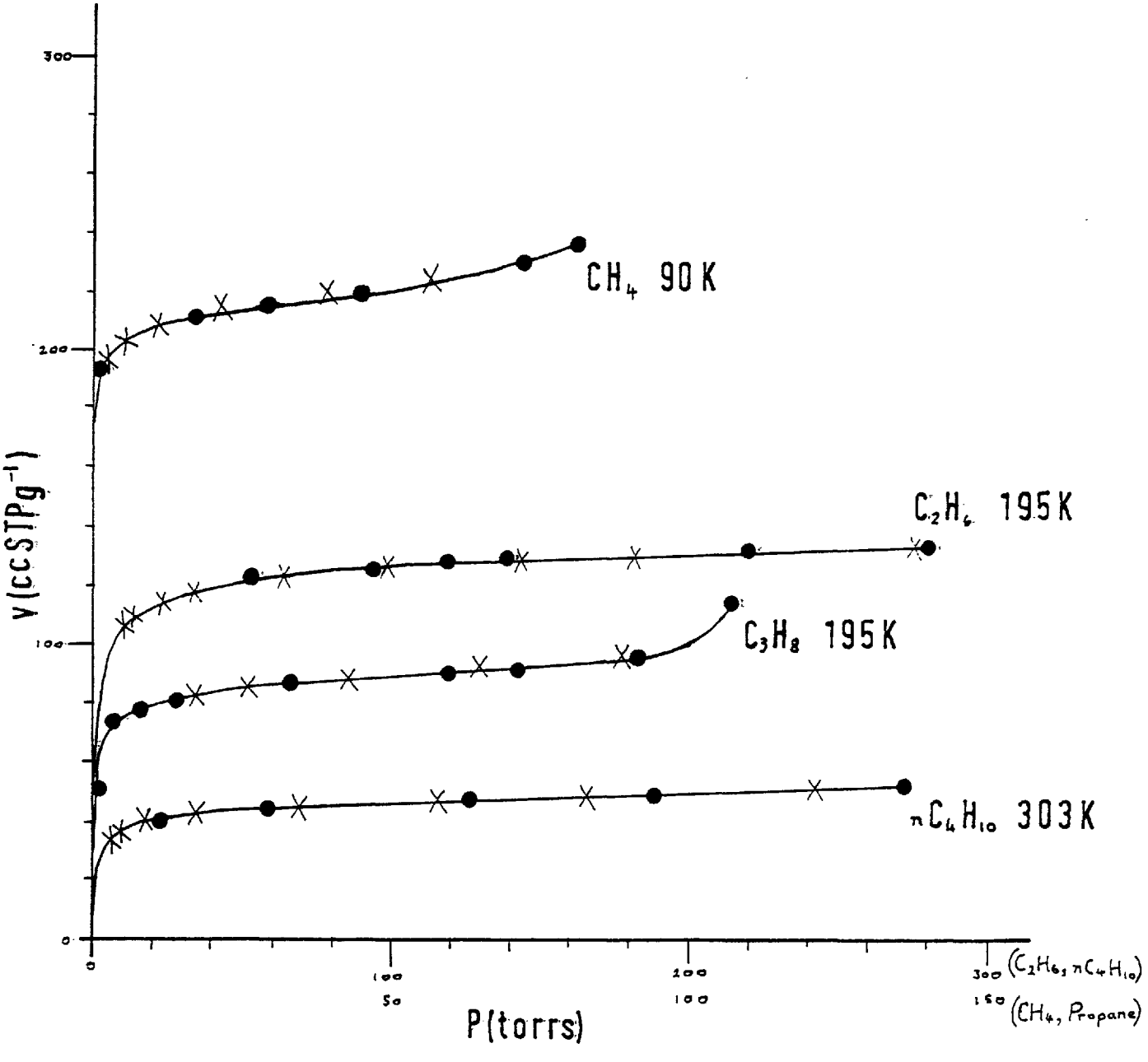
300
200
100
0
V(ccSTPg⁻¹)
CH₄ 90K
C₂H₆ 195K
C₃H₈ 195K
nC₄H₁₀ 303K
0
100
50
200
100
300 (C₂H₆, nC₄H₁₀)
150 (CH₄, Propane)
P(torrs)

N_2, 77 K			
Sample	p/p_o	cc STP g^{-1}	V_p (cc g^{-1})
A	0.26	240	0.37
B	0.26	252	0.39
C	0.26	274	0.42

This explains why sorption of Ar is larger than that of O_2 when in fact they have comparable molecular volumes. It also explains the difference observed between CO_2 and CH_4 and in part the change of V_p between propane and butane.

(2) For N_2 we have the highest value of V_p. This has been observed also in zeolite A (64) but no clear explanation can be given.

(3) For the noble gases we see that the values of V_p decrease when the size of the gas molecule increases. The same can be observed for the paraffins. This is because larger molecules can pack less economically in spatial terms in a cage, specially when the cage dimensions are of the order of the molecule and therefore the density of the larger molecules in the crystals is less than in the liquid.

After considering these points it can be concluded that in fact all the pore volume of H-RHO is accessible to all the sorbates studied. It is interesting to compare the number of molecules of, for example, argon, adsorbed per unit cell in zeolite CaA with the number in H-RHO. Assuming for zeolite H-RHO that the unit cell composition is $H_{12}Si_{36}Al_{12}O_{96}$ $F_w = 2880$, we have that the number of unit cells per gram is :

$$n = \frac{1}{2880} \times 6.02 \times 10^{23} = 2.1 \times 10^{20} \text{ unit cells/g}$$

and the number of Ar molecules at saturation per unit cell :

$$\frac{272}{22400} \times \frac{6.02 \times 10^{23}}{2.10 \times 10^{20}} = 34.8 \text{ molecules}$$

It can be determined (65) for zeolite CaA that this number is 14.8.

Per unit cell in RHO there are two 26 hedron and six octagonal prisms. In the unit cell of A there are one 26 hedron, one 14 hedron

and three cubic units. Only the 26 hedron is involved in the sorption of argon.

Therefore in half unit cell of RHO there are one 26 hedron and three octagonal prisms and the number of molecules sorbed is 17.4. If we assume one molecule of argon in each octagonal prism of RHO we have that in one 26 hedra for RHO there are 14.4 molecules while in the 26 hedra for A this number is 14.8. In making this calculation the volume of the calcium cations has been neglected. The agreement found looks to be an argument in favour of the structure proposed for zeolite RHO.

The Heat of Adsorption

(A) Gases

In order to determine heats of adsorption for N_2, O_2, CO_2, Ar, Kr and Xe isotherms were measured for each sorbate at four temperatures. The isotherms are shown in Figures 4.4 to 4.9. The isosteric heats were calculated according to equation 20.

$$q_{st} = \frac{-R \ln(p_2/p_1)}{\frac{1}{T_2} - \frac{1}{T_1}}$$

and were evaluated by two methods :

(a) At a given amount sorbed values of p_1 and p_2 were read on the isotherms at T_1 and T_2 respectively and the value of q_{st} calculated with equation (20).

(b) Plots of log v/p vs v were made and at a given amount sorbed values of log v/p_1 and log v/p_2 were read on the curves at T_1 and T_2 respectively and the value of q_{st} calculated with equation (20).

Deviations were smaller in method (b) and this was preferred. An average was taken between the values obtained for the different pairs of isotherms. Heats were determined only for small amounts of sorption. The fractions of saturation and the number of molecules per unit cell up to which heats were determined are shown below

Gas	θ	Molecules per unit cell	Molecules per unit cell at saturation
N_2	0.12	3.8	31.7
O_2	0.14	4.4	31.4

Gas	θ	Molecules per unit cell	Molecules per unit cell at saturation
CO_2	0.28	6.4	22.9
Ar	0.20	7.0	35.0
Kr	0.20	6.4	32.0
Xe	0.32	5.8	18.1

The values of q_{st} are plotted vs amount sorbed in Figure 4.10. These plots show that H-RHO is a rather homogeneous sorbent, the heats start decreasing very slightly with amount sorbed and then approach a limiting value. The difference between the heats at $\theta \rightarrow 0$ and the limiting values are about 0.5 kcal/mol for all the sorbates studied.

In order to interpret heats we consider equation (22) :

$$\phi = \phi_D + \phi_R + \phi_P + \phi_{\dot{F}Q} + \phi_{Fu} + \phi_{SP}$$

We can neglect ϕ_{SP} because at the amounts for which we have measured q_{st} the contribution to ϕ due to the interaction between sorbed molecules is very small. ϕ_{Fu} is zero because none of our sorbates has a dipole moment. Then equation (22) reduces to :

$$\phi = \phi_D + \phi_R + \phi_P + \phi_{\dot{F}Q}$$

The small variation of q_{st} with amount sorbed is not due to the existence of sites where $\dot{F}$ is large because the variations are approximately equal for the quadrupolar molecules and noble gases. It does not seem to arise from the term ϕ_P since the variation would be larger for the heavier noble gases which are more polarizable. It could then arise from the $\phi_D + \phi_R$ term but this would be larger for the heavier noble gases and therefore the variation of q_{st} with amount sorbed would be larger for Xe than for Kr and than for Ar.

A possible explanation is the following. We have assumed that q_{st} would be given by ϕ when in fact it is given, neglecting zero point energy, by equation (21)

$$q_{st} = -\phi + RT - F(T)$$

which shows the temperature dependence of q_{st}. It can easily be shown that :

Figure 4-4

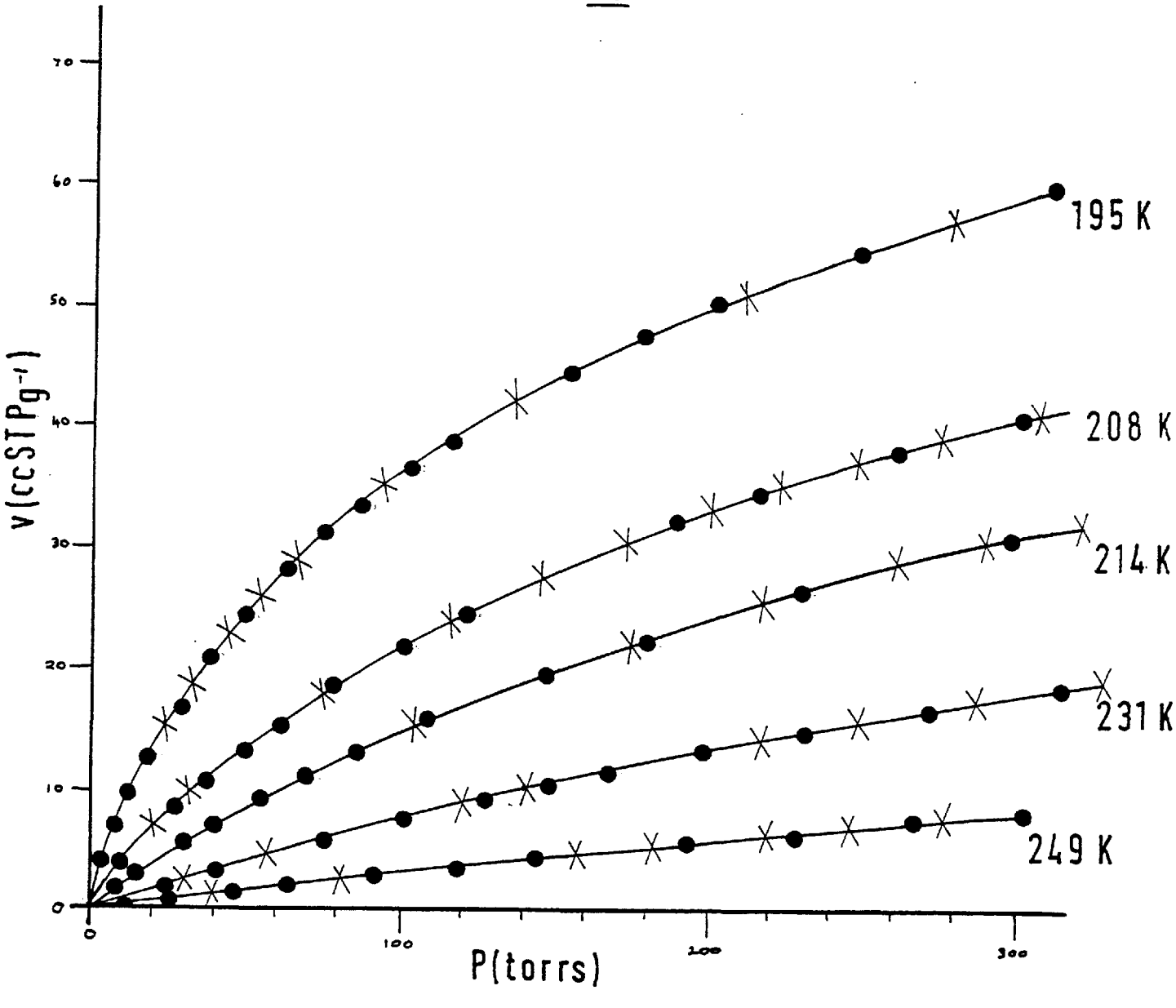
N2
V(ccSTPg-1)
P(torrs)
0
10
20
30
40
50
60
70
100
200
300
195 K
208 K
214 K
231 K
249 K

Figure 4-5

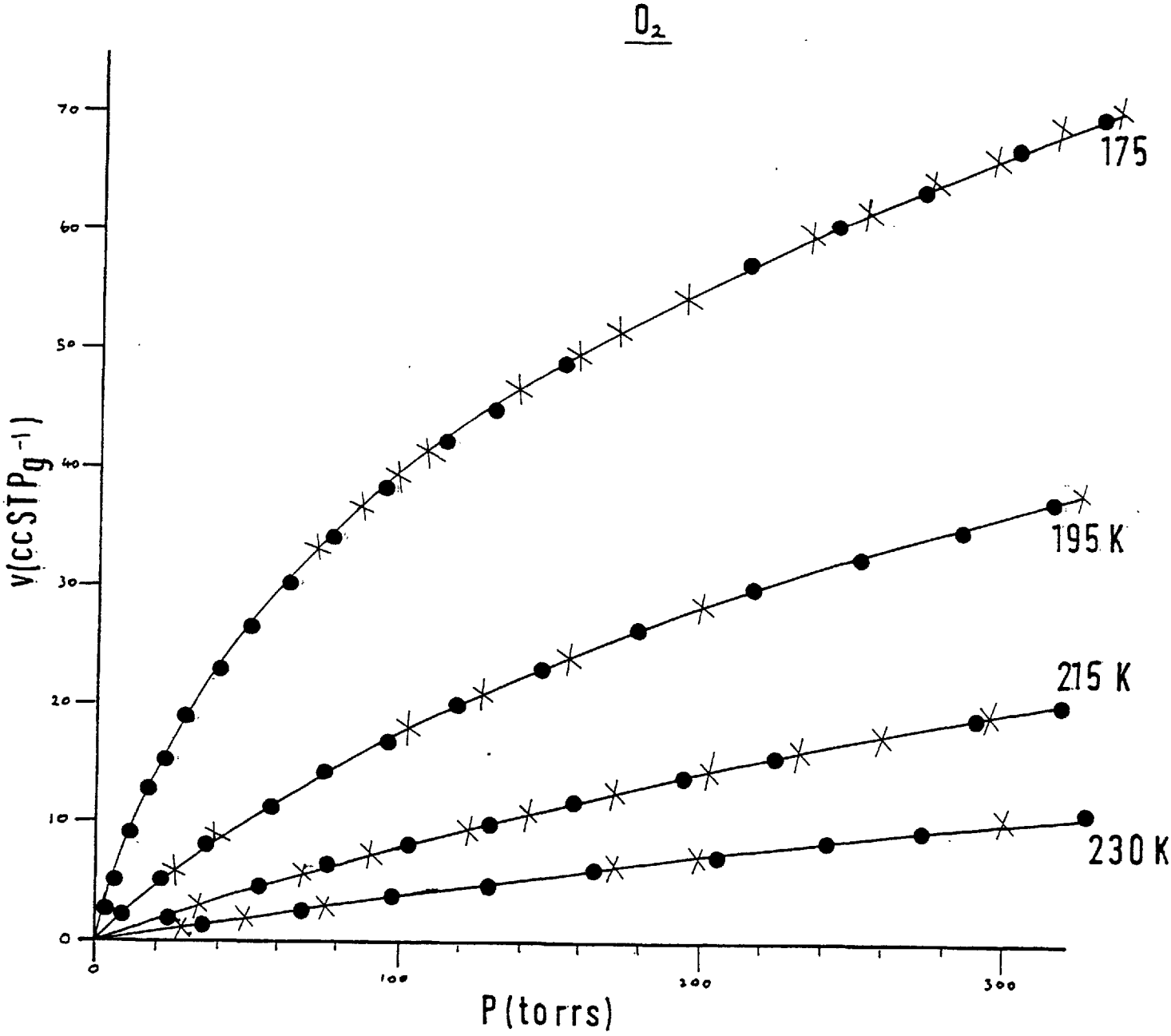
O_2
V(ccSTPg^{-1})
P(torrs)
175
195 K
215 K
230 K
0
10
20
30
40
50
60
70
100
200
300

Figure 4-6

CO_2

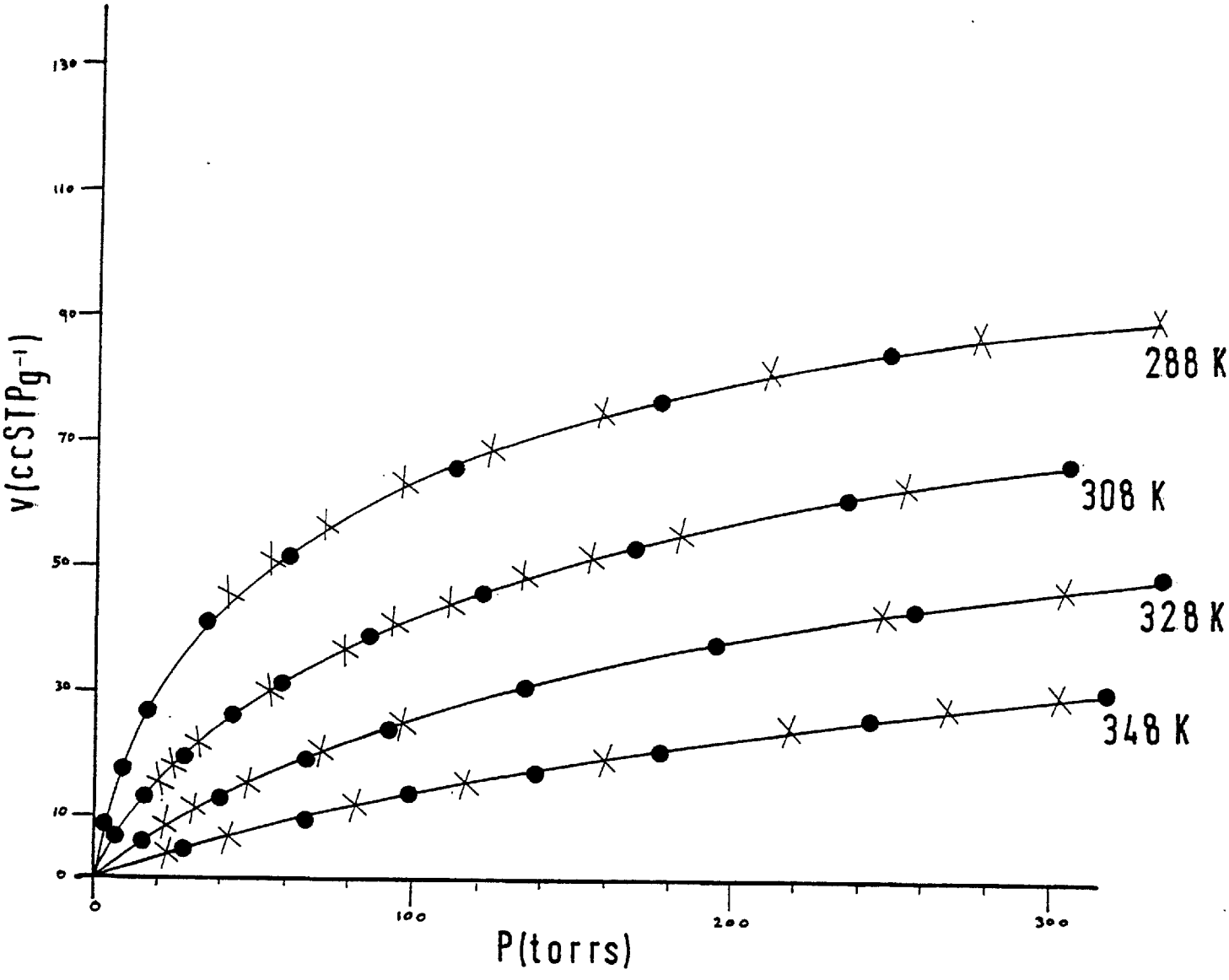

Figure 4-7

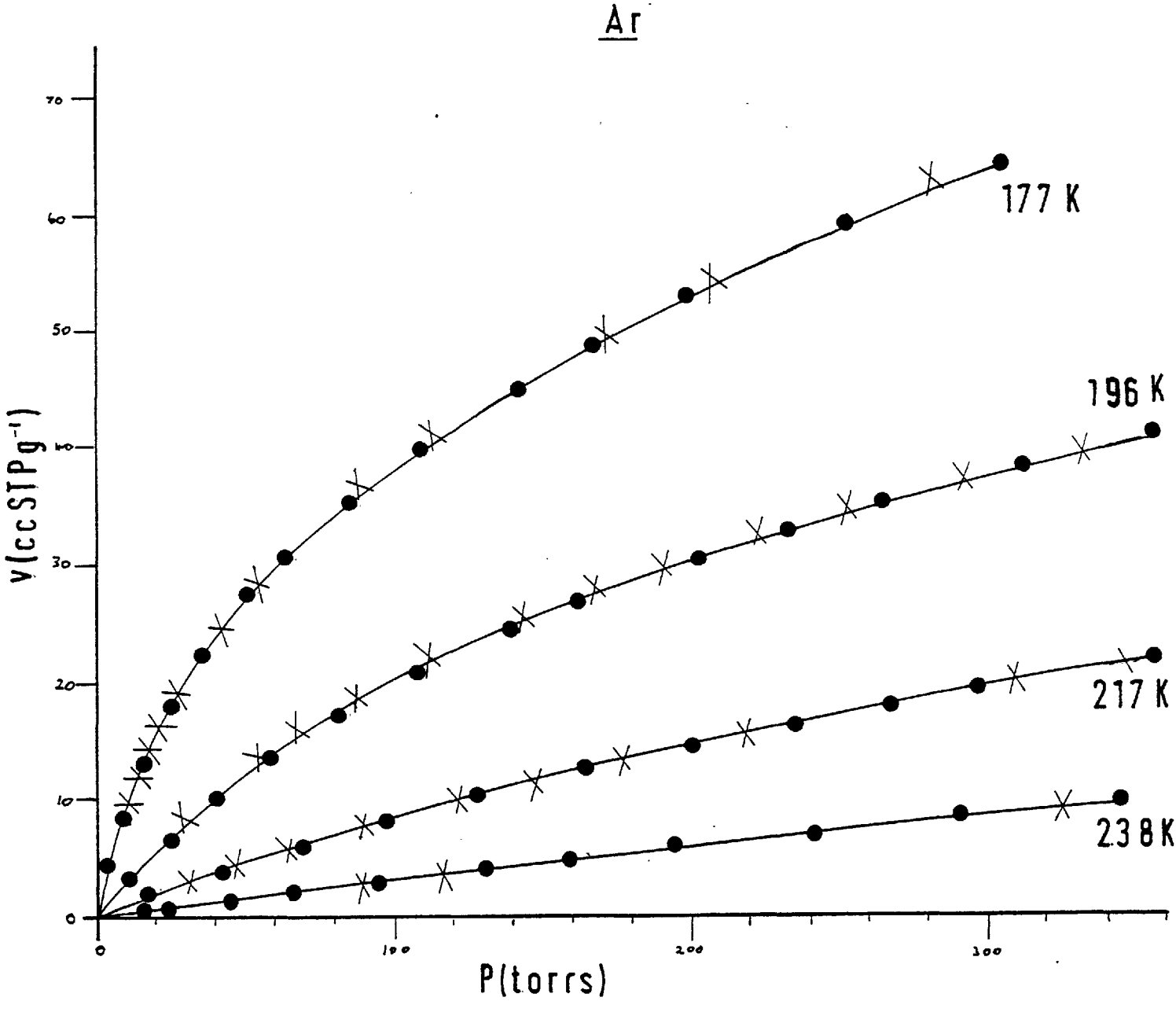
Ar
177 K
196 K
217 K
238 K
V(cc STP g⁻¹)
P(torrs)
0
10
20
30
50
60
70
100
200
300

Figure 4-8

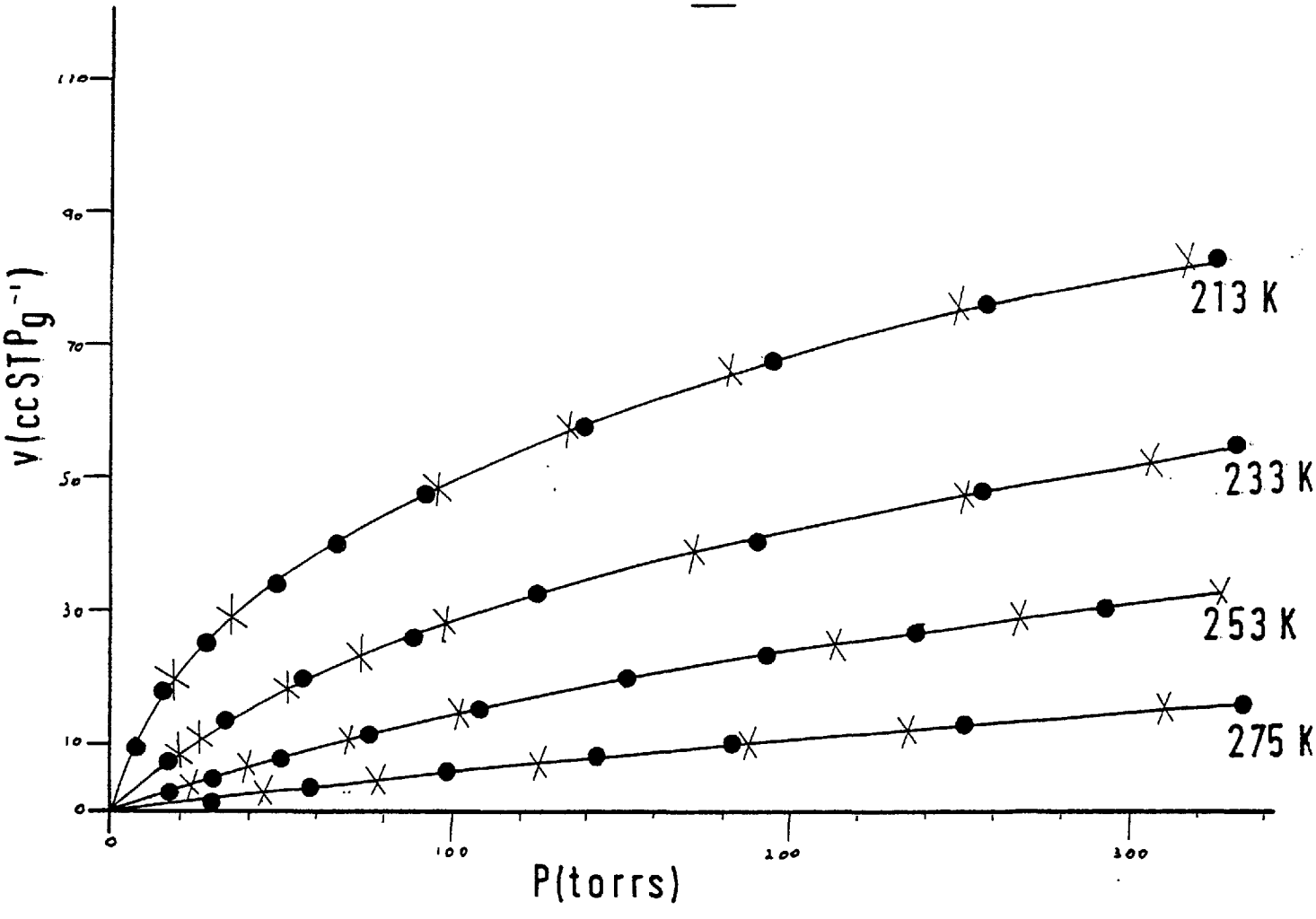
Kr
V(ccSTPg⁻¹)
P(torrs)
213 K
233 K
253 K
275 K
0
10
30
50
70
90
110
100
200
300

Figure 4-9

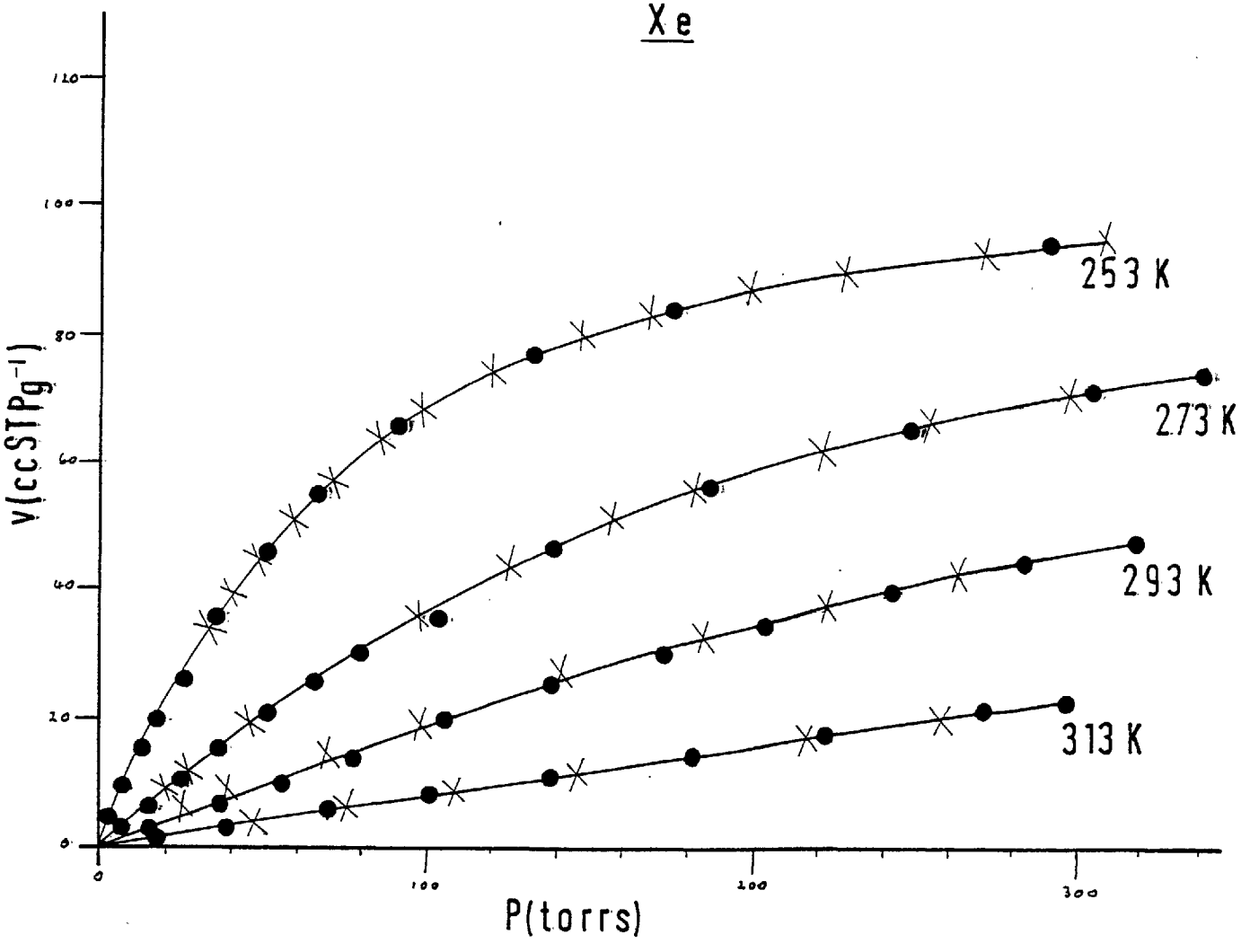
Xe
V(ccSTPg⁻¹)
P(torrs)
253 K
273 K
293 K
313 K
0
100
200
300
40
60
80
100
120

Figure 4-10

The Heat Of Adsorption vs Amount Sorbed

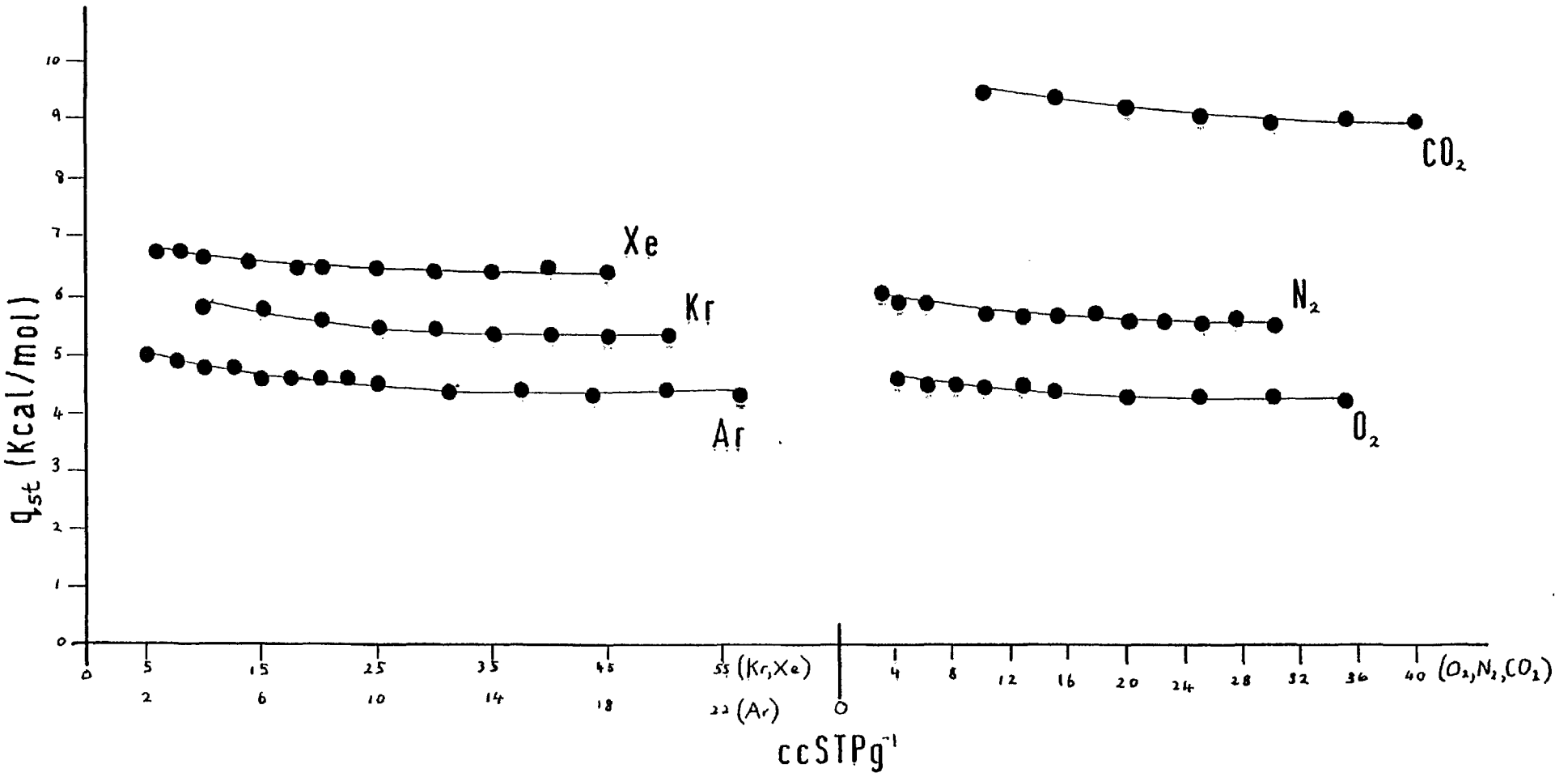

$$q_{st(T_2)} - q_{st(T_1)} = \int_{T_1}^{T_2} (\tilde{C}_g - \bar{C}_s)\, dT$$

where $\tilde{C}_g$ is the heat capacity at constant pressure of the gaseous molecules and $\bar{C}_s$ the differential heat capacity of sorbed molecules. Since q_{st} for the smaller amounts are determined from the isotherms at higher temperatures and for the larger amounts from the isotherms at lower temperatures one could think that the difference between the heats at $\theta \to 0$ and the limiting values would be given by the integral in the last equation. (71). But $\bar{C}_s$ is larger than $\tilde{C}_g$ and therefore one would expect that the heats decrease as the temperature increases.

It would be interesting to know for the quadrupolar molecules how much is the contribution to the heat of the term ϕ_{FQ} compared with the contribution of $\phi_D + \phi_R + \phi_P$ (67). For the noble gases (and gases without u and Q) a plot of q_{st} vs α is made and a curve is drawn. If we assume that for the quadrupolar gases the contribution of $\phi_D + \phi_R + \phi_P$ is given by their polarizability according to that curve, then the difference between the value of q_{st} and $\phi_D + \phi_R + \phi_P$ would be ϕ_{FQ}. When this is done we obtain :

quadrupolar gas	quadrupolar moment Q^3	q_{st}*	$\phi_D + \phi_R + \phi_P$	ϕ_{FQ}
O_2	0.10	4.3	3.6	0.7
N_2	0.31	5.5	4.0	1.5
CO_2	0.64	9.0	4.9	4.1

* limiting values

For the larger quadrupolar gas CO_2 the contribution of ϕ_{FQ} is almost as much as the contribution of $\phi_D + \phi_R + \phi_P$. For N_2 the contribution of ϕ_{FQ} to the heat is about thirty per cent, and for the small quadrupolar O_2 the contribution is very small.

It would also be interesting to compare the values of q_{st} of zeolite RHO with those of zeolite A (68).

	v = 30 cc STP g^{-1}		
	O_2	Ar	N_2
NaA	3.1	3.2	4.2
H-RHO	4.5	4.4	5.5

The value of 30 cc STP g^{-1} has been chosen for the comparison because at that amount the effect of the Na^+ ions in the energy of adsorption is less important than at smaller amounts. We see that the values for zeolite RHO exceed the ones for A by more than one kilocalorie. This difference might arise because zeolite RHO contains, apart from the 26 hedron, octagonal prisms where the energy of adsorption might be much enhanced. To test this the following calculation was made. An argon atom was placed at the centre of an octagonal prism and $\phi_D + \phi_R$ calculated. The contribution from Si and Al was neglected as well as that from oxygens other than the ones forming the prisms. The Lennard-Jones 12:6 potential was assumed (69):

$$\phi_D + \phi_R = 16\ A\left(\frac{r_o^6}{2r^{12}} + \frac{1}{r^6}\right)$$

The factor 16 accounts for the 16 oxygen atoms of the prism. A was calculated according to the Kirkwood-Muller expression, equation (11) :

$$A = -\frac{6\ mc^2\ \alpha_o\ \alpha_{Ar}}{\frac{\alpha_o}{\chi_o} + \frac{\alpha_{Ar}}{\chi_{Ar}}}$$

The following dara were required (70) :

$\alpha_o = 3.89 \times 10^{-24}$ cgs

$\chi_o = 20.92 \times 10^{-30}$ cgs

$\alpha_{Ar} = 1.63 \times 10^{-24}$ cgs

$\chi_{Ar} = 32.6 \times 10^{-30}$ cgs

$m = 9.108 \times 10^{-28}$ g

$c = 299792\ 10^5$ cm sec^{-1}

1 erg = 2.39×10^{-8} cal.

r_o is half the equilibrium distance between two argon atoms plus the radius of oxygen, (r_o = 3.255 Å). The value of r was determined in this way. An octagonal window with a free diameter of 4.2 Å was assumed, and the radius of oxygen was taken as 1.35 Å. Therefore the distance between centres of oxygens on diametrically opposite sides in an octagonal window is (4.2 + 2 x 1.35)Å = 6.9Å.

Since oxygen atoms almost touch in zeolites the distance between the planes of octagonal windows in the prism was considered 2 x 1.35 = 2.70Å. Then the argon atom at the centre of the prism is at a distance r from any of the oxygens given by :

$$r = \sqrt{(1.35)^2 + (3.45)^2} = 3.70 \text{ Å}$$

The value of $\phi_D + \phi_R$ was then calculated and a value of 9.0 kcal/mol was obtained. When the argon atom is at the centre of an octagonal window a value of 5.7 kcal/mol is obtained. Therefore the octagonal prism provides sites where the energy of adsorption is much enhanced and is not surprising that the heats in zeolite RHO are larger than the ones in zeolite A. (In such calculations the Kirkwood-Muller approximation to the dispersion constant, A, is known to give a high value for A, but this is not likely to account fully for such high energies.)

Entropy and Heat Capacity of the Sorbed Phase

A) Gases

Differential entropies of the sorbed phase were calculated according to equation (26) :

$$\bar{S}_s = \tilde{S}^o_g + R \ln \frac{p_o}{p} + C^o_p \ln \frac{T}{T_o} - \frac{q_{st}}{T}$$

$T_o = 298$ K

$p_o = 760$ mm Hg

$\tilde{S}^o_g$ and C^o_p were obtained from tables (72). p is the equilibrium pressure at temperature T for a given amount sorbed. $\bar{S}_s$ was evaluated at most of the temperatures at which isotherms were measured. $\bar{S}_s$ was plotted vs amount sorbed in Figures 4.11 to 4.16. It decreases continuously with amount sorbed. This is what one expects for a homogeneous sorbent as explained below :

In terms of an ideal localized model we can write :

$$\bar{S}_s = \tilde{S}_{th} + \bar{S}_c$$

$\bar{S}_c$ is given by equation 29 :

$$\bar{S}_c = R \ln \frac{1 - \theta}{\theta}$$

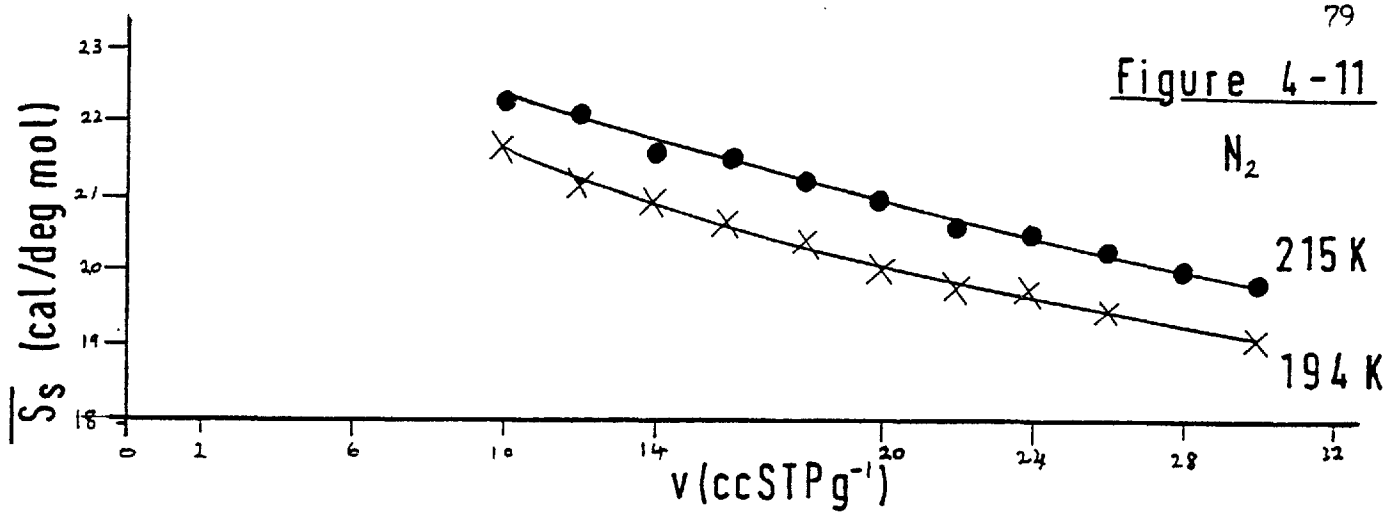

Figure 4-11

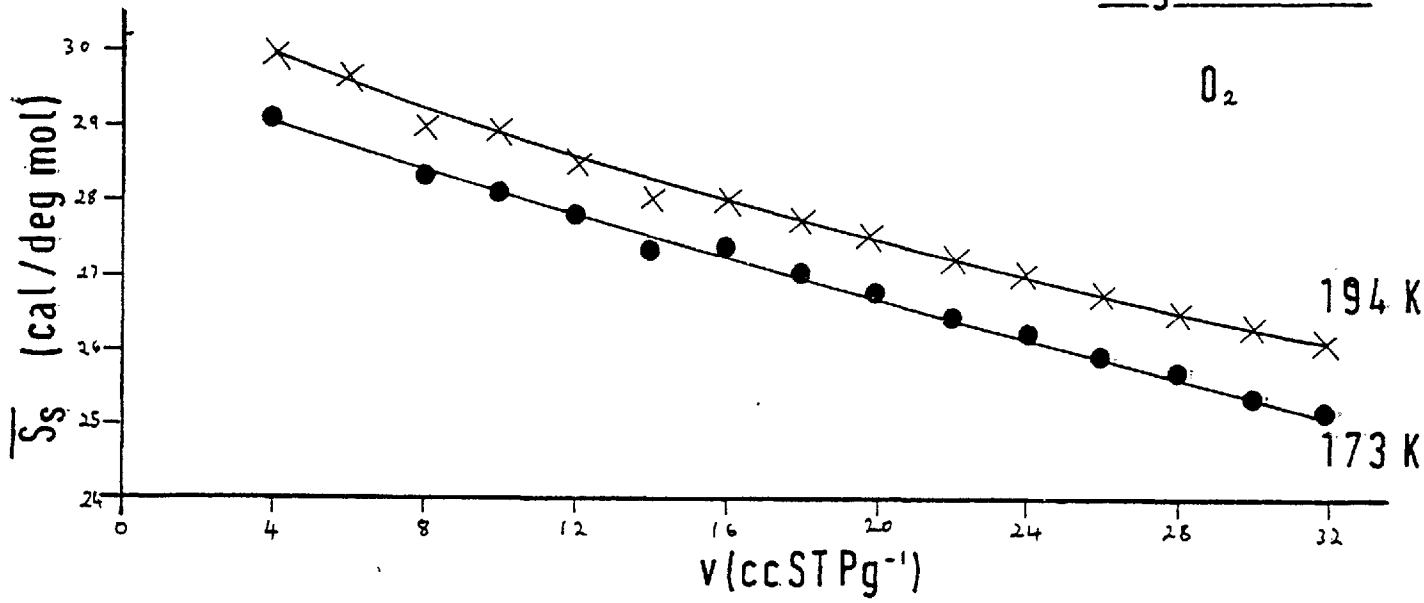

Figure 4-12

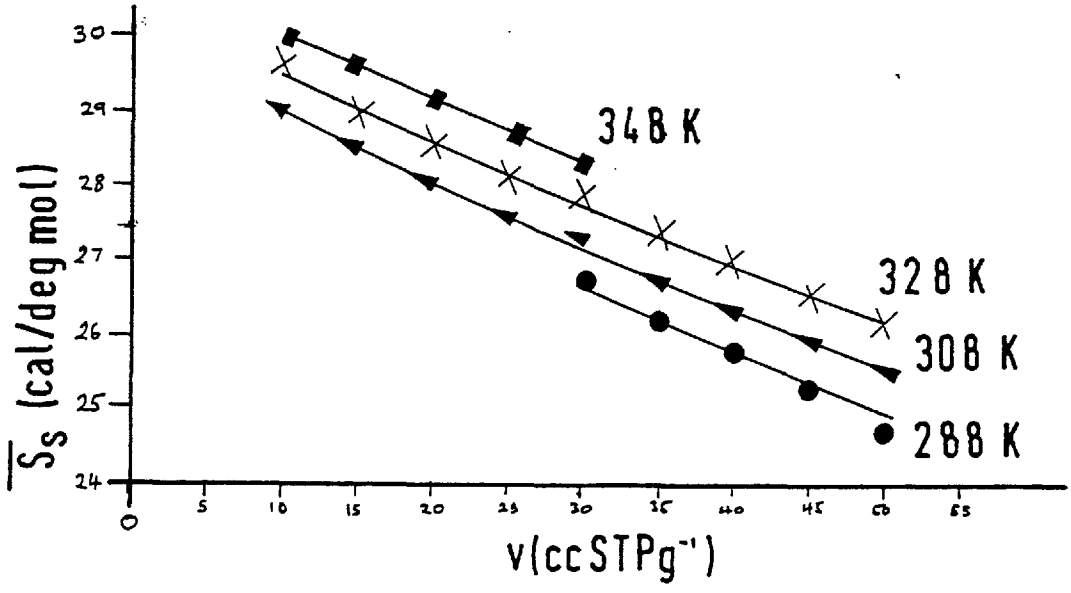

Figure 4-13

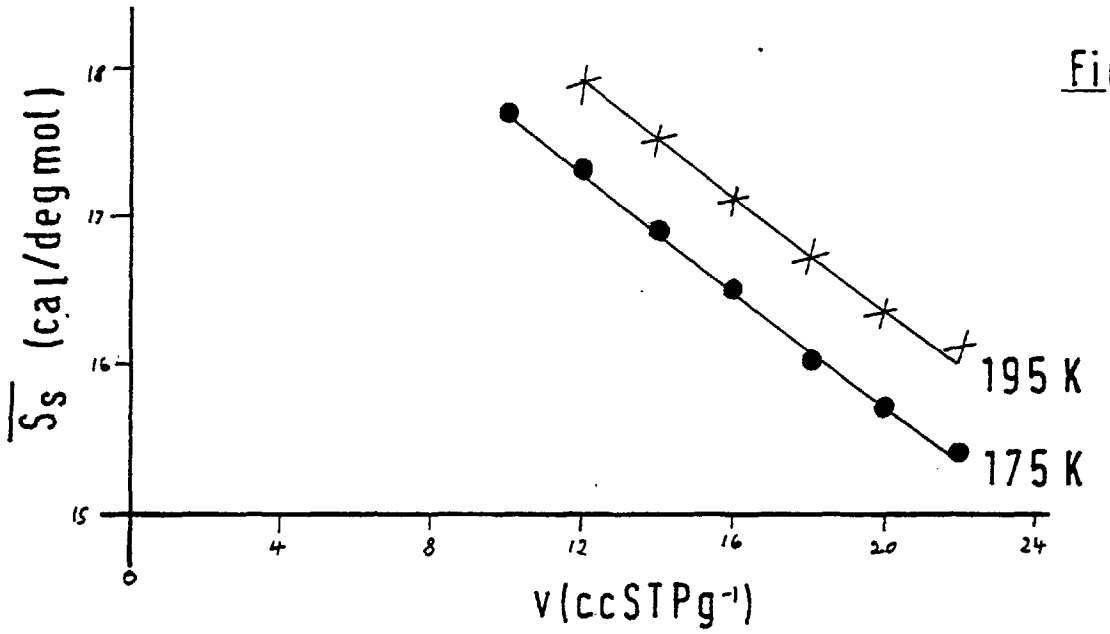

Figure 4-14

Ar

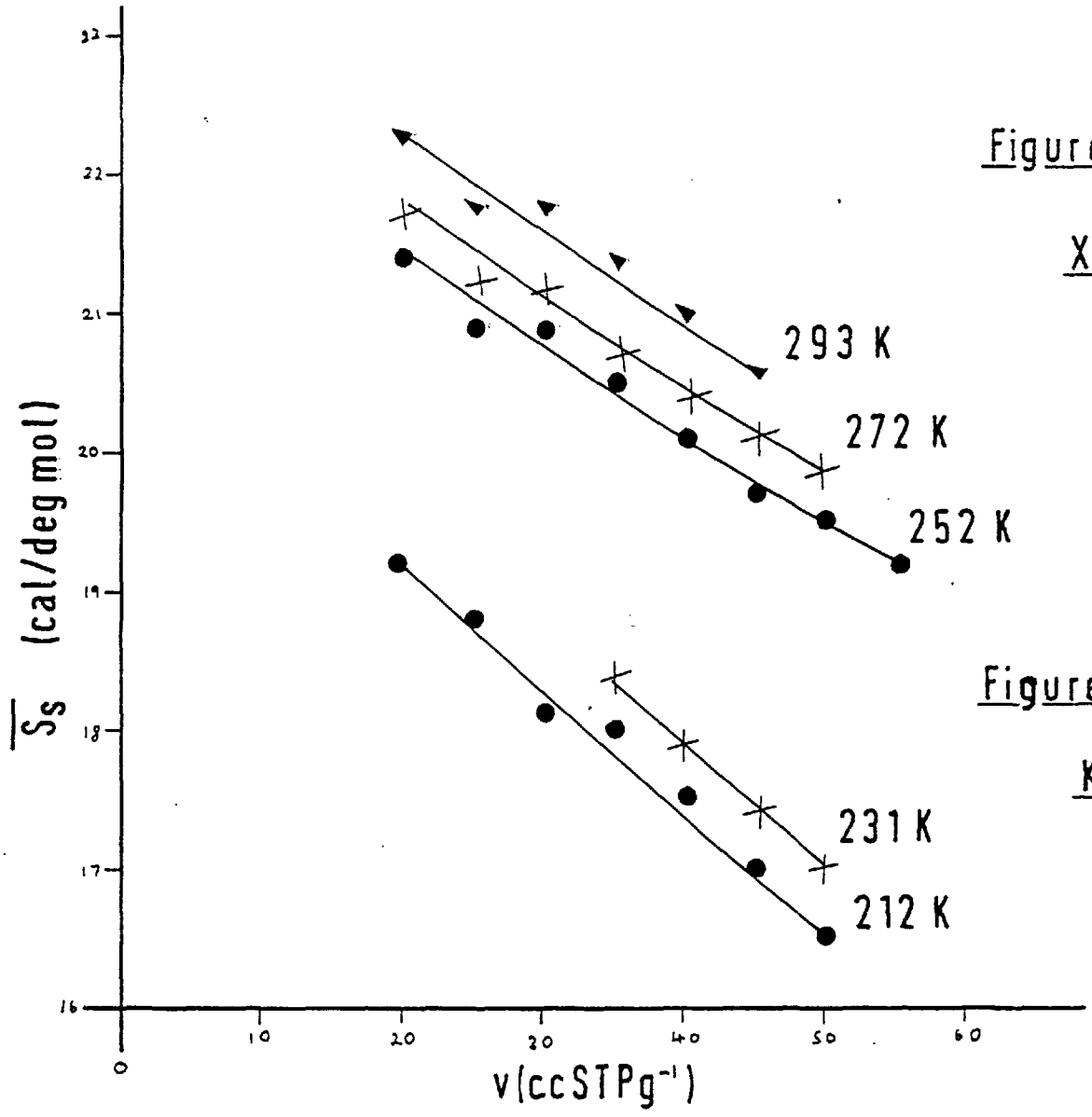

Figure 4-15

Xe

Figure 4-16

Kr

Since $\tilde{S}_{th}$ for a homogeneous surface remains constant with amount sorbed and $\bar{S}_c$ decreases continuously, $\bar{S}_s$ must also decrease continuously with amount sorbed.

In terms of ideal mobile models we have :

$$\bar{S}_s = S'_{th} + {}_1\bar{S}_T$$
$$\bar{S}_s = S''_{th} + {}_2\bar{S}_T$$

${}_1\bar{S}_T$ and ${}_2\bar{S}_T$ include the translational entropy, the configurational entropy and part of the thermal entropy and are given by equation (35) and (33) respectively. $\tilde{S}'_{th}$ and $\tilde{S}''_{th}$ remain constant with amount sorbed but ${}_1\bar{S}_T$ and ${}_2\bar{S}_T$ decrease continuously and therefore $\bar{S}_s$ decrease continuously with amount sorbed.

For heterogeneous sorbents the plots $\bar{S}_s$ vs v are more complicated, often increasing with amount sorbed, passing through a maximum and then decreasing again as saturation is approached (73).

It can be seen from the plots of $\bar{S}_s$ vs v that $\bar{S}_s$ increases with temperature. Since :

$$C_v = T \frac{dS}{dT}$$

the heat capacity of the sorbed phase can be evaluated at a given amount sorbed from the $\bar{S}_s$ vs v plots as $\Delta S/\Delta T \times T_m$, where T_m is the mean temperature of the interval ΔT. The values of C_v are :

Sorbate	$\bar{C}_v$ (cal/deg.mol)
N_2	7.8
O_2	7.4
CO_2	8.7
A	5.8
Kr	5.8
Xe	5.6

If in the sorbed phase the inert gases were localized and behave as a set of simple harmonic oscillators (3v) then for monatomic gases one would expect a value of $C_v = 3R = 6$ cal/deg.mol. If they had one degree of translational freedom replacing one vibration (2v, lt) $C_v = 2R + \frac{1}{2}R = 5$ cal/deg.mol, and if they had two translational degrees

of freedom (1v,2t) C_v = 4 cal/deg.mol. Our values agree with states (3v) and (2v,1t).

For the linear molecules N_2, O_2 and CO_2 if they are localized we can have the following states. If there are three vibrations plus two rotations (3v, 2v) $C_v = 3R + \frac{2}{2}R$ = 8 cal/deg. mol. If one rotation is substituted by a vibration (4v, 1r) C_v = 9 cal/deg. mol. If the two rotations are substituted by vibrations (5v) C_v = 10 cal/deg. mol. If mobility is introduced substituting the vibrational by translational degrees of freedom we have for (2v, 1t, 2r) C_v = 7 cal/deg. mol. and for (1v, 2t, 2r) C_v = 6 cal/deg. mol. The values obtained for O_2 and N_2 agree with states (3v, 2r) and (2v, 2r, 1t). For CO_2 the value agrees with (3v, 2r) and (4v, 1r).

The heat capacities of the sorbed phase can be dependent on the amount sorbed (74) since changes in the state of the sorbed molecules can occur as the concentration of the sorbed molecules increase inside the channels of the zeolite. For example C_v can increase with amount if translational degrees of freedom become vibrational. Nevertheless in the small range of sorption studied the heat capacities should remain constant, in fact our data is not accurate enough to detect any possible variation.

Heat of Adsorption

B) Hydrocarbons

In order to determine heats of adsorption for CH_4, C_2H_4, C_3H_8 and nC_4H_{10} isotherms were measured for each sorbate at four temperatures. The isotherms are shown in Figures 4.17 to 4.20. The isosteric heats were calculated according to :

$$q_{st} = \frac{-R \ln(p_2/p_1)}{\frac{1}{T_2} - \frac{1}{T_1}}$$

and were evaluated from log v/p vs v plots. The values of q_{st} are plotted (Figure 4.21) versus relative amount sorbed $\theta = v/v_{sat}$, where v_{sat} is the saturation capacity at 90 K for methane, 195 K for ethane and propane and 303 K for n-butane and v is the amount sorbed at p and T. These plots show that for methane the heat decreases slowly with amount sorbed and for the other hydrocarbons the heat increases with amount sorbed due to interactions between sorbed molecules.

Figure 4 17

Methane

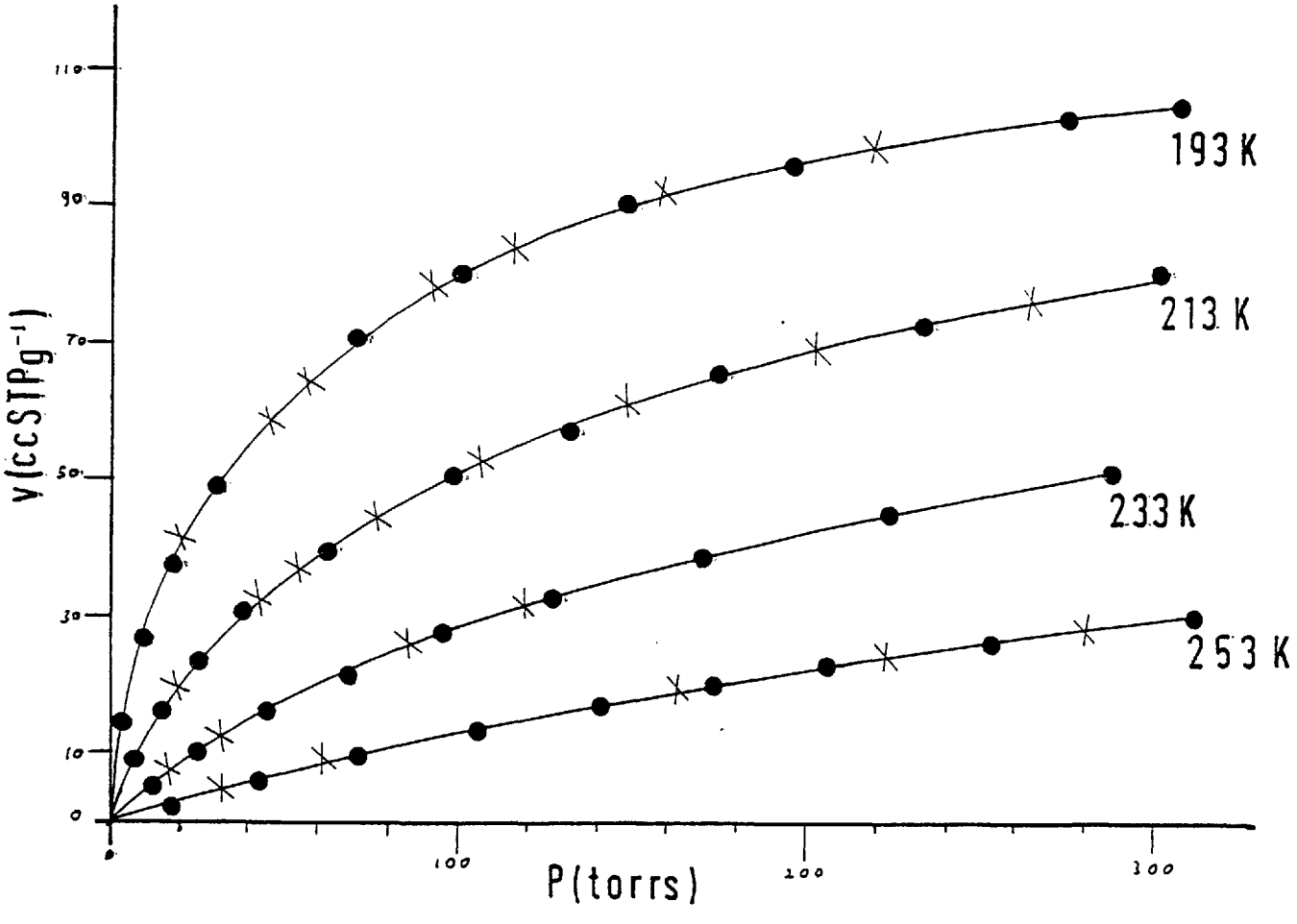

Figure 4-18

Ethane

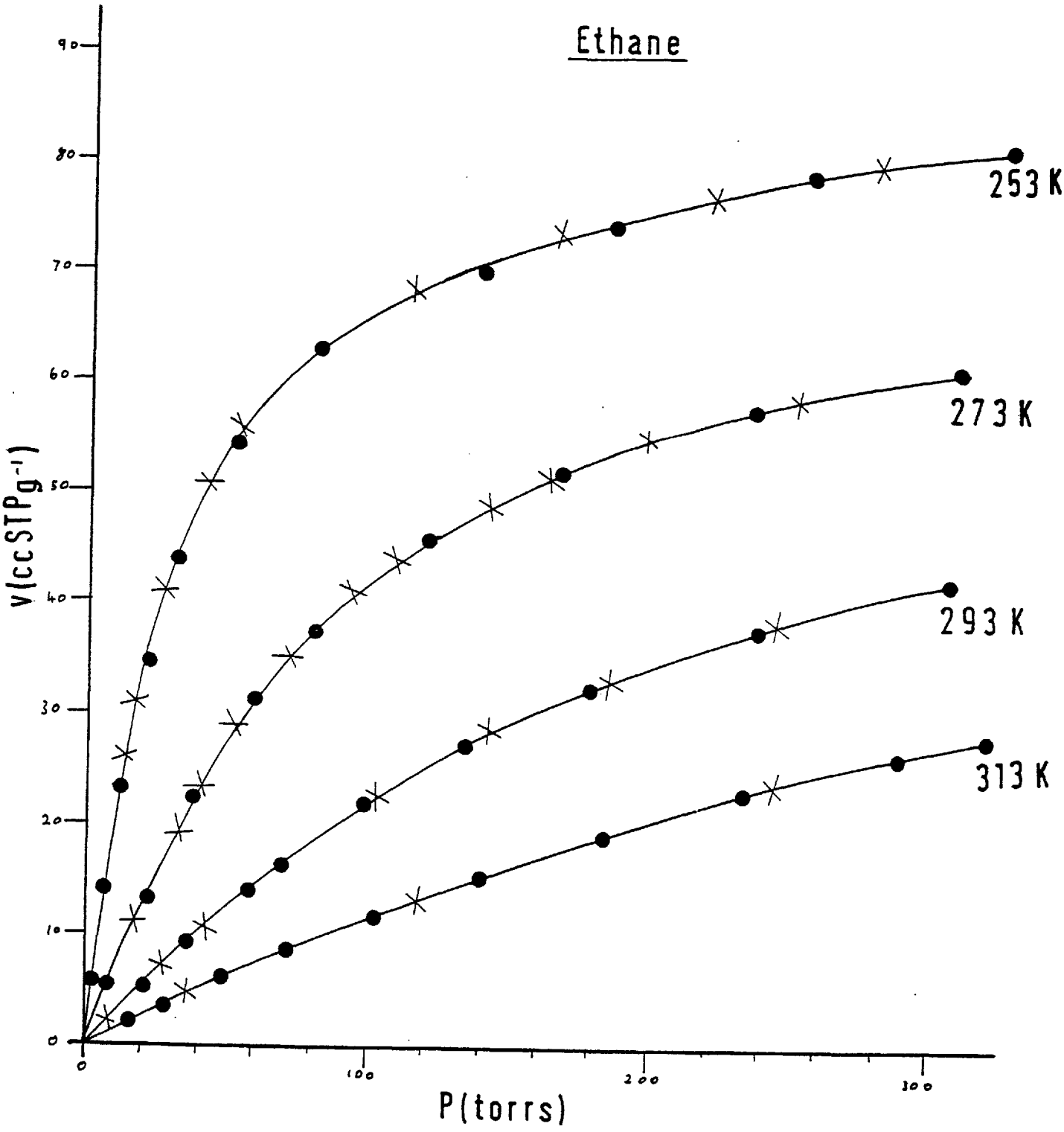

Figure 4-19

Propane

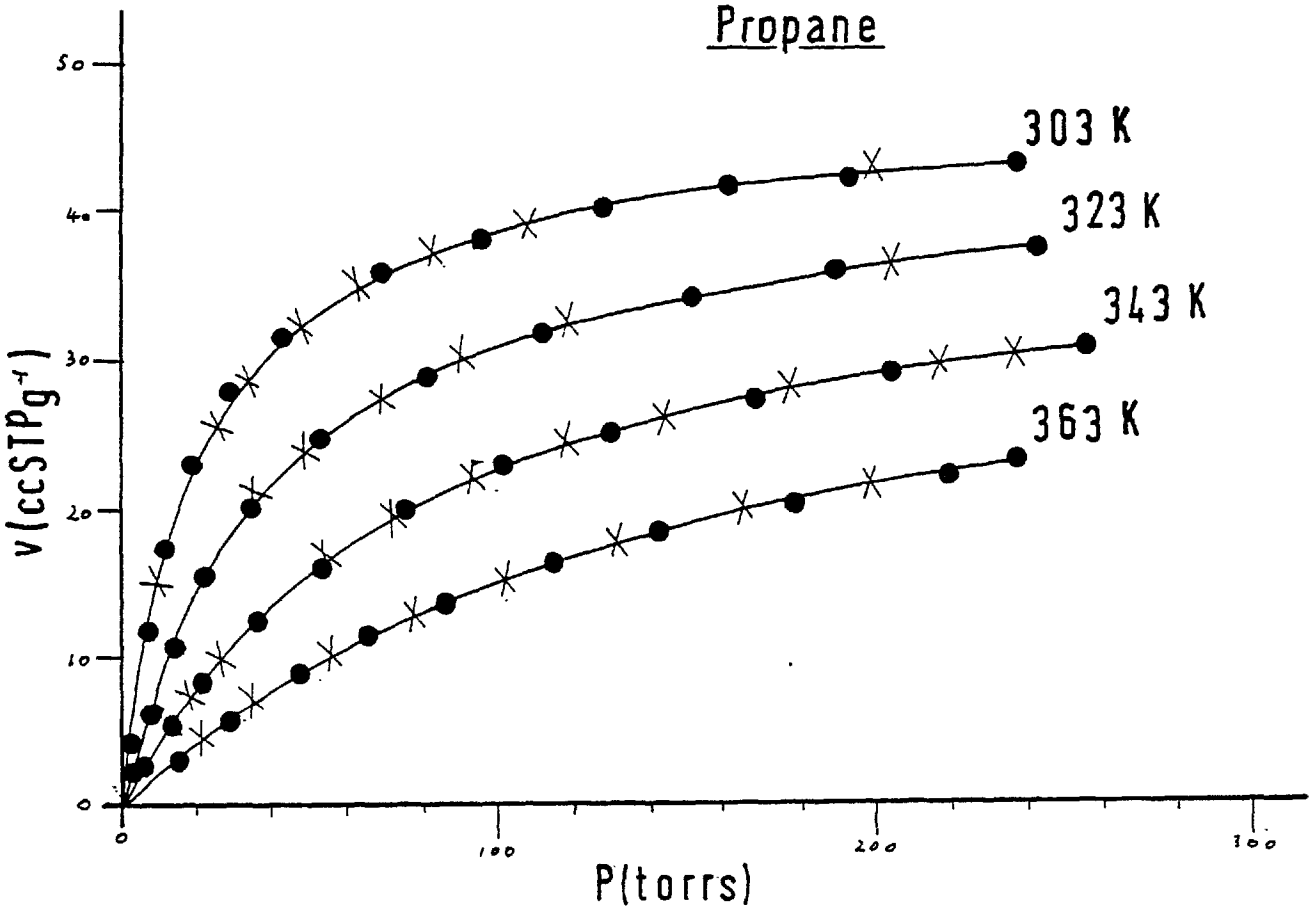

Figure 4-20

n-Butane

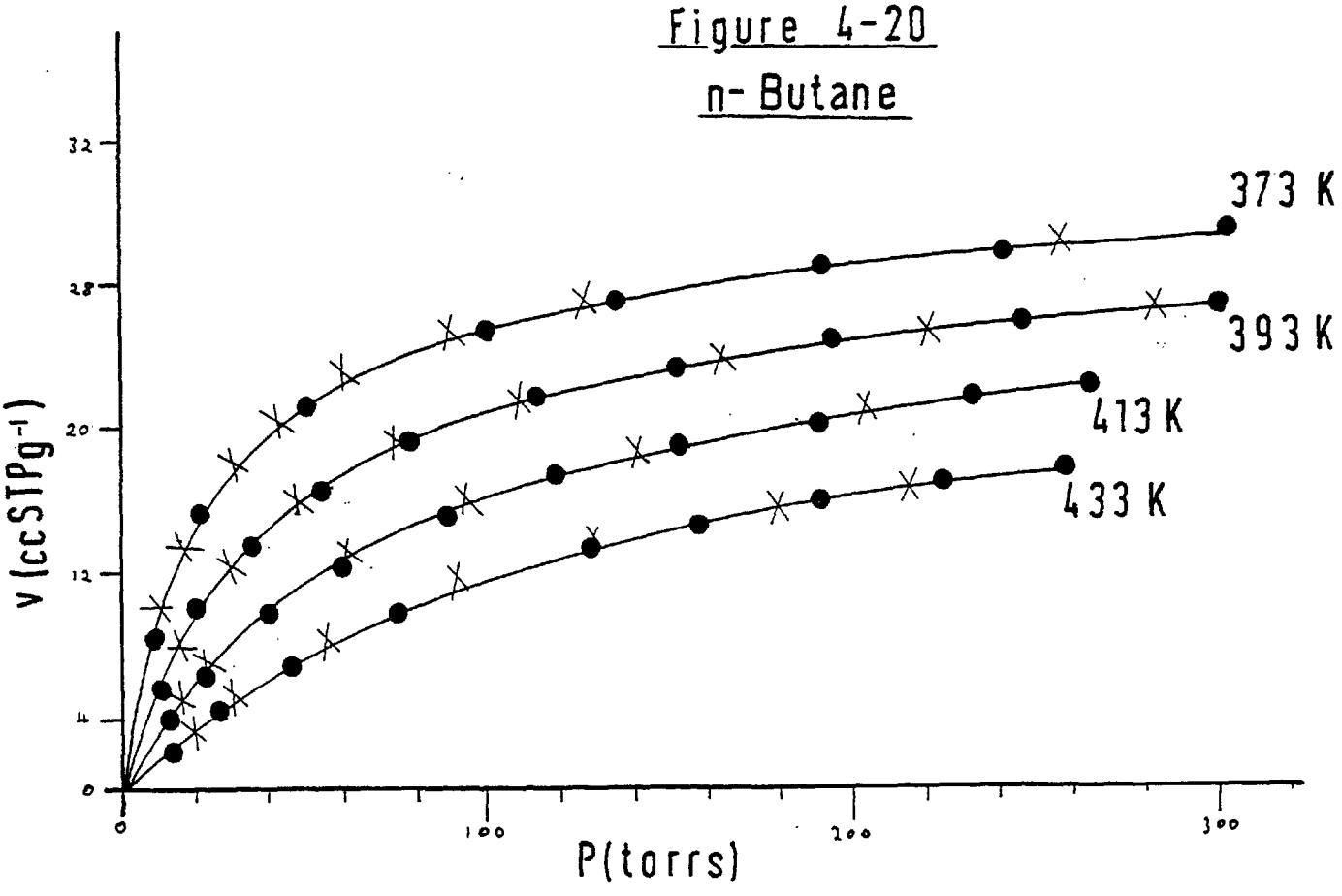

The relation between the initial isosteric heats and the number of carbon atoms in the n-paraffin is seen in Figure 4.22. The value for methane is about 0.8 kcal above the line, but this high value could be understood if one considers that the methane molecules occupy the octagonal prisms at low amounts. For the other paraffins the prisms would not be places of large interaction because only one part of the molecule would be in them while the other part would not. If one takes the limiting value of the heat for methane instead of the initial heat, the point fits much closer in the line. The general deviations of the points are in part due to the difficulty in estimating the initial heats. This linearity is commonly found in other zeolites. The equations for H-RHO and other zeolites may be compared (for C_1 to C_4 paraffins):

$$q_{st} = 3.2 + 1.8\ N \quad \text{H-RHO}$$

$$q_{st} = 2.75 + 2.0\ N \quad \text{H-chabazite} \quad (75)$$

$$q_{st} = 2.5 + 2.0\ N \quad \text{H-L} \quad (76)$$

When hydrocarbons are considered equation 22 reduces to:

$$\phi = \phi_D + \phi_R + \phi_P + \phi_{SP}$$

since ϕ_{Fu} and ϕ_{FQ} are zero. For initial heats Q_{SP} is also zero. The linearity of q_{st} vs N plots is due to heats arising mainly from $(\phi_D + \phi_R)$.

Below the initial heats are compared with the heats of liquefaction of the hydrocarbons :

	CH_4	C_2H_6	C_3H_8	nC_4H_{10}
q_{st}	5.5	7.1	8.4	10.8
ΔH_{liq}	1.9	3.5	4.5	5.4
$q_{st}/\Delta H_{liq}$	2.9	2.0	1.9	2.0

The isosteric heats double the values of the heat of liquefaction, indicating the stronger interaction of the molecule in the zeolite cavity than in the liquid. There is another reason contributing to larger heats in the sorbed state which is that when a molecule evaporates from the liquid the other molecules re-arrange to occupy the site left, while in the zeolite the cavity does not collapse into the site (77).

Figure 4-21

isosteric heat vs θ

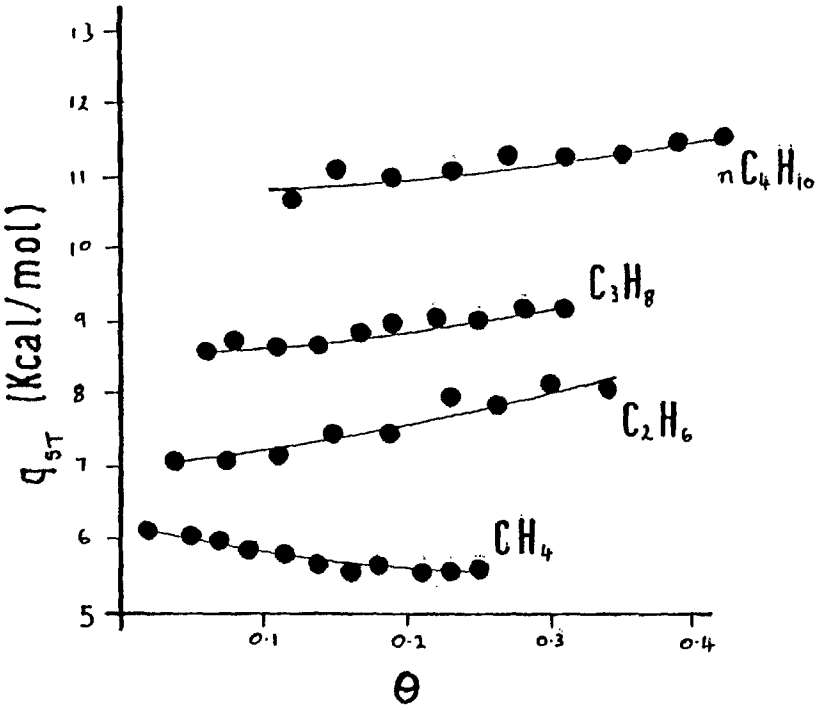

Figure 4-22

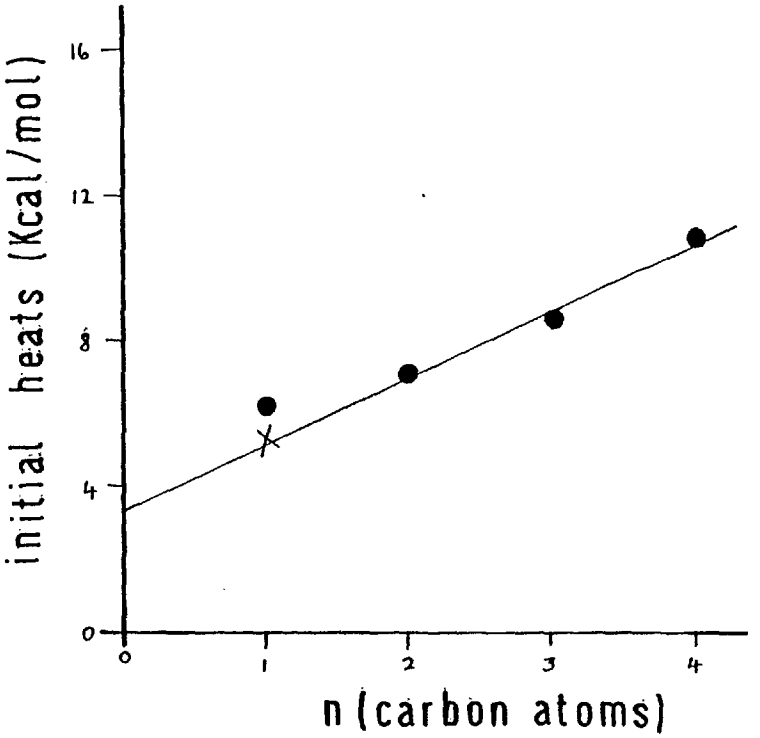

Entropy of the Sorbed Phase

(B) Hydrocarbons

Differential entropies of the sorbed phase were calculated from the relation

$$\bar{S}_s = \tilde{S}^o_g + R \ln \frac{p_o}{p} + C^o_p \ln \frac{T}{T_o} - \frac{q_{st}}{T}$$

where $T_o = 298$ K; and $p_o = 760$ mm Hg.

$\tilde{S}^o_g$ and C^o_p were obtained from Tables (78). $\bar{S}_s$ was evaluated at the temperatures at which isotherms were measured, and it is plotted vs amount sorbed in Figures 4.23 to 4.26. $\bar{S}_s$ decreases with amount sorbed in the way one expects for a comparatively homogeneous sorbent.

Since interpretation of the state of the sorbed molecules through the values of the heat capacity is much more difficult for polyatomic molecules, two possible states were considered and analyzed in the following way :

(1) Molecules were assumed to be localized having three degrees of vibrational freedom. For this case we can write :

$$\bar{S}_s = \bar{S}_{th} + \bar{S}_c$$

where $\bar{S}_{th}$ includes the entropy associated with the three vibrational degrees of freedom, the rotational and the internal degrees of freedom of the sorbed molecule. The configurational entropy is given by :

$$\bar{S}_c = R \ln \frac{1 - \theta}{\theta} \qquad \theta = v/v_{sat}$$

(2) Molecules were assumed to have one translational degree of freedom, then :

$$\bar{S}_s = \bar{S}'_{th} + {}_1\bar{S}_T$$

$\bar{S}'_{th}$ includes the entropy associated with the two vibrational, the rotational and internal degrees of freedom. ${}_1\bar{S}_T$ is the entropy of the translational degree of freedom and includes part of the thermal entropy and also the whole of the configurational entropy. It is given by :

$${}_1\bar{S}_T = R \ln \frac{(2\pi m KT)^{\frac{1}{2}}}{h} b^{\frac{1}{3}} \frac{(1 - \theta)}{\theta} + R\left(\frac{1}{2} - \frac{\theta}{1-\theta}\right)$$

Figure 4-23

Methane

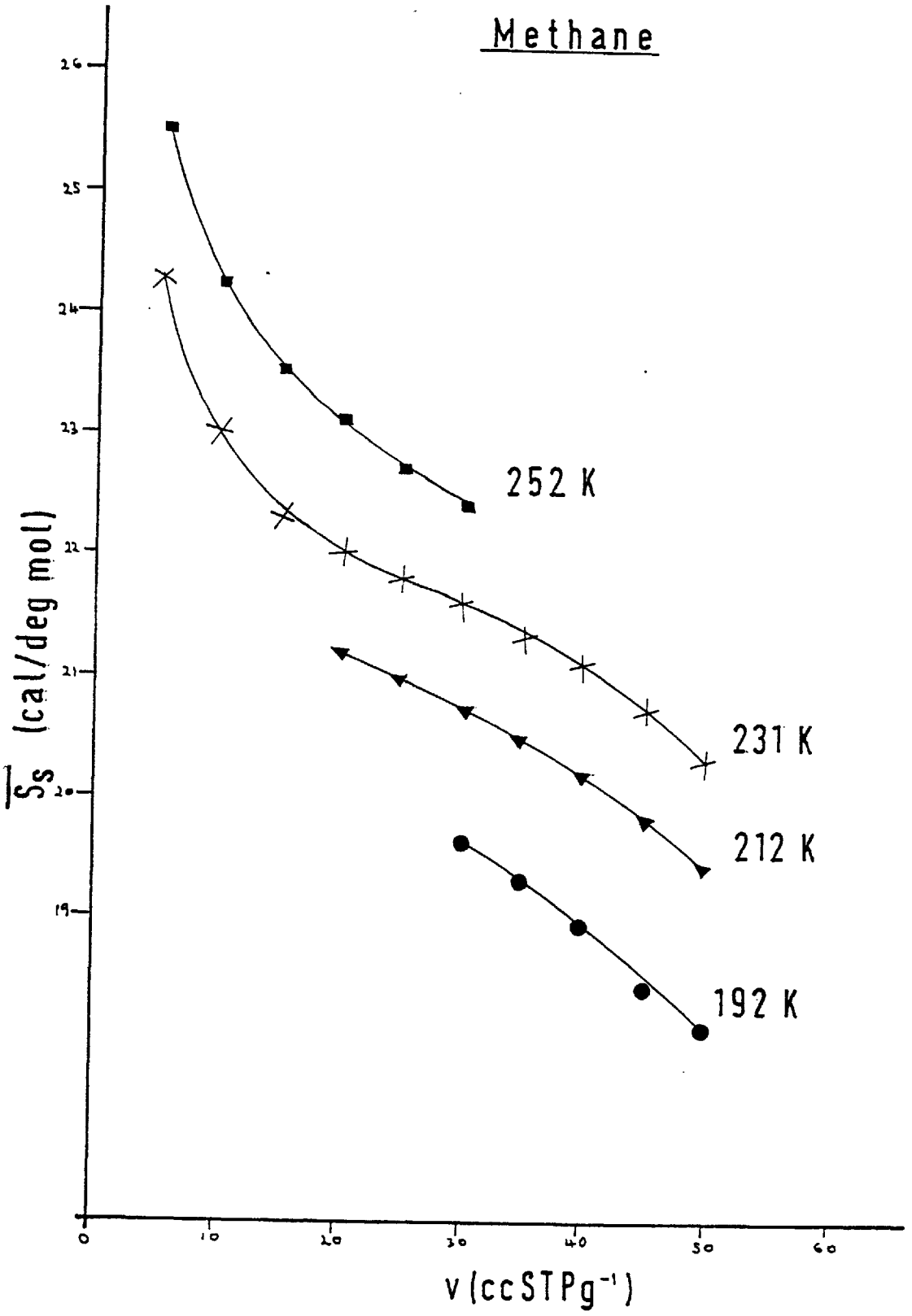

Figure 4-24

Ethane

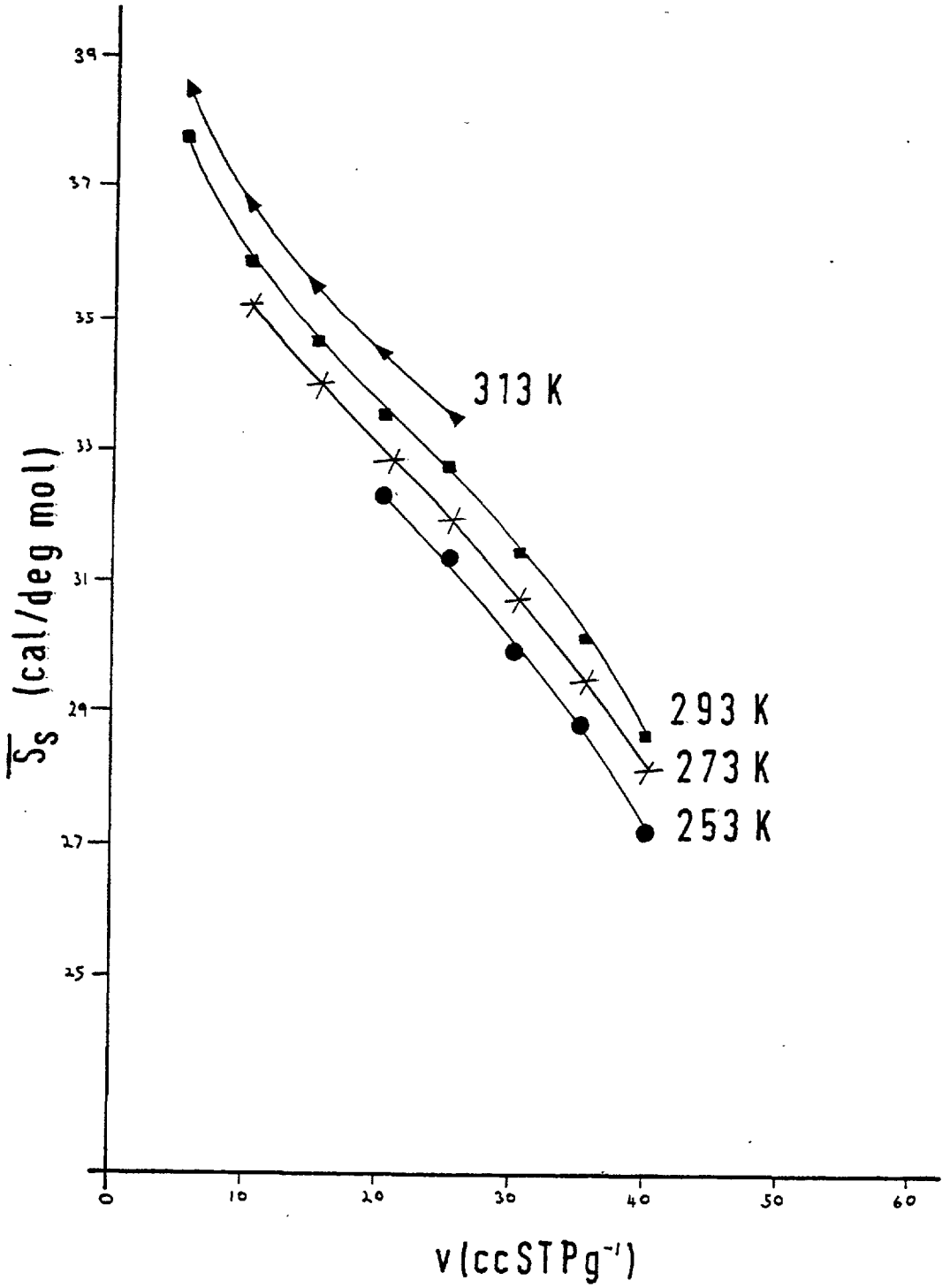

Figure 4-25

Propane

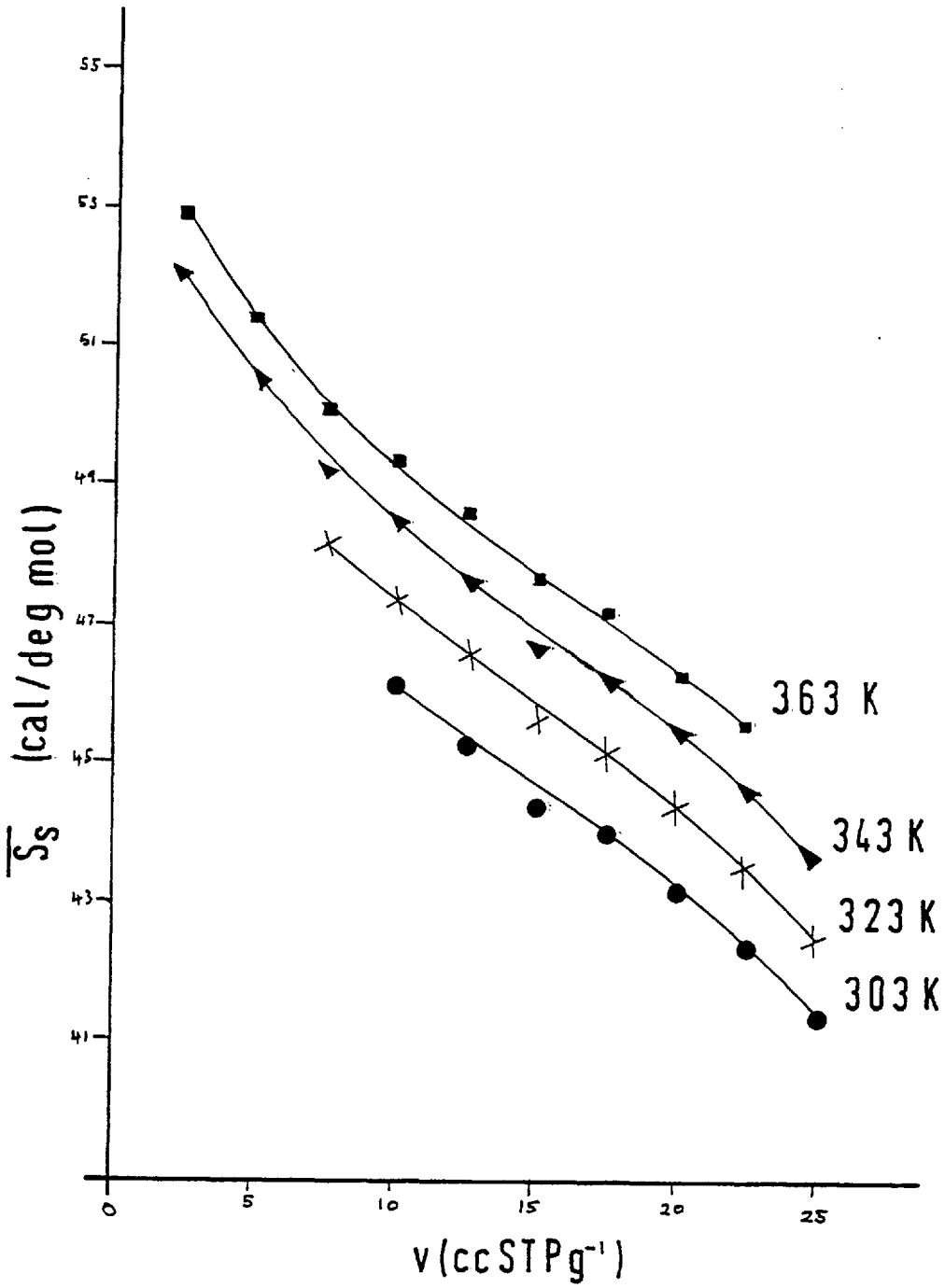

Figure 4-26

n-Butane

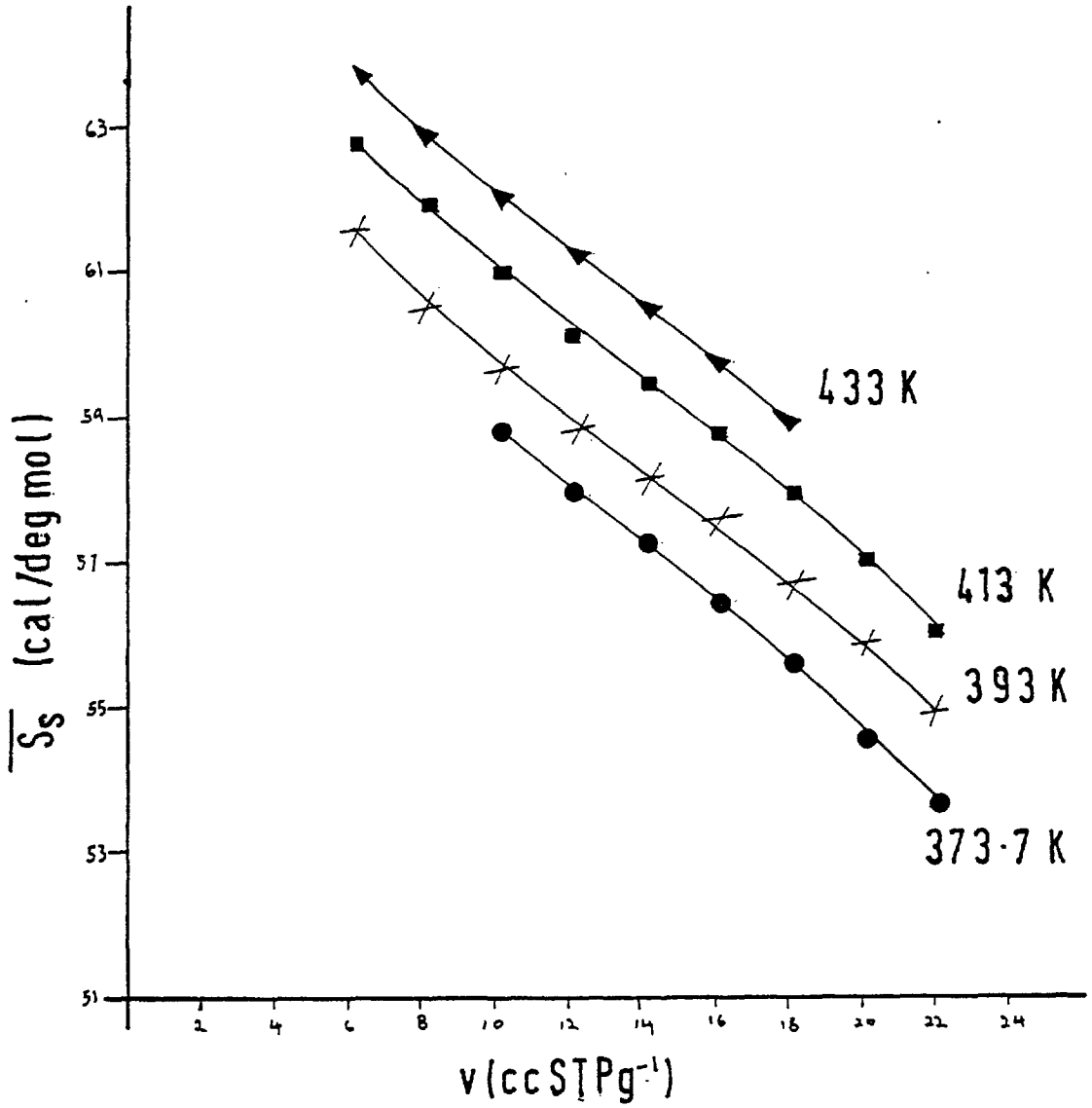

Therefore we can calculate the thermal entropies at any amount sorbed by :

For 1 $\quad \bar{S}_{th} = \bar{S}_s - \bar{S}_c$

For 2 $\quad \bar{S}'_{th} = \bar{S}_s - 1\bar{S}_T$

They should be independent of θ if the respective model is applicable. They are plotted vs amount sorbed in Figures 4-27 and 4-28. We see that $\bar{S}_{th}$ and $\bar{S}'_{th}$ both change a little with amount sorbed indicating that none of the situations considered is quite applicable.

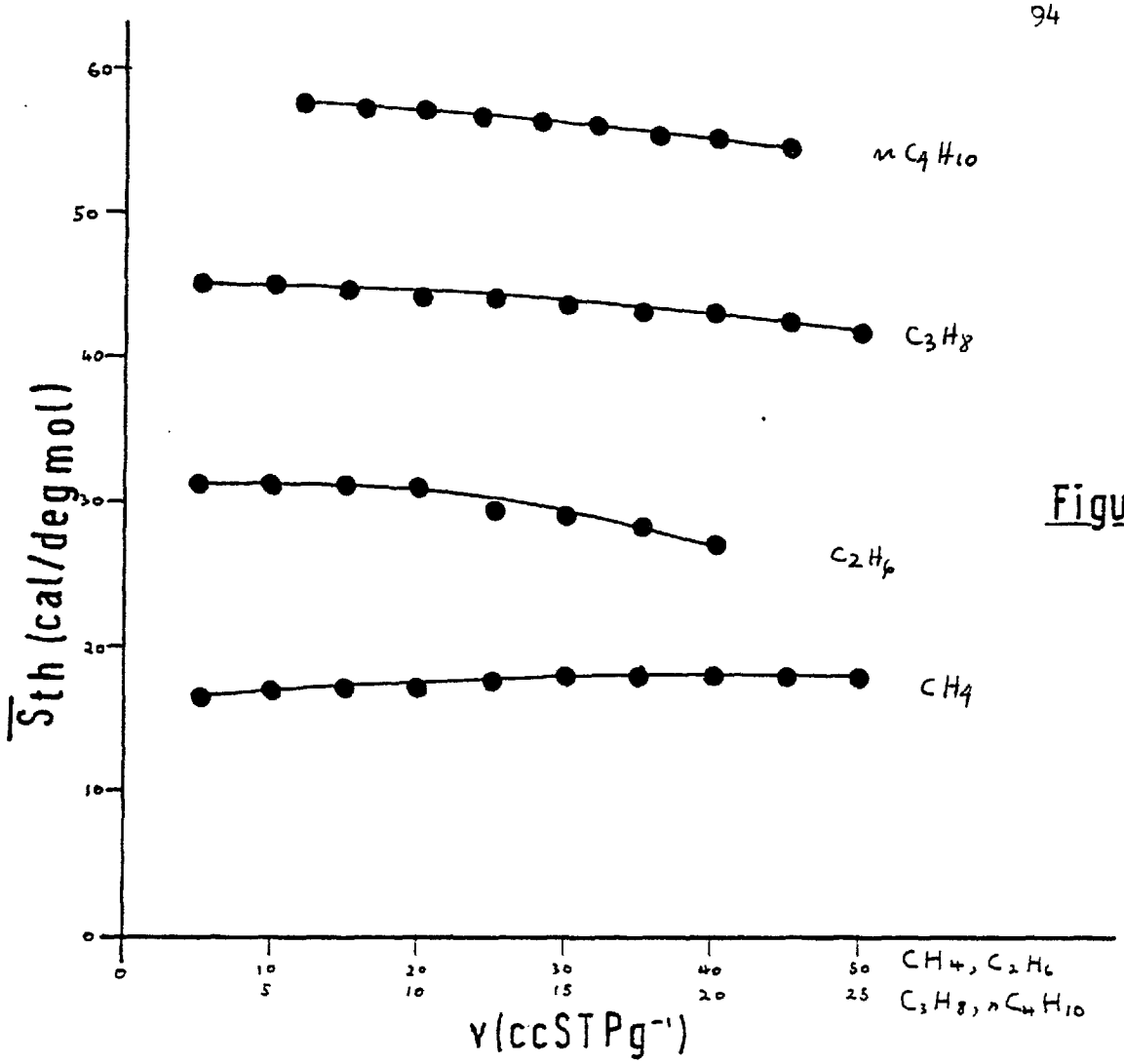

Figure 4-27

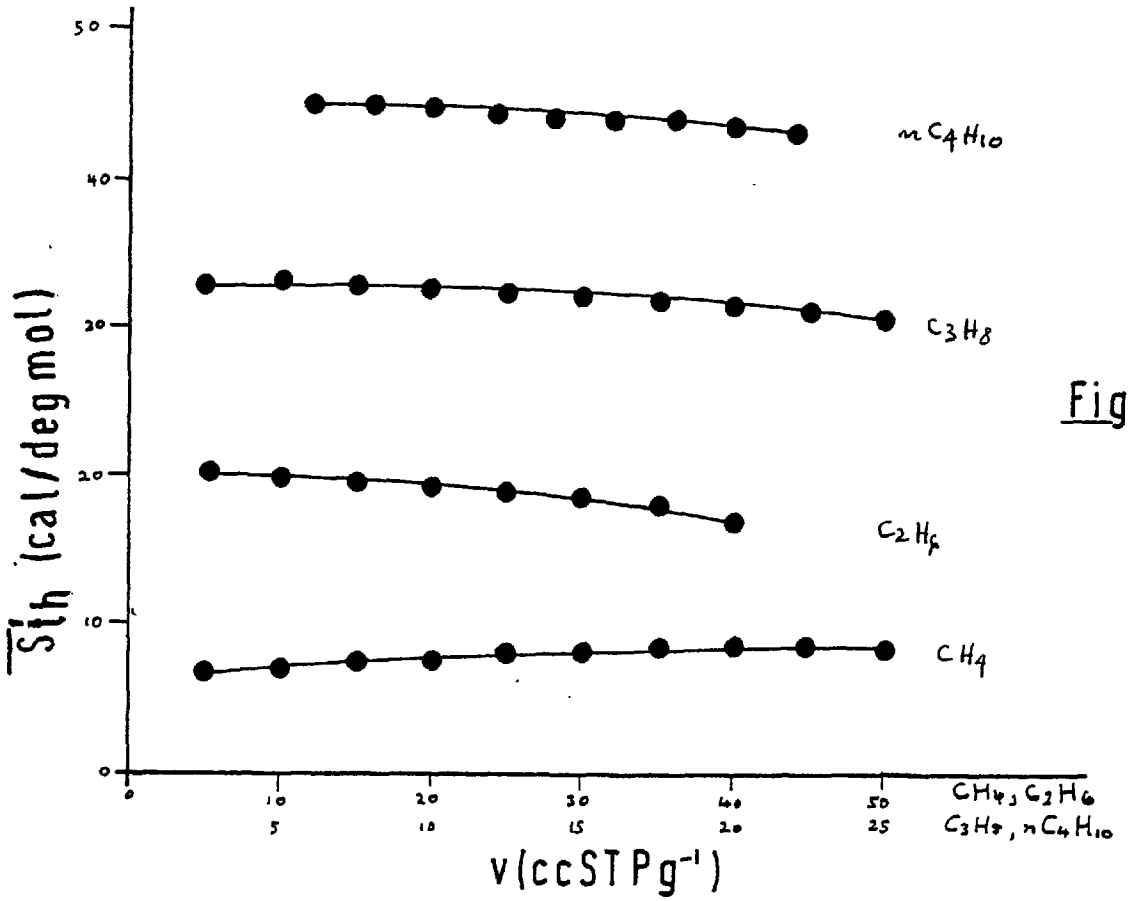

Figure 4-28

10

Kinetic Experiments in H-RHO

Sorption and desorption kinetic runs of n-hexane in H-RHO were performed at several temperatures. The rates (Q_t/Q_∞ vs t, Q_t is the quantity sorbed at time t and Q_∞ the quantity sorbed at equilibrium) are plotted in Figure 4.29.

On sorption the aim was to make runs in samples initially free of n-hexane and at a constant pressure (p_x = 45 torrs) to try to meet the boundary conditions :

$c \simeq o$ in the crystals at $t = o$

$c \simeq c_o$ just within the surfaces of crystals at $t > o$

After equilibrium was achieved in a sorption kinetic run at pressure p_x, desorptions were carried out by immersing the n-hexane bulb in liquid nitrogen to try to satisfy the boundary conditions :

$c \simeq c_o$ in the crystals at $t = o$

$c \simeq o$ just within the surfaces of crystals at $t > o$

Sorption and desorption will be called ideal when the boundary conditions already referred to are fully satisfied. We then expect for control by intracrystalline diffusion ($D = D_o \exp -E/RT$) that both sorption and desorption kinetics will have positive temperature coefficients and that curves of Q_t/Q_∞ vs time will coincide for sorption and desorption. Contrary to this expectation it is seen from Figure that :

(1) Sorption rates decrease when temperature increases.

(2) Desorption rates are much slower than the sorption rates (a difference which is too big to be understood in terms of heating on sorption and cooling in desorption or the concentration dependence of D), the difference being reduced at higher temperatures. These features require interpretation.

Let us assume first that the isotherms at two temperatures T_1 and T_2 ($T_1 < T_2$) are :

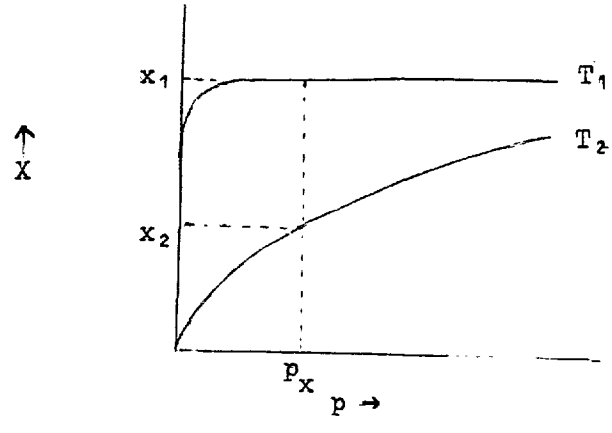

v = intracrystalline volume

Figure 4-29

n-hexane

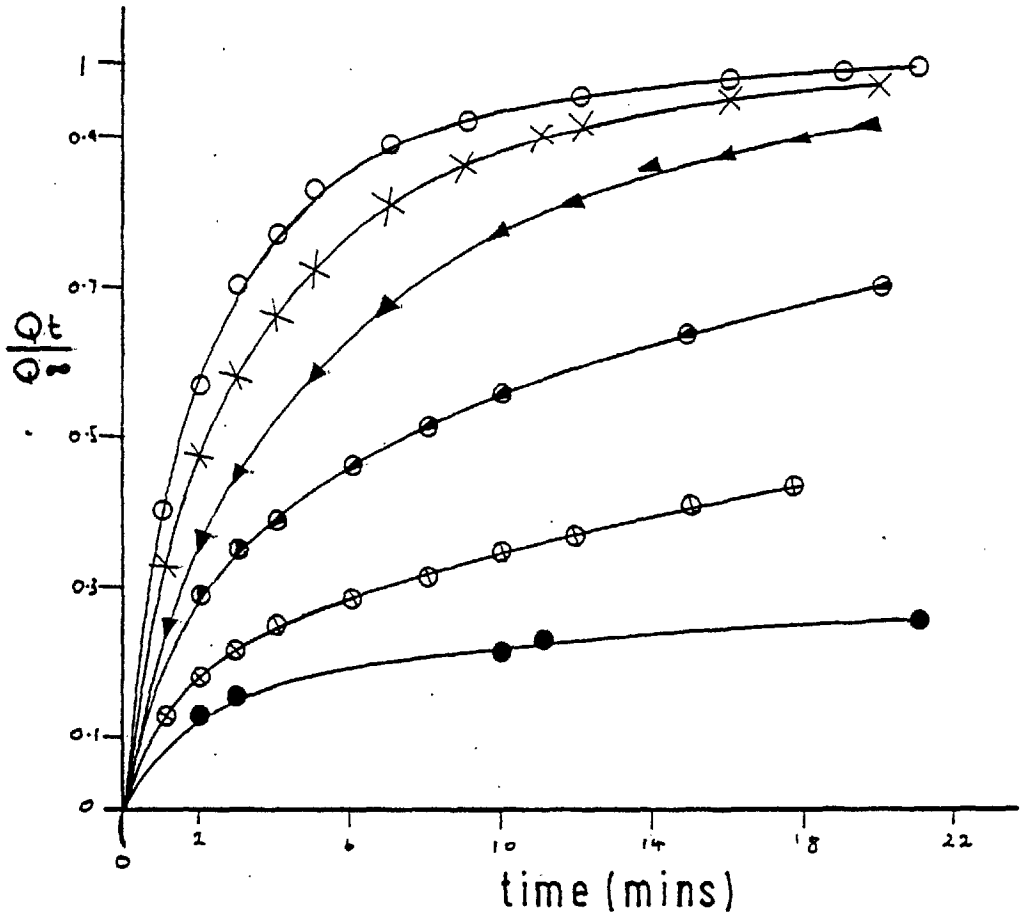

Sorption ○ 33·4°C
× 95·6°C
◄ 141·4°C

Desorption ● 33·4°C
⊕ 95·6°C
⊖ 141·4°C

Feature 1 can be explained in two ways :

(i) The true value of the pressure is not p_x but smaller than that. Thus when the vapour is admitted to the balance case the pressure drops as a result of the expansion and it can take more than ten minutes to re-establish to the value of p_x. If we compare this time with the half times of the kinetics (at 33.4°C $t_{\frac{1}{2}}$ = 1.5 min., at 95.6°C $t_{\frac{1}{2}}$ = 2.2 min., at 141.4°C $t_{\frac{1}{2}}$ = 3.5 min.) we realize that most of the sorption is taking place at a pressure smaller than p_x.

Let us see how our values of Q_t/Q_∞ compare with the ideal ones Q'_t/Q'_∞ :

At T_1 :

$Q_\infty = Q'_\infty$ because at the end of the run the pressure is re-established at p_x.

$Q_t \simeq Q'_t$ because although in our runs the pressure is smaller than p_x the concentration of sorbate just within the surface of the crystals is approximately constant at x_1/v due to the rectangular shape of the isotherms at T_1.

Therefore

$$\frac{Q_t}{Q_\infty} = \frac{Q'_t}{Q'_\infty} \text{ at } T_1$$

At T_2 :

$Q_\infty = Q'_\infty$ for the same reason as at T_1.

$Q_t < Q'_t$ The isotherm is less rectangular at T_2 and while in our experiments the concentration just within the surfaces of the crystals is less than x_2/v, in the ideal case it is x_2/v.

Therefore

$$\frac{Q_t}{Q_\infty} < \frac{Q'_t}{Q'_\infty} \text{ at } T_2.$$

Hence one could think that what is going on is as represented below :

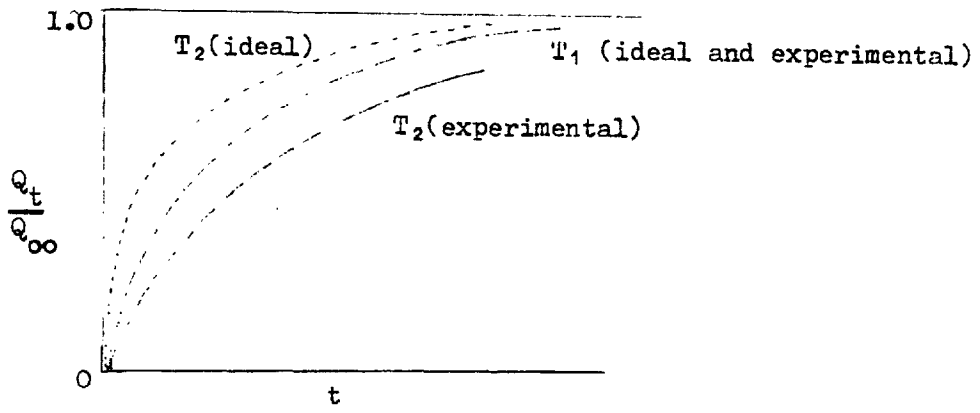

While at T_1 the experimental and ideal curves are equal, the experimental curve at T_2 is shifted below the experimental curve at T_1.

(ii) A further possibility is that there exists a pressure gradient along the bed :

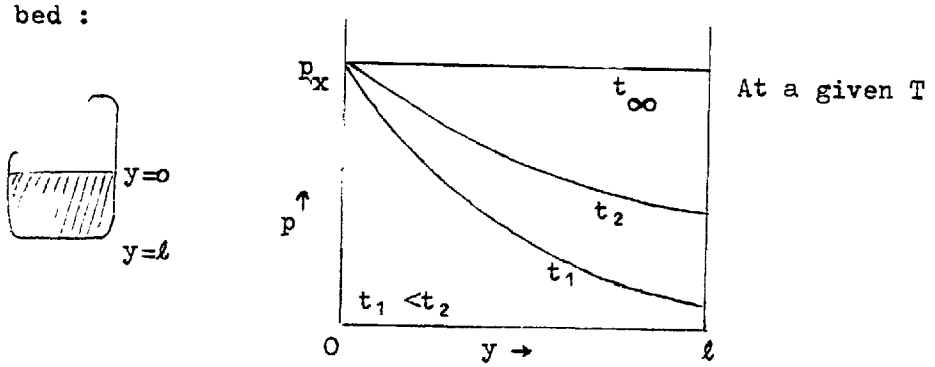

At T_1 notwithstanding the difference in pressure along y, the concentrations of sorbate just within the surfaces of the crystals are still approximately x_1/v for $0 \leq y \leq \ell$ because of the rectangular shape of the isotherm, and therefore the quantity, Q_t, sorbed at a given time is nearly equal to Q'_t for the ideal case. Since it is true as well that $Q_\infty = Q'_\infty$ then $Q_t/Q_\infty = Q'_t/Q'_\infty$.

At T_2 however at a given time, t, the concentrations of sorbate just within the surfaces of the crystals are less than x_2/v for $0 < y \leq \ell$ because the isotherm is less rectangular. Therefore :

$$Q_t = \int_0^\ell q_{yt}\, dy < Q'_t$$

$q_{yt}\, dy$ is the quantity sorbed at time t in a layer if the bed of thickness dy at a depth y

and since at the end of the run this pressure gradient has disappeared $Q_\infty = Q'_\infty$. Hence $Q_t/Q_\infty < Q'_t/Q'_\infty$ and therefore the existence of a pressure gradient would shift the rate at T_2 even more to smaller values.

The presence of a pressure gradient along the bed depends on the relative rates of diffusion of sorbate molecules in the crystals and between the crystals. If sorption in the crystals is much slower, then for the moment we begin to record values of Q_t the pressure along the bed should be constant, but when the rates in the crystals are fast it can happen that when we can record values of Q_t the pressure in the bed may not be uniform. Sorption rates of n-hexane in H-RHO are very fast and a pressure gradient is not unlikely to be present.

The second feature, which concerns the desorption kinetics, can also be explained by the presence of a pressure gradient along the bed:

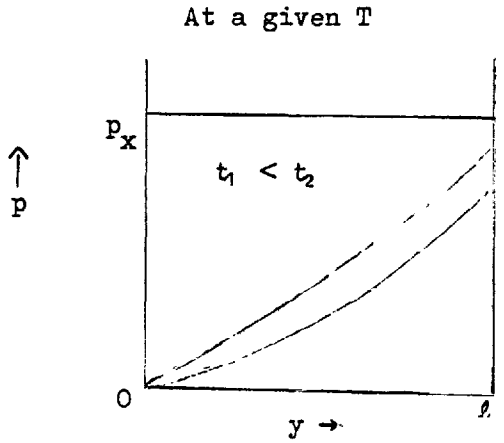

At T_1 due to the rectangular shape of the isotherm the existence of residual pressures in the region $0 < y \leq \ell$ means that the concentration of sorbate just within the surfaces of the crystals does not differ too much from x_1/v, the concentration at $t = o$, and therefore the rates of desorption from these crystals are much reduced.

At T_2 the isotherm is less rectangular and the concentration just within the surfaces of crystals will be small and the diffusion from them approach more the boundary condition $c = o$ at the surface for $t \geq o$

Conclusion :

The anomalous behaviour of sorption kinetics of n-hexane in H-RHO can be explained in terms of the failure to satisfy fixed boundary conditions. Because of this it is not possible to evaluate accurate diffusivities from the kinetics of sorption when the isotherms are very rectangular. The nearest to success in evaluating a diffusivity

within the crystals would be from sorption kinetics at the lowest temperature of 33.4°C. Under none of the conditions of this work could an intracrystalline diffusivity be evaluated from desorption kinetics of n-hexane.

Sorption kinetics runs were carried out as well for n-butane at 0°C, 30°C and 57°C. The sorption rates were very fast, the half life times for all the runs were less than a minute and in fact all fitted well in a unique plot (Figure 4.30). Therefore an apparent zero temperature coefficient is found with n-butane instead of the negative one found with n-hexane, probably because the range of temperatures is too small to observe it.

The large differences between sorption and desorption found with n-hexane were also obtained with n-butane. In agreement with the explanation given for n-hexane this difference was very small at 57°C. The same conclusion given for the n-hexane sorption kinetics applies for n-butane.

In another sample it was found that the rates of sorption of n-butane, although still fast, were slower than in the previous sample (Figure 4.30). Surprisingly the sorption rate of n-hexane was very small. Moreover this slow sorption has a very small temperature coefficient as one can see from the minor difference in rates in a range larger than 100°C. This is contradictory since if a sorption is slow E_a is large and the rates should have a large temperature coefficient. It was thought that the n-hexane bulb could be contaminated and the rate controlled by diffusion through impurities in the gas phase but sorption of the same n-hexane in the other sample was still fast. It was finally thought that some damage of the structure could have occurred in this sample. Both samples used were taken off the system and X-rayed showing that both were apparently equally well crystalline. A third sample of the H-RHO was prepared and the rates obtained with the first one were reproduced.

Figure 4-30

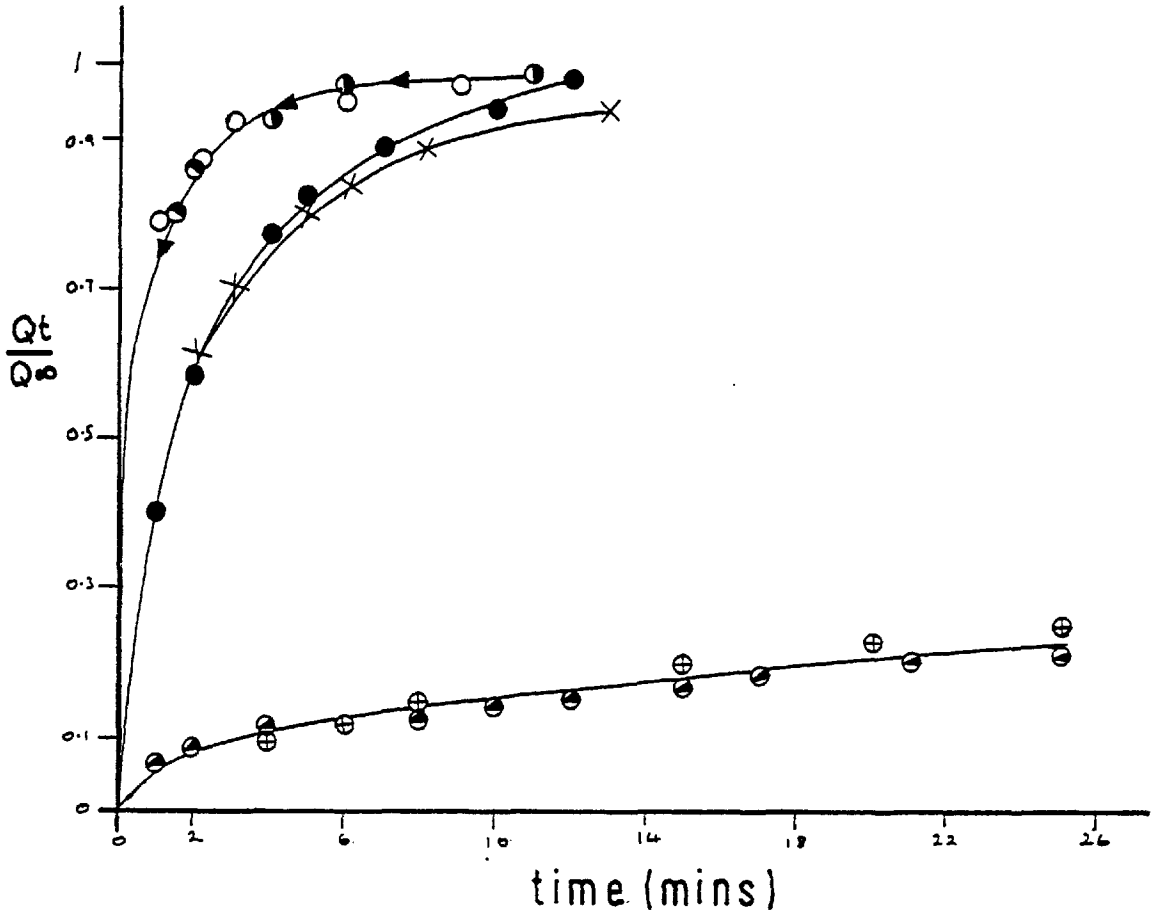

n-butane

sample 1 ◄ 37·1°C
◑ 0°C
○ 30°C

sample 2 ● 56·4°C

n-hexane

sample 1 × 33·4°C

sample 2 ⊖ 35°C
⊕ 156°C

Diffusion coefficient of n-hexane in H-RHO

Due to the anomalous behaviour of the sorption kinetics in H-RHO a study of the diffusion of the normal hydrocarbons was not possible. Nevertheless an average diffusion coefficient of n-hexane at 33.4°C was calculated using the time lag procedure (page [illegible]). The plot of $\int_0^t Q_t/Q_{oo}$ vs t is shown in Figure 4.31. It approaches a straight line of unit slope and the time lag was then obtained as the intercept of the line with the time axis. The value of D was then obtained with equation (46).

$$D = \frac{r_o^2}{15L}$$

where r_o the average radius of crystals was made equal to $\sqrt{\frac{2a^2}{2}}$ where a is the average side of the crystals.

The value of D is then :

$$D = \frac{2(5.6 \times 10^{-5})^2}{15 \times 3.2 \times 60} \times 10^{-1} = 2.18 \times 10^{-16} \ m^2 sec^{-1}$$

Figure 4-31

$\int_0^t \frac{Qt}{Q\infty}$ vs t

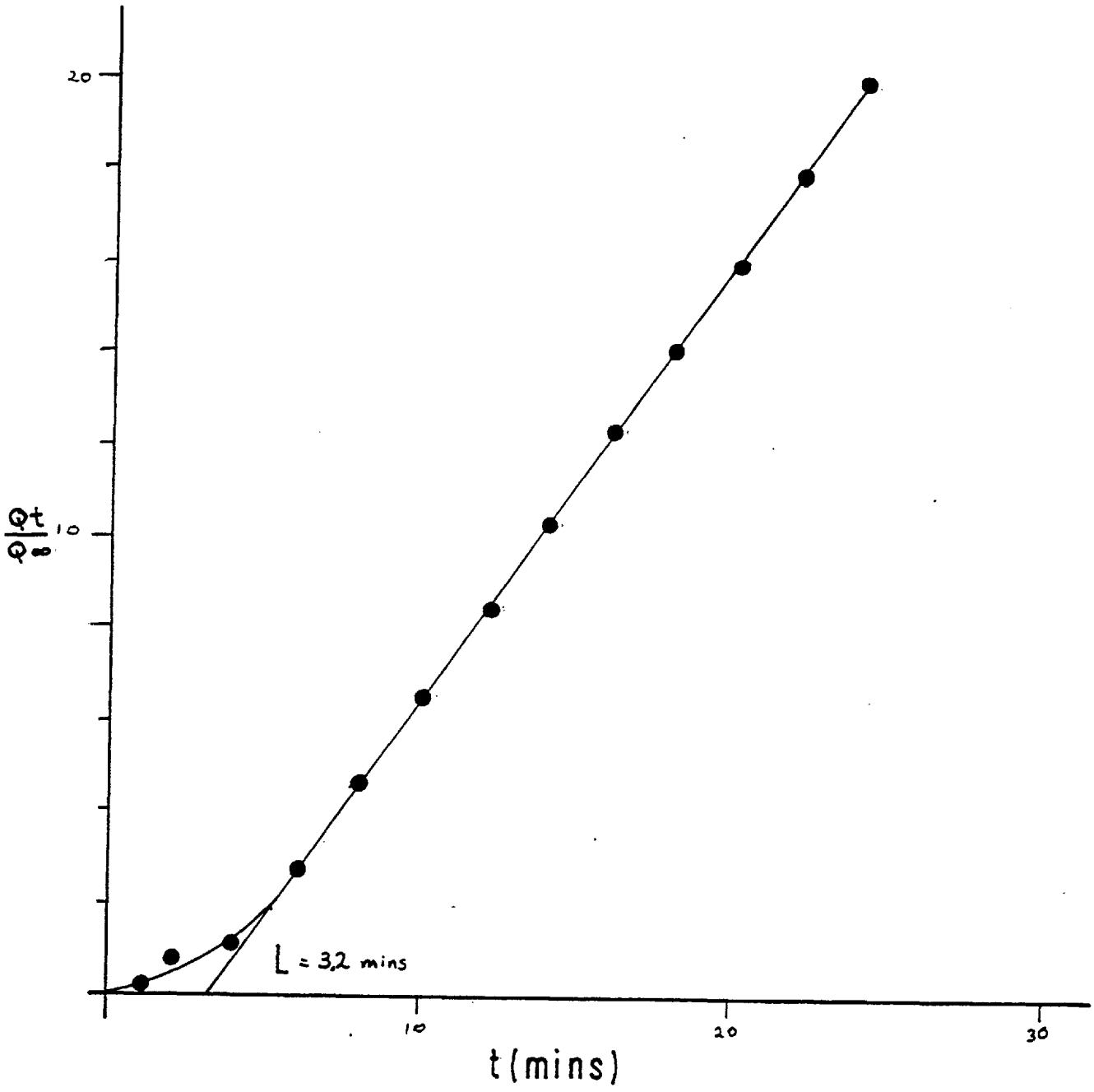

Summary

Zeolite RHO was synthesized according to Robson et al. (54). X-ray photographs were taken and the lines indexed. The lattice constant was 15.0 Å. When dehydrated a unit cell of 14.6 Å was produced. Some impurity lines were detected. Electron micrographs were taken showing that the crystals of RHO were of similar shape, and appeared to grow as simple cubes. An average size of the side of the crystals was measured. The as synthesized material was analysed, the unit cell composition is 7.8 Na^+, 5.1 Cs^+, 12.4 AlO_2, 35.6 SiO_2, 46.6 H_2O. Our ion exchange experiments showed that Cs^+ was difficult to remove with Na^+ or Ca^{+2}, concentrated exchange solutions and temperatures of 90°C being required, but it could be exchanged by NH_4^+ using 0.5 N solutions at room temperature.

Our first sorption experiments were carried out in a calcium form using n-butane, N_2, O_2 and CO_2 as sorbates. It was found that sorption was a small fraction only of the value expected since if the structure of RHO is correct the same volume accessible to water should be accessible to these sorbates. Still the sorption was too big to be taking place only at the external surfaces of the crystals and it is believed to occur mainly in the impurity crystals. The structure of RHO was thus blocked presumably because calcium cations are located in the octagonal prisms hindering the passage of molecules into the zeolite. Only dipolar molecules H_2O and NH_3 were sorbed, probably because they can move the cations from the prisms and squeeze into the zeolite. It was however surprising to find that the hydrogen form was still blocked after activating the NH_4-form by outgassing to 360°C.

Flank (63) then also reported that sorption of O_2 in cationic forms and hydrogen forms of zeolite RHO was very small but that when the hydrogen form is outgassed at 400°C instead of the usual outgassing temperature of 360°C, O_2 and even n-butane were sorbed copiously. According to him only at that temperature had enough NH_4^+ from the zeolite been decomposed to make the pore volume of the zeolite available for sorption. This is not indeed unreasonable since if the octagonal prisms are very good places to locate cations (there would be sixteen oxygen atoms surrounding them) higher temperatures than those usually needed might be required to liberate the NH_3 from them.

We then proceeded to repeat Flank's activation process. The preparation of a good sorbent was not however straightforward. Long treatments with ammonium chloride solutions were required and the outgassing procedure was important since (and this was also reported by Flank) H-RHO was unstable to water vapour at outgassing temperatures. A stabilizing procedure was developed and the highest capacity was obtained with the stabilized materials.

A sorption study was then made using the stabilized H-RHO. Sorption isotherms were measured for O_2, N_2, CO_2, Ar, Kr, Xe and CH_4, C_2H_6, C_3H_8, $n\text{-}C_4H_{10}$. It was concluded that all the pore volume is accessible to all the sorbates studied, an observation which is in agreement with the structure proposed by Robson. A calculation also showed that within the experimental error the number of molecules adsorbed per α cage (26-hedron) in RHO is equal to the number sorbed per α cage in A, which is a further corroboration of the structure and of the reliability of our stabilized materials.

From a set of accurate isotherms at four temperatures, heats of adsorption were determined versus amount sorbed at small and intermediate amounts. For O_2, N_2, CO_2 and the rare gases the heat is rather constant with amount sorbed indicating that H-RHO is a homogeneous sorbent. The magnitude of the heats is higher than in zeolite A by about 1 kcal/mol which can be due to the fact that zeolite RHO contains apart from the 26-hedron, (which is the cavity involved in sorption by A) octagonal prisms and the energy of adsorption in them as was demonstrated by a calculation is much enhanced.

Entropies of the sorbed phase were also calculated and plotted versus amount sorbed. For O_2, N_2, CO_2, Ar, Kr, Xe the entropies decrease continuously as required for a homogeneous sorbent. From the shift of these curves with temperature the heat capacity of the sorbed phase was evaluated and the physical state of the sorbed molecules relative to their intracrystalline environment considered. The state was never determined without ambiguity and two possible states were assigned to each sorbate.

For C_2H_6, C_3H_8 and nC_4H_{10} the heat of adsorption increases to some extent as the amount sorbed increases presumably due to interaction

between the sorbed molecules. For CH_4 the heat decreases a little with amount sorbed much in the same way as for O_2, N_2, CO_2, Ar, Kr and Xe. The initial heats increase linearly with the number of carbon atoms in the hydrocarbon indicating they depend mainly on $\emptyset_D + \emptyset_R$. The value for CH_4 was a little above the line but this is probably because at low uptakes the methane molecules occupy the octagonal prisms. For the larger paraffins the octagonal prisms are not sites of high interaction because when one part of the molecule is in the prism the rest is not. When for CH_4 a value of q_{st} is taken at larger amounts sorbed the point is much closer to the line. The entropies of the sorbed phase were also determined for the hydrocarbons. The curves of entropy versus amount sorbed indicated again the homogeneous character of the sorbent. Two possible physical states for the sorbed hydrocarbons were considered: (1) the molecules are localized and have three degrees of vibrational freedom, and (2) the molecules have some mobility, one translational degree of freedom replacing one vibration. None of the models was quite applicable.

Finally sorption kinetics of n-hexane were investigated. The sorption was very fast and it showed a negative temperature coefficient. Also a large difference was observed between the sorption and desorption rates. Both anomalous features were explained in terms of the failure to satisfy fixed boundary conditions. Because of this a study of diffusion of the n-paraffins in H-RHO was not possible to carry out.

REFERENCES

1. e.g. Walker, J. Geology, 68, 515 (1960).
2. e.g. Deffeyes, J. Sediment. Petrol. 29, 602 (1959).
3. Breck, "Zeolite Molecular Sieves", p.38, John Wiley and Sons (1974).
4. Lowenstein, Amer. Mineralog., 39, 92 (1954).
5. Deer, "Rock Forming Minerals", Vol. 4, John Wiley and Sons (1963).
6. Smith, Mineral. Soc. Amer. Spec. paper No.1 (1963).
7. Meier, "Molecular Sieves", The Soc. of Chem. Ind., p.10, London (1968).
8. Breck, "Zeolite Molecular Sieves", p.45, John Wiley and Sons (1974).
9. Barrer, "Zeolites and Clay Minerals", p.44, p.51, Academic Press (1978).
10. Barrer and Kerr, Trans. Faraday Soc., 55, 1915 (1959).
11. Barrer, Chem. in Britain, 3, 380 (1967).
12. Zhdanov, "Molecular Sieves", The Soc. of Chem. Ind., p.62, London (1968).
13. Barrer and Denny, J. Chem. Soc., 983 (1961).
14. Zhdanov, "Molecular Sieve Zeolites", Adv. Chem. Ser., 101, p.20, American Chemical Society, Washington D.C. (1971).
15. Kerr, J. Phys. Chem., 70, 1047 (1966).
16. Breck and Reed, J. Amer. Chem. Soc., 78, 5963 (1956).
17. Gregg, "The Surface Chemistry of Solids", p.285, Chapman and Hall Ltd (1961).
18. Breck, "Molecular Sieves", Adv. Chem. Ser., 121, p.319, American Chemical Society, Washington D.C. (1971).
19. Keough and Sand, J. Amer. Chem. Soc., 83, 3534 (1961).
20. Barrer and Makki, Can. Jour. Chem., 42, 1481, 1964.
21. Barrer, Nature, 164, 112 (1949).
22. ed. by Rabo, "Zeolite Chemistry and Catalysis", p. 285 ACS monograph 171, 1976.
23. Kerr, J. Phys. Chem., 71, 4155 (1967).
24. Langmuir, J. Amer. Chem. Soc., 40, 1361 (1918).
25. Volmer, Z. Phys. Chem., 115, 253 (1925).
26. Fowler, Proc. Camb. Phil. Soc., 31, 260 (1935).
27. Brunauer, Emmett, Teller, J. Amer. Chem. Soc., 60, 309 (1938).
28. Polanyi, Trans. Faraday Soc., 28, 316 (1932).
29. Dubinin, Chem. Rev., 2, 235 (1960).
30. London, Trans. Faraday Soc., 33, 8 (1937).
31. Salem, Mol. Phys., 3, 441 (1960).

32. Kington, McLeod, Trans. Faraday Soc., 55, 1799 (1959).
33. Barrer and Stuart, Proc. Roy. Soc., 249, 479 (1959).
34. Barrer and Davies, Proc. Roy. Soc. Lond. A, 320, 289-308 (1970).
35. Barrer and Gibbons, Trans. Faraday Soc., 59, 2569 (1963).
36. Barrer and Stuart, Proc. Roy. Soc., 249, 464-483 (1959).
37. Barrer and Coughlan, "Molecular Sieves", Soc. Chem. Ind., 241 (1968).
38. Barrer and Gibbons, Trans. Faraday Soc., 61, 948 (1965).
39. Hill, J. Chem. Phys., 14, 441 (1946).
40. Garden, Kington, Laing, Proc. Roy. Soc., A234, 35 (1956).
41. Crank, Mathematics of Diffusion, Oxford Univ. Press, 2nd edition (1975).
42. Barrer, Trans. Faraday Soc., 45, 368 (1949).
43. Ash, Barrer, Craven, J. Chem. Soc., Faraday Trans. 74, 40 (1978).
44. Ruthven and Derrah, J. Chem. Soc., Faraday I, 71, 2031 (1975).
45. Walker, Chemistry and Physics of Carbon, Volz, 257 (1966).
46. Barrer, Trans. Faraday Soc., 45, 358 (1949).
47. Barrer and Ibbitson, Trans. Faraday Soc., 45, 358 (1949).
48. Eberly, Ind. Eng. Chem. Prod. Res. and Dev., 8, 140 (1969).
49. Barrer and Clarke, J. Chem. Soc., Faraday I, 70, 535 (1974).
50. Barrer, "Molecular Sieve Zeolites", Adv. Chem. Ser. 102, p.1 (1971).
51. Satterfield and Frabetti, Am. Int. Chem. Eng., 13, 731 (1967).
52. Ruthven and Loughling, Chem. Eng. Sci., 26, 577 (1971).
53. Barrer, "Molecular Sieve Zeolites", Adv. Chem. Ser. 102, p.11, (1971).
54. Robson et al., "Molecular Sieves", 106, Adv. Chem. Ser. 121 (1973).
55. Erdey, "Gravimetric Analysis", Part I, 302, Pergamon Press (1963).
56. Erdey, "Gravimetric Analysis", Part III, 194, Pergamon Press (1963).
57. Erdey, "Gravimetric Analysis", Part I, 36, Pergamon Press (1963).
58. Erdey, "Gravimetric Analysis", Part II, 296, Pergamon Press (1963).
59. Erdey, "Gravimetric Analysis", Part III, 193, Pergamon Press (1963).
60. Erdey, "Gravimetric Analysis", Part II, 732, Pergamon Press (1963).
61. Vogel, "Qualitative Inorganic Analysis", 256, Longmans (1961).
62. Barri, D.I.C. Thesis, Imperial College (1978).
63. Flank, "Molecular Sieves II" A.C.S. Symp. series 40, Ed. Katzer P. 43 (1977).
64. Breck, "Molecular Sieves", Adv. Chem. Ser. 121, p.319, American Chemical Society (1973).
65. Breck and Grose, "Molecular Sieve Zeolites", p.428, John Wiley and Sons (1973).

66. Barrer, "Zeolites and Clay Minerals", p.174, Academic Press (1978).
67. Barrer, J. Coll. and Interface Sci., 21, 415 (1966).
68. Harper et al., Can. Jour. Chem. 47, 4661 (1969).
69. Hirschfelder, "Molecular Theory of Gases and Liquids", p.32, Wiley (1954).
70. Salem, Molec. Phys., 3, 441 (1960).
71. Orr, Trans. Faraday Soc., 35, 1247 (1939).
72. Selected Values of Chemical Thermodynamic Properties, Nat. Bur. of Standards (1952).
73. Barrer and Bratt, Phys. Chem. Solids, 12, 146 (1959).
74. Barrer and Coughlan, "Molecular Sieves", Soc. Chem. Ind., Lond. (1968), p.241.
75. Barrer and Davies, Proc. Roy. Soc., A322, 1 (1971).
76. Barrer and Lee, Surface Science, 12, 341 (1968).
77. Barrer and Langley, J. Chem. Soc., 3817 (1958).
78. 'Selected Values of Properties of Hydrocarbons and Related Compounds', American Petroleum Institute Research Project 44 (U.S.A.).

22

APPENDIX A

Sorption experiments in samples outgassed at 360°C. (All samples prepared from the synthesis 1 material except where indicated).

p in mm Hg
v in cc STP per outgassed gram of zeolite
x in grams per outgassed gram of zeolite.

n-butane Ca-RHO

T = 25°C		T = 97°C	
p	x	p	x
60.6	0.030	65	0.017

Oxygen Ca-RHO

T = 77 K

p	v
1.77	24.79
2.44	36.40
21.08	44.03
34.90	45.50
45.07	46.90
71.78	48.72
90.58	50.47
100.20	52.50
109.0	53.20
147.49	68.18
160.0	89.81

Nitrogen Ca-RHO

T = 77 K

p	v
0.01	14.14
23.51	35.52
108.88	37.04
207.46	37.60
289.42	37.76
391.50	38.40
419.95	38.96
459.73	39.20

Carbon dioxide Ca-RHO

T = 195 K

p	v
1.3	16.04
60.9	28.56
130.1	30.14
222.5	30.60
338.01	31.36
401.7	31.82
459.4	31.97

Oxygen H-RHO

T = 77 K

p	v
3.67	38.57
43.20	49.10
85.89	52.36
145.07	69.86

Nitrogen H-RHO

T = 77 K

p	v
88.22	34.10
192.82	36.50
254.68	37.33
328.92	38.91
380.15	40.40
423.08	40.98

H_2O Ca-RHO
T = 34.01°C

p	v
-	85.96
-	116.94
-	146.79
2.79	263.85
9.20	295.01
14.90	342.60
21.10	367.11

NH_3 Ca-RHO
T = 101°C

p	v
16.29	119.6
31.15	127.15
52.11	135.19
72.98	141.12
106.59	145.73
223.11	156.67

Oxygen Ca-RHO Synth. 2
77 K

p	v
10.59	56.63
70.45	65.08
146.54	74.83

Oxygen Ca-RHO Synth. 3
77 K

p	v
0.71	15.61
39.48	22.89
73.96	24.43
116.15	27.86
124.27	28.77
144.47	33.88
159.89	44.03

APPENDIX B

Oxygen sorption experiments in hydrogen forms outgassed at 400°C (see Table page) T = 77 K p in torrs v in cc STP g^{-1}

Sample 1

p	v
17.81	39.48
65.71	44.31
102.01	49.28

Sample 2a

p	v
0.98	45.08
3.52	69.86
42.21	81.13
94.22	84.00
164.69	88.06

Sample 2b

p	v
-	65.03
0.88	120.19
24.93	147.14
51.50	175.98
62.74	182.0
86.5	193.76
139.5	205.8
150.25	211.96

24

3a		3b A		3b B		3b C		3b D	
p	v	p	v	p	v	p	v	p	v
-	182.56	-	247.45	-	199.9	-	223.26	1.85	213.85
10.64	220.29	9.6	265.55	1.32	249.9	7.55	286.66	34.7	286.3
64.54	230.93	28.86	269.22	5.95	267.3	43.9	297.90	67.02	290.8
83.8	233.8	55.73	273.0	24.57	272.6	58.59	299.87	93.15	294.9
118.14	240.17	74.13	274.96	90.09	281.4	90.48	303.17	116.69	299.1
140.72	251.93	100.19	278.11	113.17	284.5	113.87	306.35	132.48	309.6
151.30	269.22	121.32	280.63	142.9	303.9	139.0	311.92	155.34	360.8
		148.57	301.63	151.94	358.6	157.79	325.3		
		129.83	289.1	155.17	326.1	135.75	314.44		
		100.18	279.65	140.37	304.0	111.76	308.57		
		65.46	275.73	102.37	289.9	77.43	304.19		
		44.25	272.44	63.23	286.3	48.54	301.26		
		23.95	264.25	40.31	280.7	31.7	295.87		
		13.53	261.80	25.07	277.3	19.81	292.63		
		8.09	259.91	11.22	274.5	12.27	290.57		
		6.44	258.16	5.8	272.3	8.89	219.02		
				4.05	270.7				

25

APPENDIX C

Sorption of gases.

Isotherms, p in torrs, v in cc STP g^{-1}

Nitrogen

77 K		195 K				216 K	
p	v	p	v	p	v	p	v
0.77	196.8	4.37	4.13	32.58	19.62	8.69	1.89
1.92	203.2	8.56	6.84	25.03	15.68	14.97	2.96
3.19	215.76	13.33	9.53	19.56	13.10	29.85	5.29
9.32	224.32	18.95	12.36	15.54	10.98	40.1	7.14
35.42	231.2	28.51	16.67	12.53	9.30	54.99	9.29
59.44	234.32	38.1	20.27	10.37	7.88	70.31	11.29
99.82	236.96	50.13	24.39	8.5	6.75	85.48	13.00
139.8	238.24	63.29	29.02	7.39	5.72	108.97	15.80
193.69	240.0	75.25	30.97			147.08	19.47
255.37	243.68	86.54	34.32			180.27	22.39
357.49	246.16	103.17	37.54			231.02	26.48
228.5	242.4	115.63	39.61			297.51	30.48
138.97	239.2	155.15	45.43			354.22	33.86
83.97	237.2	179.37	48.27			322.85	32.26
54.62	234.48	201.77	50.95			289.49	30.66
24.89	230.32	248.0	55.61			261.82	28.65
15.22	226.88	311.37	61.04			218.01	25.47
10.49	224.72	374.70	64.11			175.92	21.84
		325.39	60.95			139.39	18.83
		247.06	54.83			105.01	15.13
		210.73	51.28			82.57	12.74
		182.18	48.25			59.67	10.16
		156.88	45.13			43.61	8.03
		137.13	42.45			31.05	6.21
		114.33	39.36			21.98	5.19
		95.43	36.07			13.65	3.48
		84.33	33.30			8.39	2.44
		66.89	29.13				
		56.17	26.16				
		44.64	23.27				

208 K		231 K		249 K	
p	v	p	v	p	v
3.97	1.83	11.21	1.08	11.86	0.30
10.12	3.47	23.53	1.97	25.48	0.67
28.19	8.43	30.49	2.47	46.74	1.42
38.17	10.65	41.52	3.34	65.02	1.98
50.71	13.23	56.78	4.52	92.12	2.99
60.56	15.20	76.05	5.91	118.38	3.67
78.96	18.36	101.98	7.65	144.01	4.41
100.55	21.59	126.78	9.17	193.66	5.60
120.64	24.32	148.07	10.54	228.65	6.38
145.65	27.47	167.58	11.55	267.14	7.41
189.97	32.02	198.46	13.34	302.16	8.47
215.69	34.63	230.53	14.87	275.98	8.25
261.73	37.95	272.34	16.61	247.01	7.57
302.27	40.80	314.73	18.72	219.23	6.82
342.61	43.23	329.0	19.56	180.92	5.85
306.56	41.00	286.78	17.89	156.8	5.19
276.9	39.08	249.01	15.93	118.37	4.15
249.4	37.26	218.19	14.65	81.82	3.02
222.35	34.88	196.77	13.63	62.35	2.50
198.93	32.82	174.34	12.51	39.74	1.85
171.97	30.43	141.19	10.41	23.25	1.43
145.41	27.50	120.44	9.46	15.67	1.24
115.78	23.98	99.35	7.97	5.4	0.76
87.81	20.36	77.81	6.50		
74.55	18.18	56.83	5.17		
61.93	16.09	44.39	4.16		
51.95	14.29	29.41	3.07		
41.13	12.3	18.85	2.31		
32.03	10.54	8.76	1.35		
23.9	8.75	4.01	0.92		
18.91	7.50				
14.14	6.35				
10.02	5.04				

27

Oxygen

90 K		195 K		175 K			
p	v	p	v	p	v	p	v
-	159.6	9.35	2.22	3.0	2.85	138.75	47.00
1.56	202.65	22.21	4.93	6.12	5.36	126.12	44.80
1.65	215.6	36.07	7.92	10.86	9.31	109.73	41.25
10.50	231.63	57.97	11.65	17.18	12.96	99.38	39.8
18.80	239.54	74.51	13.99	23.11	15.51	87.36	37.07
44.27	244.65	96.61	17.29	29.38	18.95	71.49	33.76
74.51	247.24	119.32	20.07	39.62	23.03	59.45	30.65
125.67	249.69	147.21	23.34	50.38	26.54	48.11	27.36
156.74	251.37	179.35	26.50	62.66	30.17	39.03	24.97
200.99	252.28	216.96	29.83	77.14	34.11	32.08	22.59
238.67	253.19	252.28	32.62	94.58	38.24	26.18	20.01
247.98	253.89	286.02	35.21	115.3	42.09	20.85	17.22
209.43	252.49	315.97	37.38	131.29	45.02	16.95	14.93
155.37	250.25	368.75	40.85	153.03	48.59	13.89	13.06
108.23	248.08	411.99	43.34	186.67	52.52	11.59	11.48
83.48	247.24	373.39	41.17	214.22	57.37	10.00	10.11
52.1	245.77	327.19	38.25	243.41	60.95		
30.92	243.81	283.68	35.38	272.2	64.23		
12.76	239.89	250.85	32.68	301.87	67.58		
10.84	237.65	199.58	28.48	330.95	70.38		
8.55	235.34	156.90	24.34	355.73	73.04		
6.6	233.73	128.35	21.29	336.65	71.26		
		103.42	18.17	317.29	69.53		
		75.35	14.57	295.21	67.01		
		55.06	11.52	274.4	64.83		
		40.25	8.99	254.52	62.39		
		24.97	8.99	234.96	60.23		
		15.40	4.18	211.63	57.36		
		9.66	3.06	193.95	55.05		
				171.11	51.86		
				157.67	49.80		

28

215 K		230 K	
p	v	p	v
24.57	2.22		
55.06	4.76		
77.18	6.46		
102.86	8.35	11.49	0.35
130.11	10.13	36.18	1.44
159.12	12.02	69.39	2.73
194.91	14.00	97.45	3.76
225.36	15.75	129.8	4.86
260.06	17.62	164.8	6.19
291.34	19.08	205.69	7.40
319.55	20.38	241.89	8.45
368.1	22.58	274.13	9.44
337.87	21.35	328.7	11.05
297.05	19.37	381.66	12.70
259.54	17.47	338.84	11.47
233.04	16.17	300.9	10.29
202.72	14.58	273.14	9.47
171.82	12.73	239.51	8.63
142.95	10.84	200.9	7.27
123.97	9.50	173.19	6.44
91.82	7.35	133.41	5.07
68.93	5.63	98.71	3.75
50.7	4.30	77.15	3.07
33.67	2.97	50.36	2.09
23.24	2.17	28.6	1.09
10.71	1.05	15.09	0.77
		5.27	0.45

29

Carbon dioxide

195 K		288 K		308 K		328 K		348 K	
p	v	p	v	p	v	p	v	p	v
0.47	9.44	3.0	8.20	6.9	6.78	15.27	6.19	26.85	4.75
0.38	25.13	8.84	17.81	15.95	13.01	39.67	13.21	66.54	10.12
0.46	41.65	17.12	27.17	28.71	19.89	66.4	19.15	98.66	13.73
0.83	59.21	35.44	40.74	42.29	25.84	92.06	23.93	130.26	17.63
1.10	77.08	60.00	51.52	58.58	31.16	135.12	30.57	176.58	20.92
2.09	108.46	112.27	65.92	86.05	38.76	194.38	37.68	243.26	25.92
4.85	137.09	175.75	77.06	120.65	45.70	255.83	43.53	318.08	30.68
7.38	145.45	249.1	85.35	168.6	53.29	334.73	49.40	361.04	33.08
13.39	153.05	349.3	93.07	234.75	61.09	357.11	50.74	302.81	29.91
20.81	158.44	388.86	95.6	304.6	67.27	304.17	47.36	268.26	27.87
42.1	165.51	331.1	92.12	351.69	70.59	246.97	42.96	217.94	24.45
78.65	170.62	277.12	88.21	302.33	67.14	193.77	37.78	159.55	19.85
139.1	175.39	210.25	81.88	254.31	63.28	137.31	31.00	116.15	15.76
218.8	178.6	159.05	75.57	231.96	61.18	95.36	24.80	80.77	12.05
313.8	180.82	122.75	69.32	208.35	58.64	68.56	19.79	41.75	7.13
360.61	182.41	95.57	63.58	181.99	55.58	48.05	15.22	23.47	4.34
266.28	180.58	70.53	56.92	154.5	51.91	31.42	11.34		
195.47	178.61	70.91	56.27	133.56	48.68	22.08	8.52		
130.17	175.58	54.15	51.19	111.13	44.68				
88.47	172.53	41.4	45.60	95.85	41.48				
59.05	169.38	32.12	41.25	77.82	37.15				
38.35	165.88	24.86	37.54	55.53	31.21				
26.85	162.61			40.59	25.98				
20.44	160.06			30.92	21.95				
16.84	157.77			24.06	18.83				
				19.63	16.28				

Argon

90 K		177 K		196 K		217 K		238 K	
p	v	p	v	p	v	p	v	p	v
-	143.16	3.72	4.60	10.97	3.25	18.12	1.81	15.72	0.39
0.17	188.74	9.15	8.69	24.95	6.60	42.45	3.88	25.38	0.69
2.17	235.87	15.7	12.98	39.99	10.09	70.45	6.12	45.67	1.31
51.98	263.98	24.72	17.90	59.31	13.61	98.27	8.20	67.06	2.07
138.3	268.86	35.85	22.63	81.44	17.16	128.95	10.44	94.54	2.94
209.67	271.36	50.83	27.26	109.32	21.02	165.12	12.57	130.47	4.10
269.15	273.64	63.71	30.77	138.55	24.43	200.86	14.53	158.72	4.89
327.88	275.07	85.37	35.58	167.95	26.80	235.89	16.33	194.08	5.79
201.58	272.94	108.72	39.90	202.49	30.51	269.5	18.17	241.18	7.23
148.25	270.05	142.25	45.17	232.98	33.06	297.85	19.56	291.41	8.58
110.11	268.18	167.32	48.86	265.1	35.56	356.59	22.07	344.67	9.87
61.38	265.44	198.92	53.05	312.7	38.80	398.9	23.94	397.02	10.95
38.66	263.25	252.35	59.62	356.44	41.54	347.26	21.70	356.91	9.94
25.15	261.38	305.33	64.72	330.67	40.09	310.14	20.40	324.89	9.13
12.78	256.47	357.41	70.4	290.95	37.46	266.61	18.37	288.02	8.36
8.24	253.81	311.83	66.26	251.62	34.87	219.31	15.95	239.58	7.13
5.85	251.31	279.58	63.12	222.43	32.78	178.4	13.51	196.76	6.00
		241.25	59.1	191.4	30.09	148.3	11.71	156.28	4.90
		205.71	55.0	166.77	27.98	122.08	10.10	116.91	3.74
		167.56	50.18	141.34	25.49	89.61	7.91	89.57	2.82
		142.15	45.7	111.97	22.25	65.37	6.07	64.37	1.94
		111.36	41.6	86.64	19.03	46.94	4.56	46.44	1.61
		86.89	37.10	66.53	16.01	30.69	3.26	24.73	0.83
		69.35	23.79	53.59	13.92	15.13	1.70	7.97	0.32
		53.73	28.14	39.72	11.50	6.82	1.08		
		41.11	24.92	27.73	9.20				
		33.27	22.4	17.45	7.17				
		24.9	19.2	13.01	5.68				
		20.38	16.58						
		15.74	14.64						
		14.38	12.8						
		11.72	11.4						

31

Krypton

90 K		213 K		233 K		253 K		275 K	
p	v	p	v	p	v	p	v	p	v
-	186.36	6.85	9.66	16.46	7.52	16.81	3.03	28.3	1.79
-	230.95	15.51	17.96	34.01	13.89	29.72	5.12	59.09	3.60
-	241.20	27.58	25.43	56.72	19.85	50.12	8.11	99.21	5.81
1.25	215.27	47.63	34.09	88.51	26.39	75.9	11.49	142.69	7.99
2.86	240.46	66.14	40.29	125.52	32.77	109.41	15.61	183.18	9.86
3.85	243.67	91.83	47.46	189.9	40.72	152.05	19.93	251.87	12.94
4.59	245.77	138.63	57.84	256.7	48.40	193.3	23.53	333.74	16.22
5.44	247.81	194.2	67.60	331.52	54.88	237.14	27.03	383.23	18.23
6.39	249.80	258.08	76.11	372.85	58.13	292.58	30.90	311.08	15.47
10.6	252.63	325.05	83.04	306.95	53.03	368.07	35.52	236.0	12.31
15.8	256.19	320.49	86.66	252.77	48.32	380.35	36.33	188.0	10.21
18.79	262.1	317.99	82.53	215.0	44.36	328.23	33.17	126.65	7.15
		249.08	75.41	171.7	39.33	268.18	29.43	77.4	4.45
		181.19	65.95	128.05	33.37	212.82	25.18	44.45	2.57
		134.03	57.51	98.78	28.81	154.98	20.28	17.4	0.936
		94.09	48.52	74.61	23.94	103.21	14.99		
		64.07	40.41	52.35	19.18	69.81	10.83		
		46.34	34.44	35.26	14.61	41.41	7.06		
		34.62	29.94	25.6	11.28	23.48	4.37		
		27.22	26.41	19.23	8.85				
		15.46	19.73	14.65	6.95				

32

Xenon

195 K		313 K		293 K		273 K		253 K	
p	v	p	v	p	v	p	v	p	v
0.75	11.71	17.98	1.37	14.77	2.83	7.13	3.34	3.66	4.47
1.5	24.72	38.68	3.07	36.8	6.75	15.55	6.66	7.88	9.58
1.83	41.11	69.68	5.64	56.02	10.04	25.06	10.98	13.59	15.43
2.67	74.08	101.29	8.32	77.6	13.78	36.35	25.77	18.42	19.87
5.25	91.59	138.18	11.13	104.89	20.21	51.5	21.06	24.94	25.78
19.42	116.09	181.56	14.49	138.61	25.28	66.19	25.94	36.5	36.08
29.12	125.76	223.18	17.58	173.05	30.35	79.65	30.66	52.35	45.97
110.13	135.01	270.98	21.03	203.83	34.76	103.9	37.89	66.78	54.55
169.08	139.11	296.55	22.50	243.75	39.46	138.55	46.72	91.92	65.39
257.65	140.98	258.16	19.90	284.08	43.95	186.61	56.03	132.9	76.67
363.77	142.81	217.43	17.00	317.87	47.38	248.81	65.20	175.93	83.60
231.3	140.20	184.17	14.50	273.11	42.89	303.74	70.75	227.36	89.33
166.66	138.48	147.28	11.70	227.71	38.19	337.19	73.52	290.64	93.87
109.86	136.2	107.89	8.63	184.03	32.81	297.52	70.31	358.8	96.69
74.08	134.18	74.95	6.04	141.7	26.83	254.31	65.81	312.14	94.61
48.15	131.04	48.18	3.70			221.79	62.0	269.56	92.36
27.27	126.18	21.74	1.57	24.59	7.38	182.72	55.99	228.26	89.50
19.57	122.84	10.38	0.47			156.52	51.14	199.33	86.60
14.92	119.9					124.69	43.77	167.98	82.75
12.7	117.6					98.36	36.7	145.95	19.47
						78.51	30.76	119.98	74.41
						63.64	25.80	98.88	68.29
						46.5	19.82	84.93	63.53
						34.56	18.41	70.37	57.23
						26. 9	11.91	58.67	51.38
						21.07	9.31	48.21	44.8
						15.51	7.39	33.91	34.68
								29.43	30.62
								24.68	27.2
								20.93	27.88

Heats of Adsorption

(Kcal/mol.)

N_2		O_2		CO_2	
v	q_{st}	v	q_{st}	v	q_{st}
3	6.0	4	4.6	10	9.5
4	5.9	6	4.5	15	9.4
6	5.9	8	4.5	20	9.2
10	5.7	10	4.4	25	9.1
12.5	5.7	12.5	4.5	30	9.0
15	5.7	15	4.4	35	9.0
17.5	5.7	20	4.3	40	9.0
20	5.6	25	4.3	45	9.0
22.5	5.6	30	4.3	50	9.0
25	5.5	35	4.2		
27.5	5.6				
30	5.5				

Ar		Kr		Xe	
v	q_{st}	v	q_{st}	v	q_{st}
2	5.0	10	5.8	6	6.8
3	4.9	15	5.8	8	6.8
4	4.8	20	5.6	10	6.7
5	4.8	25	5.4	14	6.6
6	4.6	30	5.4	18	6.5
7	4.6	35	5.3	20	6.5
8	4.6	40	5.3	25	6.5
9	4.6	45	5.3	30	6.4
10	4.5	50	5.3	35	6.4
12.5	4.4			40	6.5
15	4.4			45	6.4
17.5	4.3				
20	4.4				
22.5	4.3				

34

Entropy of the Sorbed Phase

(cal/deg. mol)

Nitrogen

	$\bar{S}_s$			
v	194 K	229 K	215 K	248 K
4	23.1	23.4	23.3	25.4
6	21.9	22.7	22.6	24.8
8	21.8	22.8	22.3	24.4
10	21.6	22.6	22.3	
12	21.3	22.3	22.1	
14	21.2	21.9	21.6	
16	20.9	21.9	21.6	
18	20.5	21.6	21.3	
20	20.2		21.0	
22	19.9		20.6	
24	19.8		20.6	
26	19.6		20.3	
28	19.3		20.1	
30	19.0		19.9	

Oxygen

	$\bar{S}_s$			
v	173 K	194 K	214 K	228 K
4	29.1	30.0	30.9	30.5
6	28.9	29.6	30.4	30.1
8	28.1	28.9	29.8	29.5
10	28.1	28.9	29.6	29.3
12	27.7	28.4	29.2	
14	27.2	28.0	28.9	
16	27.3	28.1	29.0	
18	27.0	27.7	28.7	
20	26.7	27.5	28.4	
22	26.4	27.2		
24	26.1	27.0		
26	25.9	26.8		
28	25.7	26.5		
30	25.4	26.3		
32	25.2	26.1		
34	25.6	26.4		

Carbon dioxide

	$\bar{S}_s$			
v	288 K	308 K	328 K	348 K
10		29.0	29.7	30.0
15		28.6	29.1	29.6
20		28.0	28.6	29.1
25		27.6	28.3	28.7
30	26.8	27.4	28.1	28.4
35	26.2	26.8	27.5	
40	25.7	26.4	27.1	
45	25.2	25.9	26.5	
50	24.7	25.4		
55				

Argon

	$\bar{S}_s$			
v	175 K	195 K	216 K	236 K
2			19.7	19.8
4			19.0	19.2
6		18.6	19.0	19.0
8		18.4	18.9	18.8
10	17.7	18.3	18.6	18.8
12	17.3	17.9	18.6	
14	16.9	17.5	18.6	
16	16.5	17.1	18.6	
18	16.0	16.7	18.6	
20	15.7	16.4	18.6	
22	15.4	16.1		
24				
26				

Krypton

$\bar{S}_s$

v	212 K	231 K	252 K	274 K
10		19.5	20.0	
15	19.2	19.8		
20	19.2	19.3	19.9	
25	18.8	19.0	19.6	
30	18.1	18.4	19.0	
35	18.0	18.4		
40	17.5	17.9		
45	17.0	17.4		
50	16.5	17.0		
55				

Xenon

$\bar{S}_s$

v	252 K	272 K	293 K	313 K
5		22.9	23.7	23.4
10	22.2	22.5	23.1	23.0
15	22.2	22.3	22.9	22.8
20	21.4	21.7	22.3	22.2
25	20.9	21.2	21.8	
30	20.9	21.2	21.8	
35	20.5	20.7	21.4	
40	20.1	20.4	21.0	
45	19.7	20.1	20.6	
50	19.5	19.9		
55	19.2	19.5		
60				

37

APPENDIX D

Sorption of hydrocarbons.

Isotherms p in torrs; v in cc STP g^{-1}

Methane

90 K		193 K		213 K		233 K		253 K	
p	v	p	v	p	v	p	v	p	v
0.09	66.25	3.08	15.03	6.87	9.73	12.38	5.70	17.63	2.90
0.17	96.90	8.87	27.35	14.95	17.19	25.44	10.47	43.15	6.61
0.24	122.70	17.67	38.29	24.78	24.00	45.06	16.35	72.1	10.23
0.33	141.73	30.37	49.69	37.66	30.85	68.89	22.15	105.76	14.08
0.44	172.09	58.35	62.46	61.13	39.84	96.33	27.72	140.86	17.63
1.26	193.00	70.12	70.85	99.11	51.13	127.43	32.87	174.26	20.63
10.21	207.02	98.95	80.13	130.86	58.34	170.17	38.93	205.54	23.23
16.47	210.73	147.99	90.27	174.0	65.97	222.99	45.20	253.17	26.83
28.89	215.76	195.16	96.41	232.85	72.85	287.38	51.45	310.74	30.71
44.95	220.49	273.2	102.67	299.99	80.33	349.7	56.51	365.21	34.36
59.43	224.43	304.53	104.60	348.29	84.10	389.02	59.26	281.97	29.38
71.9	230.21	219.0	98.61	273.06	78.12	342.18	56.11	222.85	25.15
81.3	236.05	158.6	91.86	202.71	70.40	278.24	50.91	162.81	20.29
79.8	241.97	116.37	84.53	147.77	61.81	224.97	45.66	107.29	14.89
71.52	233.38	93.06	78.85	106.98	53.30	169.07	39.17	60.57	9.58
56.72	226.26	72.7	72.43	75.82	45.05	119.53	32.01	32.25	5.95
39.65	221.44	55.69	65.18	54.41	38.04	87.41	26.33	17.9	3.92
27.78	218.09	44.36	59.30	41.06	32.67	64.45	21.70		
20.9	215.49	31.01	51.13	18.63	20.52	47.97	17.80		
10.23	207.44	18.85	42.42	11.22	15.54	32.33	13.66		
4.65	202.48	17.27	42.69			23.23	10.68		
2.1	196.37					17.28	8.45		

Ethane

195 K		253 K		273 K		293 K		313 K	
p	v	p	v	p	v	p	v	p	v
1.01	29.38	3.06	6.16	8.34	5.60	20.66	5.27	16.63	2.15
2.38	72.48	7.32	14.31	21.49	13.52	36.57	9.23	29.3	3.68
3.21	81.92	12.42	23.35	38.17	22.64	58.43	14.05	49.07	6.05
15.7	106.42	20.72	34.84	59.19	31.35	68.8	16.19	71.91	8.64
33.4	116.79	30.76	44.16	80.39	37.67	99.32	21.90	102.0	11.79
52.88	121.68	50.99	54.71	119.9	45.76	134.73	27.35	139.88	15.53
94.38	126.41	81.33	62.88	168.42	52.03	178.51	32.43	183.7	19.26
118.65	128.02	128.97	69.82	236.6	57.49	237.75	37.75	234.01	22.90
138.78	128.82	185.87	74.70	309.25	61.26	306.21	42.12	288.45	26.26
219.63	131.94	257.18	78.67	252.19	58.51	363.25	45.04	319.49	27.98
279.1	133.40	326.38	81.36	197.95	54.81	301.76	42.22	246.07	24.06
362.3	134.89	279.79	79.74	162.61	51.61	242.55	38.54	182.47	19.47
415.81	135.93	222.45	77.24	141.56	49.31	185.96	33.56	117.69	13.84
348.93	134.92	166.32	73.82	107.95	44.17	143.34	28.76	72.19	9.06
276.26	133.44	114.85	68.85	92.85	41.29	102.59	22.80	35.62	4.95
192.03	131.04	78.79	63.08	70.51	35.50	69.02	16.51	18.71	2.73
143.89	129.43	53.23	56.26	50.96	28.89	43.48	11.02		
97.54	126.87	39.92	50.97	38.94	23.67	28.41	7.38		
63.91	123.86	24.75	40.79	30.5	19.55	9.26	2.27		
49.21	121.33	16.49	31.35	17.2	11.65				
32.57	118.09	11.85	26.22						
22.74	114.53								
17.36	111.72								
14.26	109.55								
12.16	107.74								
10.96	105.7								

39

Propane

195 K		303 K		323 K		343 K		363 K	
p	v	p	v	p	v	p	v	p	v
0.84	29.07	2.25	4.71	3.05	2.81			14.54	3.20
1.02	50.6	6.84	2.12	7.64	6.84	7.00	3.08	29.08	5.96
3.39	73.4	11.17	17.52	13.74	11.05	13.78	5.73	47.03	8.93
8.02	78.1	18.54	23.09	21.87	15.48	22.35	8.66	65.76	11.45
14.23	81.3	28.71	27.84	34.27	20.25	35.97	12.68	85.84	13.74
32.97	86.3	41.88	31.57	52.4	24.76	53.08	16.18	113.77	16.28
60.29	90.1	68.9	35.88	81.75	29.20	75.55	19.82	143.14	18.42
70.65	91.3	94.88	38.21	112.01	31.97	102.11	22.84	177.64	20.36
91.49	95.34	128.27	40.19	151.24	34.29	128.77	25.01	218.88	22.18
107.43	114.6	161.28	41.45	189.17	35.88	167.45	27.44	237.42	23.11
101.77	102.2	192.77	42.42	243.18	37.39	205.19	29.22	199.18	21.63
88.46	96.9	237.57	43.40	204.45	36.45	254.62	30.69	165.28	20.03
65.09	92.5	199.25	42.64	152.98	34.56	236.93	30.23	130.89	17.90
42.49	89.4	162.77	41.62	118.12	32.59	216.52	29.62	100.89	15.60
25.74	85.0	138.3	40.78	90.24	30.35	176.45	28.09	76.86	13.18
16.62	82.5	108.38	39.36	68.74	27.64	143.6	26.33	55.19	10.40
		81.5	37.42	48.82	24.25	117.84	24.62	33.85	7.37
		62.51	35.32	34.85	20.88	92.75	22.29	34.13	7.32
		44.0	32.46	19.49	15.05	72.23	19.85	20.6	4.85
		30.17	29.01	10.7	10.24	53.95	16.85		
		22.87	26.05			37.61	13.68		
		18.27	23.68			25.82	10.44		
		10.22	17.8			18.41	8.09		
		10.14	17.8			7.77	4.11		
		7.69	14.76			7.64	4.14		

n-butane

298 K		373.7 K		393 K		413 K		433 K	
p	v	p	v	p	v	p	v	p	v
7.37	22.79	8.57	8.72	10.43	5.74	12.86	4.02	13.8	2.48
10.72	32.06	21.01	15.20	19.6	9.30	23.22	6.52	27.14	4.49
24.28	39.08	50.4	21.44	35.09	13.55	39.87	9.77	46.24	6.98
58.90	43.70	71.09	23.60	54.34	16.75	58.95	12.49	74.87	9.84
125.48	47.04	99.4	25.61	77.83	19.33	87.63	15.37	94.85	11.31
187.62	49.32	134.29	27.21	111.6	21.81	117.86	17.50	127.43	13.42
271.53	51.52	190.03	28.95	149.58	23.49	151.97	19.23	157.1	14.82
324.58	53.49	239.56	30.04	193.18	24.89	189.77	20.71	190.36	16.13
243.05	51.44	301.01	31.25	244.53	26.12	230.86	21.94	223.61	17.17
166.66	49.36	366.83	32.23	298.93	27.32	262.75	22.73	256.51	18.13
115.87	47.04	315.58	31.81	330.7	27.69	201.95	21.40	214.06	17.16
68.67	44.34	255.39	30.96	281.09	27.20	140.06	19.24	178.12	16.13
33.73	41.79	190.41	29.83	218.81	26.20	93.43	16.45	128.5	13.89
17.68	40.01	125.56	27.59	161.05	24.58	61.38	13.40	90.92	11.67
10.42	35.92	88.14	25.58	108.14	22.17	37.76	10.22	54.9	8.55
6.95	33.10	58.57	23.15	73.94	19.71	23.13	7.28	30.36	5.72
4.66	31.24	40.97	20.70	45.3	16.19	15.14	5.32	17.2	3.76
		28.25	18.10	28.39	12.56				
		20.12	15.55	20.31	9.87				
		14.72	13.67	14.88	2.89				
		8.6	10.09						

Heat of Adsorption

(Kcal/mol)

Methane

v	q_{st}
5	6.2
10	6.1
15	6.0
20	5.9
25	5.8
30	5.7
35	5.6
40	5.7
45	5.6
50	5.6
55	5.7

Ethane

v	q_{st}
5	7.1
10	7.1
15	7.2
20	7.5
25	7.5
30	8.0
35	7.9
40	8.2
45	8.1

Propane

v	q_{st}
5	8.6
7.5	8.8
10	8.7
12.5	8.7
15	8.9
17.5	9.0
20	9.1
22.5	9.0
25	9.2
27.5	9.2

n-Butane

v	q_{st}
6	10.7
8	11.1
10	11.0
12	11.1
14	11.3
16	11.3
18	11.3
20	11.5
22	11.6

Entropy of the Sorbed Phase

(cal/mol deg.)

Methane

	$\bar{S}_s$			
v	192 K	212 K	231 K	252 K
5			24.3	25.5
10			23.0	24.2
15			22.3	23.5
20		21.2	22.0	23.1
25		21.0	21.8	22.7
30	19.6	20.7	21.6	22.4
35	19.3	20.5	21.3	
40	18.9	20.2	21.1	
45	18.4	19.8	20.7	
50	18.1	19.4	20.3	
55				

Ethane

	$\bar{S}_s$			
v	253 K	273 K	293 K	313 K
5		37.4	37.8	38.6
10		35.3	35.9	36.8
15		34.1	34.7	35.6
20	32.3	32.9	33.6	34.6
25	31.4	32.0	32.8	33.5
30	30.0	30.8	31.5	
35	28.9	29.6	30.2	
40	27.2	28.0	28.7	
45				

Propane

	$\bar{S}_s$			
v	303 K	323 K	343 K	363 K
2.5			52.1	52.9
5			50.5	51.4
7.5		48.2	49.2	50.1
10	46.1	47.4	48.5	49.4
12.5	45.3	46.6	47.6	48.6
15	44.4	45.7	46.7	47.7
17.5	44.0	45.2	46.2	47.2
20	43.2	44.4	45.5	46.3
22.5	42.4	43.6	44.7	45.5
25	41.3	42.5	43.6	
27.5				

n-Butane

	$\bar{S}_s$			
v	373.7 K	393 K	413 K	433 K
6		61.6	62.8	63.8
8		60.6	62.0	63.0
10	58.9	59.7	61.1	62.1
12	58.0	58.9	60.2	61.3
14	57.3	58.2	59.5	60.5
16	56.5	57.7	58.9	59.9
18	55.7	56.8	58.0	59.0
20	54.6	56.0	57.1	
22	53.7	55.0	56.1	

APPENDIX E

Sorption and desorption kinetics in H-RHO

Q_t = quantity sorbed at time t

Q_∞ = quantity sorbed at equilibrium

p = pressure in torrs at which the kinetic run was made.

Sample 1

n-Hexane 33.4°C

Sorption p = 48.3		Desorption	
t	Q_t/Q_∞	t	Q_t/Q_∞
0	0.000	0	0.000
1	0.401	2	0.135
2	0.574	3	0.152
3	0.699	5	0.182
4	0.769	10	0.210
5	0.837	11	0.234
7	0.889	21	0.268
9	0.920	27	0.290
12	0.957	33	0.307
16	0.973	41	0.325
19	0.983	54	0.346
21	0.990	63	0.365
25	0.991	69	0.376
35	0.994		
60	1.000		
90	1.000		

n-hexane 95.6°C

Sorption

p = 45.3

t	Q_t/Q_∞
0	0.000
1	0.330
2	0.477
3	0.577
4	0.659
5	0.723
6	0.769
7	0.814
8	0.842
9	0.869
10	0.892
11	0.907
12	0.922
14	0.936
16	0.956
18	0.920
20	0.978
22	0.982
28	0.990
35	0.993
42	0.994
54	0.999

Desorption

t	Q_t/Q_∞
0	0.000
1	0.129
2	0.179
3	0.216
4	0.250
6	0.281
8	0.314
10	0.350
12	0.368
15	0.400
18	0.429
25	0.486
30	0.521
44	0.579
52	0.618
81	0.679

n-hexane 141.4°C

Sorption

p = 45.3

t	Q_t/Q_∞
0	0.000
1	0.259
2	0.379
3	0.467
5	0.591
6	0.646
7	0.681
8	0.720
10	0.729
12	0.824
14	0.860
16	0.884
18	0.903
20	0.912
23	0.935
25	0.946
30	0.963
35	0.971
43	0.983
53	0.993
63	1.000

Desorption

t	Q_t/Q_∞
0	0.000
1	0.214
2	0.291
3	0.348
4	0.394
6	0.460
8	0.513
10	0.559
15	0.642
21	0.708
31	0.790
48	0.874
59	0.908

n-butane 0°C

Sorption		Desorption	
p = 26.9			
t	Q_t/Q_∞	t	Q_t/Q_∞
0	0.000	0	0.000
1.5	0.798	1	0.176
2	0.855	2	0.228
4	0.930	3	0.286
6	0.970	4	0.322
11	0.980	5	0.347
18	0.990	6	0.373
90	1.000	7	0.401
		8	0.419
		9	0.442
		11	0.482
		15	0.536
		19	0.588
		24	0.632
		27	0.670
		30	0.692
		67	0.860
		90	0.894

n-butane 30°C

Sorption		Desorption	
p = 50			
t	Q_t/Q_∞	t	Q_t/Q_∞
0	0.000	0	0.000
1	0.790	1	0.285
2	0.858	2.5	0.343
3	0.921	3	0.366
6	0.951	3.5	0.376
9	0.966	6	0.409
16	0.972	8	0.439
36	0.977	10	0.452
69	1.000	12	0.463
		15	0.482
		18	0.519
		24	0.535
		32	0.547
		40	0.600
		48	0.853
		60	0.914
		70	0.939

n-butane 57.1°C

Sorption		Desorption	
p = 26.9			
t	Q_t/Q_∞	t	Q_t/Q_∞
0	0.000	0	0.000
1	0.239	1	0.688
2	0.843	2	0.800
3	0.906	3	0.889
4	0.935	5	0.933
7	0.972	11	0.961
11	0.996	22	0.972
23	0.998	34	0.987
46	1.000		

47

Sample 2

n-Butane 56.4°C

Sorption

p = 27.0

t	Q_t/Q_{oo}
0	0.000
1	0.396
2	0.575
3	0.664
4	0.765
5	0.821
7	0.892
10	0.940
12	0.978
16	1.000

n-Hexane 25°C

Sorption

p = 52.0

t	Q_t/Q_{oo}
0	0.000
1	0.065
2	0.085
4	0.107
8	0.132
10	0.143
12	0.153
15	0.172
17	0.184
21	0.198
25	0.209
30	0.229

n-Hexane 155.8°C

Sorption

p = 52.0

t	Q_t/Q_{oo}
0	0.000
2	0.051
4	0.100
6	0.118
8	0.140
15	0.200
20	0.228
25	0.253
33	0.286
42	0.310

Sample 3

n-hexane 33.4°C

Sorption

p = 45.5

t	Q_t/Q_{oo}
0	0.000
1	0.420
1.5	0.510
2	0.590
3	0.680
4	0.750
6	0.860
7	0.870
8	0.900
10	0.910

Sorption (continued)

t	Q_t/Q_{oo}
15	0.900
20	0.920
35	1.000